FUTURE VISION BIE

One Stop for All Study Materials

& Lab Programs

Future Vision

By K B Hemanth Raj

Scan the QR Code to Visit the Web Page

Or

Visit : https://hemanthrajhemu.github.io

Gain Access to All Study Materials according to VTU,
CSE – Computer Science Engineering,
ISE – Information Science Engineering,
ECE - Electronics and Communication Engineering
& MORE...

Join Telegram to get Instant Updates: https://bit.ly/VTU_TELEGRAM

Contact: MAIL: futurevisionbie@gmail.com

INSTAGRAM: www.instagram.com/hemanthraj_hemu/

INSTAGRAM: www.instagram.com/futurevisionbie/

WHATSAPP SHARE: https://bit.ly/FVBIESHARE

COMMUNICATION SYSTEMS ENGINEERING

John G. Proakis

Masoud Salehi

2nd Ed.

Upper Saddle River, New Jersey 07458

10

Wireless Communications

In Chapters 7 and 8, we described digital modulation and demodulation methods for transmission of information over two types of channels, namely, an additive Gaussian noise channel and a linear filter channel. Such channel models are appropriate for characterizing physical channels that are relatively static; i.e., the channel transmission characteristics are generally modeled as time invariant. In this chapter we treat modulation and demodulation techniques that are appropriate for wireless communication channels, such as radio and acoustic communication channels, whose transmission characteristics are time varying.

10.1 DIGITAL TRANSMISSION ON FADING MULTIPATH CHANNELS

Physical channels with time-varying transmission characteristics may be characterized as time-varying linear filters. Such linear filters are described by a time-varying impulse response $h(\tau; t)$, where $h(\tau; t)$ is the response of the channel at time t due to an impulse applied at time $t - \tau$. Thus, τ denotes the "age" (elapsed time) variable. The time-varying linear filter model of the channel with additive noise was previously shown in Figure 1.10. We cite the following examples of wireless communication channels that can be modeled in this manner.

Signal Transmission via Ionospheric Propagation in the HF Band. We recall from our discussion in Chapter 1 that sky-wave propagation, as illustrated in Figure 1.6, results from transmitted signals (in the HF frequency band) being bent or refracted by the ionosphere, which consists of several layers of charged particles ranging in altitude from 30–250 miles above the surface of the earth. As a consequence

of these ionospheric layers, the signal arrives at the receiver via different propagation paths at different delays. These signal components are called *multipath components*. The signal multipath components generally have different carrier-phase offsets and, hence, they may add destructively at times, resulting in a phenomenon called *signal fading*. Hence, signal fading is a result of multipath signal propagation. To characterize such channel behavior, we adopt a time-varying impulse response model.

Mobile Cellular Transmission. In mobile cellular radio transmission between a base station and a mobile telephone, the signal transmitted from the base station to the mobile receiver is usually reflected from surrounding buildings, hills, and other obstructions. As a consequence, we observe multiple propagation paths arriving at the receiver at different delays. Hence, the received signal has characteristics similar to those for ionospheric propagation. The same is true of transmission from the mobile telephone to the base station. Moreover, the speed that the mobile (automobile, train, etc.) is traveling results in frequency offsets, called *Doppler shifts,* of the various frequency components (see Problem10.1) of the signal.

Line-of-sight Microwave Radio Transmission. In line-of-sight (LOS) radio transmission of signals, the transmitting and receiving antennas are generally mounted on high towers, in order to avoid obstructions, such as buildings and hills, in the path of signal propagation. However, when there are tall obstructions or hilly terrain in the path of propagation, it is likely that signals will be reflected from the ground to the receiving antenna as illustrated in Figure 10.1. This is especially a problem under severe weather conditions. In this case, there is a received signal component that arrives via the direct path and an ensemble of secondary paths that are reflected from the ground terrain. The latter arrive at the receiver with various delays and constitute multipath propagation. Relatively narrow-beamwidth antennas are employed in microwave LOS transmission to reduce the occurrence of secondary reflections. Nevertheless, some secondary signal reflections are frequently observed in practice. Such secondary signal reflections generally vary with time, so the channel may be characterized by a time-varying impulse response.

Airplane-to-Airplane Radio Communications. In radio communications between two aircraft, it is possible for secondary signal components to be received from ground reflections, as illustrated in Figure 10.2. This is especially the case when omnidirectional antennas are employed in the communication system. The ensemble of

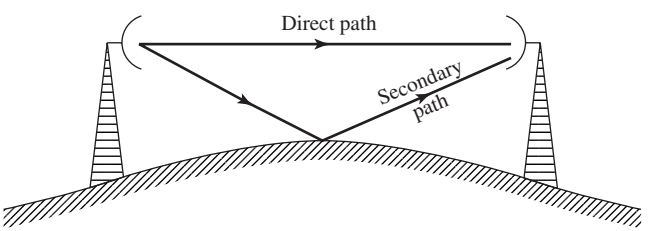

Figure 10.1 Illustration of multipath propagation in LOS microwave transmission.

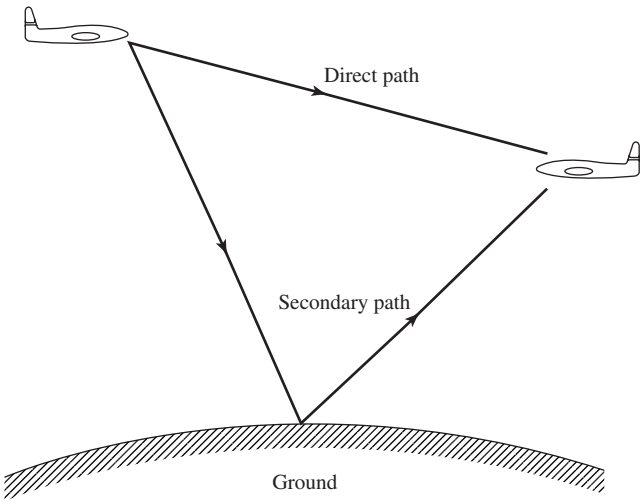

Figure 10.2 Illustration of multipath propagation in airplane-to-airplane communications.

ground-reflected signal components generally arrive at the receiver with different delays and different attenuations. In addition, the motions of the aircraft result in Doppler frequency offsets in the various signal components. In many respects, this situation is similar to that in mobile cellular communications.

Underwater Acoustic Signal Transmission. A shallow-water acoustic channel is generally characterized as a multipath channel due to acoustic signal reflections from the surface and the bottom of the sea. Because of wave motion, the signal multipath components undergo time-varying propagation delays which result in signal fading. In addition, there is frequency-dependent attenuation, which increases proportionally as the square of the signal frequency.

The channels briefly described above may be generally characterized as linear systems with time-varying impulse responses. Since it is generally difficult, if not impossible, to characterize the microscopic effects of signal transmission on channels as the ones described above in a deterministic fashion, it is logical to adopt a statistical characterization. Such an approach is described below.

10.1.1 Channel Models for Time-Variant Multipath Channels

As we have observed, there are basically two distinct characteristics of the types of radio channels described above. One characteristic is that the transmitted signal arrives at the receiver via multiple propagation paths, each of which has an associated time delay. For example, if we transmit an extremely short pulse, the channel response due to multiple scatterers (such as ionized particles in the ionosphere) might appear as shown in Figure 10.3. Because the received signal is spread in time due to the multiple scatterers at different delays, we say that the channel is time dispersive.

A second characteristic of the types of radio channels described above is concerned with the time variations in the structure of the medium. As a result of such

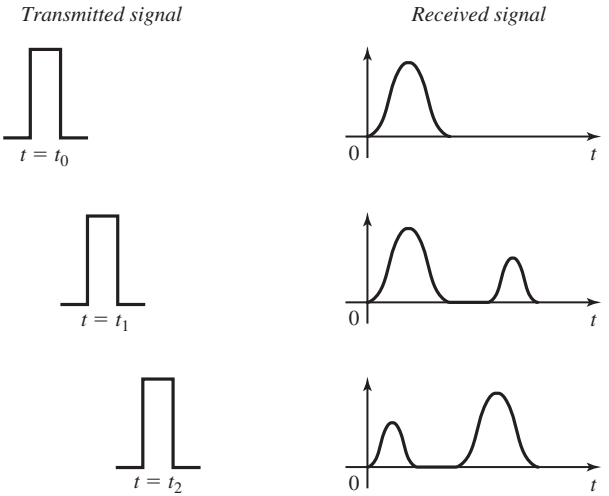

Figure 10.3 Illustration of time-variant channel response characteristics.

time variations, the response of the channel to any signal transmitted through it will change with time. Hence, if we repeat the short pulse transmission experiment over and over, we would observe changes in the received signal, which are due to physical changes in the medium. Such changes include variations in the relative delays of signals from the multiple scatterers. Hence, the received signal might appear as illustrated in Figure 10.3. In other words, the impulse response of the channel is varying with time. In general, the time variations in the received signal appear to be unpredictable to the user of the channel. This leads us to characterize the time-variant multipath channel statistically.

To obtain a statistical description of the channel, let us consider the transmission of an unmodulated carrier

$$c(t) = A \cos 2\pi f_c t \tag{10.1.1}$$

The received signal in the absence of noise may be expressed as

$$\begin{aligned} x(t) &= A \sum_n \alpha_n(t) \cos[2\pi f_c (t - \tau_n(t)] \\ &= A \,\mathrm{Re}\left[\sum_n \alpha_n(t) e^{-j2\pi f_c \tau_n(t)} \; e^{j2\pi f_c t} \right] \end{aligned} \tag{10.1.2}$$

where $\alpha_n(t)$ is the time-variant attenuation factor associated with the nth propagation path and $\tau_n(t)$ is the corresponding propagation delay. The complex-valued signal

$$\begin{aligned} z(t) &= \sum_n \alpha_n(t)\, e^{-j2\pi f_c \tau_n(t)} \\ &= \sum_n \alpha_n(t)\, e^{-j\phi_n(t)} \end{aligned} \tag{10.1.3}$$

represents the response of the channel to the complex exponential $\exp(j2\pi f_c t)$. We note that, although the input to the channel is a monochromatic signal; i.e., a signal at a single frequency, the output of the channel consists of a signal that contains many different frequency components. These new components are generated as a result of the time variations in the channel response. The r.m.s. (root-mean-square) spectral width of $z(t)$ is called the *Doppler frequency spread* of the channel and is denoted as B_d. This quantity is a measure of how rapidly the signal $z(t)$ is changing with time. If $z(t)$ changes slowly, the Doppler frequency spread is relatively small, while if $z(t)$ changes rapidly, the Doppler frequency spread is large.

We may view the received complex-valued signal $z(t)$ in Equation (10.1.3) as the sum of a number of vectors (phasors) each of which has a time-variant amplitude $\alpha_n(t)$ and phase $\phi_n(t)$. In general, it takes large dynamic changes in the physical medium to cause a large change in $\{\alpha_n(t)\}$. On the other hand, the phases $\{\phi_n(t)\}$ will change by 2π radians whenever $\{\tau_n(t)\}$ change by $1/f_c$. But $1/f_c$ is a small number and, hence, the phases $\{\phi_n(t)\}$ change by 2π or more radians with relatively small changes of the medium characteristics. We also expect the delays $\{\tau_n(t)\}$ associated with the different signal paths to change at different rates and in as unpredictable (random) manner. This implies that the complex-valued signal $z(t)$ in Equation (10.1.3) can be modeled as a random process. When there are a large number of signal propagation paths, the central limit theorem can be applied. Thus, $z(t)$ can be modeled as a complex-valued Gaussian random process.

The multipath propagation model for the channel, embodied in the received signal $x(t)$ or, equivalently, $z(t)$ given by Equation (10.1.3), results in signal fading. The fading phenomenon is primarily a result of the time-variant phase factors $\{\phi_n(t)\}$. At times, the complex-valued vectors in $z(t)$ add destructively to reduce the power level of the received signal. At other times, the vectors in $z(t)$ add constructively and, thus, produce a large signal value. The amplitude variations in the received signal due to the time-variant multipath propagation in the channel are usually called *signal fading*.

Tapped Delay Line Channel Model. A general model for a time-variant multipath channel is illustrated in Figure 10.4. The channel model consists of a tapped delay line with uniformly spaced taps. The tap spacing between adjacent taps is $1/W$, where W of the signal transmitted through the channel. Hence, $1/W$ is the time resolution that can be achieved by transmitting a signal of bandwidth W. The tap coefficients, denoted as $\{c_n(t) \equiv \alpha_n(t)e^{j\phi_n(t)}\}$ are usually modeled as complex-valued, Gaussian random processes which are mutually uncorrelated. The length of the delay line corresponds to the amount of time dispersion in the multipath channel, which is usually called the *multipath spread*. We denote the multipath spread as $T_m = L/W$, where L represents the maximum number of possible multipath signal components.

Example 10.1.1

Determine an appropriate channel model for two-path ionospheric propagation, where the relative time delay between the two received signal paths is 1 msec and the transmitted signal bandwidth W is 10 kHz.

Solution A 10-kHz signal can provide a time resolution of $1/W = 0.1$ msec. Since the [illegible] is interpreted as a tapped delay line

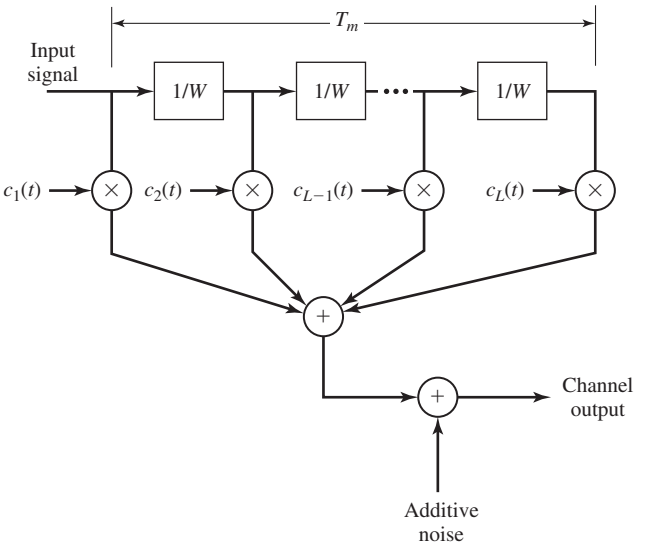

Figure 10.4 Model for time-variant multipath channel.

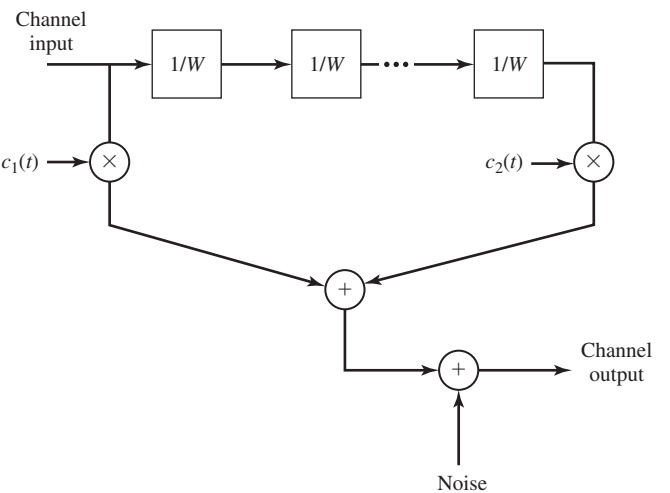

Figure 10.5 Channel model for two-path channel in Example 10.1.1.

model consists of 10 taps, with only the first tap and the last tap having non-zero, time-varying coefficients, denoted as $c_1(t)$ and $c_2(t)$, as shown in Figure 10.5. Because $c_1(t)$ and $c_2(t)$ represent the signal response of a large number of ionized particles from two different regions of the ionosphere, we may characterize $c_1(t)$ and $c_2(t)$ as complex-valued, uncorrelated Gaussian random processes. The rate of variation of the tap coefficients [illegible] of the Doppler spread [illegible]

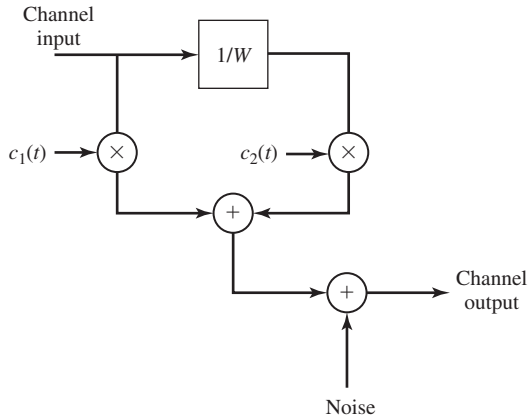

Figure 10.6 Channel model for two-path channel in Example 10.1.2.

Example 10.1.2

Determine an appropriate channel model for an airplane-to-airplane communication link in which there is a direct signal propagation path, and a secondary propagation resulting from signal scattering due to the surrounding ground terrain. The secondary path has a propagation delay of $\tau_0 = 10$ μsec relative to the propagation delay of the direct path. The signal bandwidth is $W = 100$ kHz.

Solution A 100-kHz signal provides a time resolution of $1/W = 10$ μsec. Consequently, the secondary signal path is resolvable, since its relative time delay is 10 μsec. In this case, a channel model that has two taps with tap coefficients $c_1(t) = \alpha_1(t)\, e^{j\phi_1(t)}$ and $c_2(t) = \alpha_2(t)\, e^{j\phi_2(t)}$, as shown in Figure 10.6, is appropriate. The direct path may be modeled as having a fixed (time-invariant) attenuation α_1, but a time-varying phase shift. The secondary path, which results from ground terrain, is modeled as having a time-varying attenuation and phase shift, since the ground terrain is changing with time due to the motion of the airplanes. In this case, it is appropriate to model $c_2(t)$ as a complex-valued, Gaussian random process. The rates of variation of the tap coefficients, $c_1(t)$ and $c_2(t)$, determine the value of the Doppler frequency spreads for these paths. Note that, in both the direct and the reflected signal paths, there will be Doppler frequency shifts resulting from motion of the aircraft.

Example 10.1.3

Determine the appropriate channel model for the airplane-to-airplane communication link described in Example 10.1.2, but now assume that the transmitted signal bandwidth is 10 kHz.

Solution A 10-kHz signal provides a time resolution of 100 μsec. Since the relative delay between the two signal components is 10 μsec, the two signal paths are not resolvable in time. Consequently, the channel appears as a single path channel with tap coefficient $c(t)$ that includes the direct path and the secondary path. Since the secondary path results from signal scattering from a large number of scatterers, we may characterize $c(t)$ as a complex-valued Gaussian random process with a mean value of $\alpha_1 e^{j\phi_1(t)}$, which is due to the direct path.

Rayleigh and Ricean Fading Models. In the channel models described in Examples 10.1.2 and 10.1.3, the tap coefficients in the tapped-delay line model were characterized as complex-valued Gaussian random processes. We may express each of the tap coefficients as

$$c(t) = c_r(t) + jc_i(t) \tag{10.1.4}$$

where $c_r(t)$ and $c_i(t)$ represent real-valued Gaussian random processes. We assume that $c_r(t)$ and $c_i(t)$ are stationary and statistically independent. This assumption generally holds for the tapped delay model of physical channels.

We may also express $c(t)$ in the form as

$$c(t) = \alpha(t)\, e^{j\phi(t)} \tag{10.1.5}$$

where

$$\begin{aligned} \alpha(t) &= \sqrt{c_r^2(t) + c_i^2(t)} \\ \phi(t) &= \tan^{-1} \frac{c_i(t)}{c_r(t)} \end{aligned} \tag{10.1.6}$$

In this representation, if $c_r(t)$ and $c_i(t)$ are Gaussian with zero-mean values, the amplitude $\alpha(t)$ is characterized statistically by the Rayleigh probability distribution and $\phi(t)$ is uniformly distributed over the interval $(0, 2\pi)$. As a consequence, the channel is called a *Rayleigh fading channel*. The Rayleigh fading signal amplitude is described by the PDF

$$f(\alpha) = \frac{\alpha}{\sigma^2}\, e^{-\alpha^2/2\sigma^2}, \quad a \geq 0 \tag{10.1.7}$$

and $f(\alpha) = 0$ for $\alpha < 0$. The parameter $\sigma^2 = E(c_r^2) = E(c_i^2)$.

On the other hand, if $c_r(t)$ and $c_i(t)$ are Gaussian with nonzero mean as in the airplane-to-airplane communication link described in Example 10.1.3, the amplitude $\alpha(t)$ is characterized statistically by the Rice probability distribution and the phase $\phi(t)$ is also nonzero mean. In this case the channel is called a *Ricean fading channel* and the PDF of the amplitude is given as

$$f(\alpha) = \frac{\alpha}{\sigma^2} e^{-(\alpha^2+s^2)/2\sigma^2}\, I_0\left(\frac{s\alpha}{\sigma^2}\right), \quad a \geq 0 \tag{10.1.8}$$

where the parameter s^2 represents the power of the received nonfading signal component and $\sigma^2 = \text{VAR}(c_r) = \text{VAR}(c_i)$.

Propagation Models for Mobile Radio Channels. In the link budget calculations that were described in Section 7.7.2, we had characterized the path loss of radio waves propagating through free space as being inversely proportional to d^2, where d is the distance between the transmitter and the receiver. However, in a mobile radio channel, propagation is generally neither free space nor LOS. The mean path loss encountered in mobile radio channels may be characterized as being inversely proportional

to d^p, where $2 \leq p \leq 4$, with d^4 being a worst-case model. Consequently, the path loss is usually much more severe compared to that of free space.

There are a number of factors affecting the path loss in mobile radio communications. Among these factors are base-station antenna height, mobile antenna height, operating frequency, atmospheric conditions, and presence or absence of buildings and trees. Various mean path loss models have been developed that incorporate such factors. For example, a model for a large city in an urban area is the Hata model, in which the mean path loss is expressed as

$$\begin{aligned}\text{Loss in dB} = {} & 69.55 + 26.16 \log_{10} f - 13.82 \log_{10} h_t - a(h_r) \\ & + (44.9 - 6.55 \log_{10} h_t) \log_{10} d \end{aligned} \tag{10.1.9}$$

where f is the operating frequency in MHz ($150 < f < 1500$), h_t is the transmitter antenna height in meters ($30 < h_t < 200$), h_r is the receiver antenna height in meters ($1 < h_r < 10$), d is the distance between transmitter and receiver in km ($1 < d < 20$), and

$$a(h_r) = 3.2(\log_{10} 11.75h_r)^2 - 4.97, \qquad f \geq 400\,\text{MHz} \tag{10.1.10}$$

In mobile radio communications we often encounter the effect of shadowing of the signal due to large obstructions, such as large buildings, trees, and hilly terrain between the transmitter and the receiver. Shadowing is usually modeled as a multiplicative and, generally, slowly time-varying random process; i.e., the received signal may be characterized mathematically as

$$r(t) = A_0 g(t) s(t) \tag{10.1.11}$$

where A_0 represents the mean path loss, $s(t)$ is the transmitted signal, and $g(t)$ is a random process that represents the shadowing effect. At any time instant, the shadowing process is modeled statistically as lognormally distributed. The PDF for the lognormal distribution is

$$f(g) = \begin{cases} \frac{1}{\sqrt{2\pi\sigma^2 g}}\, e^{-(\ln g - \mu)^2/2\sigma^2} & (g \geq 0) \\ 0, & (g < 0) \end{cases} \tag{10.1.12}$$

If we define a new random variable X as $X = \ln g$, then

$$f(x) = \frac{1}{\sqrt{2\pi\sigma^2}}\, e^{-(x-\mu)^2/2\sigma^2}, \qquad -\infty < x < \infty \tag{10.1.13}$$

The random variable X represents the path loss measured in dB, μ is the mean path loss in dB and σ is the standard deviation of the path loss in dB. For a typical cellular environment, σ is in the range of 5–12 dB.

The Coherence Time and Coherence Bandwidth of the Channel. Besides the multipath (time) spread T_m and the Doppler (frequency) spread B_d, there are two other parameters that are useful in characterizing fading, multipath channels. One parameter is the reciprocal of the Doppler spread. This quantity is a measure of the time interval over which the channel characteristics will change very little. We call this

parameter the *coherence time* of the channel, and define it as

$$T_{ct} = \frac{1}{B_d} \tag{10.1.14}$$

The other useful parameter is the reciprocal of the multipath spread, which has units of frequency. This quantity is a measure of the bandwidth over which the channel characteristics (magnitude $\alpha(t)$ and phase $\phi(t)$) are highly correlated. In other words, all frequency components of a signal within this bandwidth will fade simultaneously. We call this parameter the *coherence bandwidth* of the channel and define it as

$$B_{cb} = \frac{1}{T_m} \tag{10.1.15}$$

Example 10.1.4

Consider the communication link described in Example 10.1.1. Determine the coherence bandwidth of this channel.

Solution The multipath spread for this channel is $T_m = 1$ msec. Hence, the coherence bandwidth of the channel is $1/T_m = 1000$ Hz. Within this bandwidth, all frequency components of a signal will be affected similarly by the channel. For example, all frequency components of a signal that fall within the coherence bandwidth will fade simultaneously.

Examples 10.1.1, 10.1.3, and 10.1.4 provide some indication on the role that the signal bandwidth plays in relation to the characteristics of the channel model. For example, if the transmitted signal has a bandwidth W that is larger than the coherence bandwidth B_{cb} of the channel ($W > B_{cb}$), as is the case in Example 10.1.1 and 10.1.2, the multipath components are resolvable and, as a consequence, frequency components of the transmitted signal that are separated by more that B_{cb} are affected (attenuated and phase shifted) differently by the channel. In such a case we say that the channel is *frequency selective*. On the other hand, if the signal bandwidth W is smaller than $B_{cb}(W < B_{cb})$, as is the case in Example 10.1.3 , all the frequency components in the signal are affected (attenuated and phase shifted) similarly by the channel at any instant in time. In such a case, we say that the channel is *frequency nonselective*.

The Channel Spread Factor. The product $T_m B_d = T_m / T_{ct}$ is usually called the *channel spread factor*. If $T_m B_d < 1$, the channel is called *underspread* and if $T_m B_d > 1$, the channel is said to be *overspread*. The spread factor usually provides some indication on whether or not phase-coherent demodulation is possible at the receiver. In general, if the channel is overspread, due either to a large multipath spread or a large Doppler spread or both, the estimation of the carrier phase is extremely difficult because of the rapid time variations ($T_{ct} \ll T_m$) in the channel that occur in the time interval T_m. On the other hand, if the channel is underspread, the channel-time variation is slow relative to the multipath spread ($T_{ct} \gg T_m$) and, hence, the carrier phase of the received signal can be estimated with good precision. Fortunately, most physical time-varying channels encountered in practice are underspread.

Next, we describe how these channel parameters are used in the design of modulation signals for transmitting digital information over the channel. Table 10.1 lists the

TABLE 10.1 MULTIPATH SPREAD, DOPPLER SPREAD, AND SPREAD FACTOR FOR SEVERAL TIME-VARIANT MULTIPATH CHANNELS

Type of channel	Multipath duration (s)	Doppler spread (Hz)	Spread factor
Shortwave ionospheric propagation (HF)	$10^{-3} - 10^{-2}$	$10^{-1} - 1$	$10^{-4} - 10^{-2}$
Ionospheric propagation under disturbed auroral conditions	$10^{-3} - 10^{-2}$	$10 - 100$	$10^{-2} - 1$
Ionospheric forward scatter (VHF)	10^{-4}	10	10^{-3}
Tropospheric scatter	10^{-6}	10	10^{-5}
Mobile cellular (UHF)	10^{-5}	100	10^{-3}

values of these channel parameters for several multipath channels. Although we focus our treatment on binary modulation, the basic concepts carry over to M-ary modulation without exceptions.

10.1.2 Signal Design for Fading Multipath Channels

There are different approaches that one can take in the design of signals for transmitting digital information through a fading multipath channel. Although, in principle, any of the carrier-modulation methods (PAM, QAM, PM, and FSK) are applicable, signal fading generally causes large fluctuations in the received signal amplitude and, consequently, it is extremely difficult to discriminate among multiple-amplitude levels in the received signal. For this reason, PAM and QAM are often avoided for digital communications through fading channels. In our discussion, we shall focus our attention on digital-phase modulation (PSK) and frequency-shift keying (FSK).

As indicated in the previous section, the available channel bandwidth plays an important role in the design of the modulation. If the bandwidth that is allocated to the user exceeds the coherence bandwidth B_{cb} of the channel, we have basically two options. One option is to transmit the information on a single sinusoidal carrier, using a signal that occupies the entire available channel bandwidth. In this case, the multipath signal components are resolvable to within a time resolution of $1/W$. Hence, signal propagation paths that differ in time-of-arrival at the receiver by a time interval greater than or equal to $1/W$ will be distinguishable as separate propagating signal components. The number of distinct signal components depends on the channel characteristics. For example, in the airplane-to-airplane communication link, we would expect to see the direct path and the ground-reflected path. In radio-signal transmission via ionospheric propagation in the HF frequency band, the number of received signal components depends on the number of ionospheric reflecting layers and the possibility of paths arriving by multiple skips.

We observe that, when $W > B_{cb}$, the received signal may be corrupted by intersymbol interference, unless the symbol rate is selected to be significantly smaller than the multipath spread T_m. We recall that the symbol rate $1/T$ satisfies the condition

$$\frac{1}{T} \leq 2W \tag{10.1.16}$$

For example, if we select the symbol rate $1/T = W$, then, since $T_m > 1/W$, it follows that $T_m > T$. In this case, the receiver encounters intersymbol interference (ISI) and must employ some type of equalization, as previously described in Section 8.6. On the other hand, if the symbol rate is selected to be very small; i.e., $T \gg T_m$, then the ISI becomes insignificant and no equalization is necessary. Such signal design is usually accomplished by the use of spread-spectrum signals, as described in Section 10.3. Further discussion on this topic is deferred to Section 10.3.2.

Example 10.1.5 Single Carrier Signal Transmission

Suppose that an HF channel with a nominal bandwidth allocation of 3200 Hz is to be used for transmitting digital information at a rate of either (1) 4800 bits/sec or (2) 20 bits/sec. The channel multipath spread is $T_m = 5$ msec. Specify a modulation method for achieving the desired data rates and indicate whether or not an equalizer is necessary at the receiver for the intersymbol interference.

Solution For the 4800-bps system, we select a symbol rate of 2400 symbols/second and four-phase modulation (either coherent PSK or DPSK). A symbol rate of 2400 can be accommodated in a channel bandwidth of 3200 Hz, since there is an excess bandwidth of 800 Hz. A transmitting filter with a raised cosine spectral characteristic may be used to obtain the desired signal shaping. The symbol rate $1/T = 2400$ means that the received signal will be corrupted by intersymbol interference ($T_m \gg T$), which will require the use of an equalizer to reduce its effect on performance.

For the low rate of 20 bits/sec we may again employ four-phase modulation (PSK or DPSK). Thus, the symbol rate is 10 symbols/sec and, hence, $T = 100$ msec. Since $T \gg T_m$, the effect of the multipath spread is negligible and no equalization is necessary at the receiver. To use the entire channel bandwidth, we may employ a phase-modulated spread-spectrum signal as described in Section 10.3.

Example 10.1.6 Multicarrier OFDM Signal Transmission

Consider an HF channel which has a nominal bandwidth of 3200 Hz and a multipath spread of $T_m = 1$ msec. Design a multiple-carrier OFDM signal that achieves a data rate of 4800 bits/sec.

Solution We may select the number N of subcarriers to be as large as we like so as to achieve the desired condition that $T_{sc} \gg T_m$, where T_{sc} is the symbol duration for each subcarrier. However, the complexity of the demodulator increases, as $N \log_2 N$ (computational complexity of FFT algorithm) and the demodulation delay for delivering the information to the user increases (linearly) with N. Therefore, it is desirable to keep N as small as possible. Suppose we select N such that $T_{sc} = 100$ msec. Then, each subchannel may be as narrow[†] as $W_{ac} \approx \frac{1}{T_{sc}} = 10$ Hz. Note that $W_{sc} \ll B_{cb} = 1000$ Hz as desired. If we employ four-phase (PSK or DPSK) modulation in each subchannel, we achieve a bit rate of 20 bits/sec, per subchannel. With $N = 240$ subchannels, we achieve the desired data rate of 4800 bps.

As previously indicated in Section 8.7, a disadvantage of multicarrier OFDM modulation is the relatively high peak-to-average ratio (PAR) that is inherent in the

[†]In practice, it will be necessary to have some excess bandwidth in each subchannel. The excess bandwidth may be in the range of 25–50%.

transmitted signal. In general, large peaks occur in the transmitted signal when the signals in many of the subchannels add constructively in phase. Such large signal peaks may saturate the power amplifier and, thus, cause intermodulation distortion in the transmitted signal. One way to avoid intermodulation distortion is to reduce the power in the transmitted signal and, thus, operate the power amplifier at the transmitter in its linear operating range. However, this power reduction or "power backoff" results in inefficient operation of the communication system. For this reason, alternative methods have been developed to reduce the PAR in OFDM systems. The interested reader is referred to the references cited at the end of Chapter 8.

In the above discussion, we assumed that the available channel bandwidth exceeds the coherence bandwidth B_{cb} of the channel. On the other hand, if the channel bandwidth is much smaller than B_{cb}, there is no point in designing a multicarrier system. A single-carrier system can be designed using the entire bandwidth, with a symbol rate of $W \leq 1/T \leq 2W$. In this case $T \gg T_m$, so that the effect of intersymbol interference on the performance of the system is negligible.

Next, we evaluate the performance of the demodulator and detector for a PSK, DPSK, and FSK modulations in a Rayleigh fading channel under the condition that intersymbol interference is negligible.

10.1.3 Performance of Binary Modulation in Frequency Nonselective Rayleigh Fading Channels

In this section, we determine the probability of error at the receiver of a binary digital communication system that transmits information through a Rayleigh fading channel. The signal bandwidth W is assumed to be much smaller than the coherence bandwidth B_{cb} of the channel, as in Example 10.1.3. Since the multipath components are not resolvable, the channel is frequency nonselective and, hence, the channel impulse response is represented as

$$h(\tau; t) = \alpha(t)\delta(\tau - \tau_0(t)) \tag{10.1.17}$$

where $\alpha(t)$ has a Rayleigh distribution at any instant in time.

We assume that the time variations of $\alpha(t)$ and $\tau_0(t)$ are very slow compared to the symbol interval, so that within the time interval $0 \leq t \leq T$, the channel impulse response is constant; i.e.,

$$h(\tau; t) \equiv h(\tau) = \alpha\delta(\tau - \tau_0) \tag{10.1.18}$$

where the amplitude α is Rayleigh distributed; i.e.,

$$f(\alpha) = \begin{cases} \frac{\alpha}{\sigma^2} e^{-\alpha^2/2\sigma^2}, & \alpha > 0 \\ 0, & \text{otherwise} \end{cases} \tag{10.1.19}$$

Now, suppose that binary antipodal signals; e.g., binary PSK, are used to transmit the information through the channel. Hence, the two possible signals are

$$u_m(t) = \sqrt{\frac{2\mathcal{E}_b}{T}} \cos(2\pi f_c t + m\pi) + n(t), \quad m = 0, 1 \tag{10.1.20}$$

The received signal is the interval $0 \le t \le T$ is

$$r(t) = \alpha\sqrt{\frac{2\mathcal{E}_b}{T}} \cos(2\pi f_c t + m\pi + \phi) + n(t) \tag{10.1.21}$$

where ϕ is the carrier-phase offset. Let us assume that ϕ is known to the demodulator, which crosscorrelates $r(t)$ with

$$\psi(t) = \sqrt{\frac{2}{T}} \cos(2\pi f_c t + \phi), \quad 0 \le t \le T \tag{10.1.22}$$

Hence, the input to the detector at the sampling instant is

$$r = \alpha\sqrt{\mathcal{E}_b} \cos m\pi + n, \quad m = 0, 1 \tag{10.1.23}$$

For a fixed value of α, the probability of error is the familiar form

$$P_b(\alpha) = Q\left(\sqrt{\frac{2\alpha^2\mathcal{E}_b}{N_0}}\right) \tag{10.1.24}$$

We view $P_b(\alpha)$ as a conditional probability of error for a given value of the channel attenuation α. To determine the probability of error averaged over all possible values of α, we compute the integral

$$P_b = \int_0^\infty P_b(\alpha) f(\alpha)\, d\alpha \tag{10.1.25}$$

where $f(\alpha)$ is the Rayleigh PDF given by Equation (10.1.19). This integral has the simple closed form expression

$$P_b = \frac{1}{2}\left[1 - \sqrt{\frac{\bar{\rho}_b}{1 + \bar{\rho}_b}}\right] \tag{10.1.26}$$

where, by definition,

$$\bar{\rho}_b = \frac{\mathcal{E}_b}{N_0} E(\alpha^2) \tag{10.1.27}$$

Hence, $\bar{\rho}_b$ is the average received SNR/bit and $E(\alpha^2) = 2\sigma^2$.

If the binary signals are orthogonal, as in orthogonal FSK, where the two possible transmitted signals are given as

$$u_m(t) = \sqrt{\frac{2\mathcal{E}_b}{N_0}} \cos\left[2\pi\left(f_c + \frac{m}{2T}\right)t\right], \quad m = 0, 1, \tag{10.1.28}$$

the received signal is

$$r(t) = \alpha\sqrt{\frac{2\mathcal{E}_b}{T}}\cos\left[2\pi\left(f_c + \frac{m}{2T}\right)t + \phi\right] + n(t) \tag{10.1.29}$$

In this case, the received signal is crosscorrelated with the two signals

$$\begin{aligned}\psi_1(t) &= \sqrt{\frac{2}{T}}\cos(2\pi f_c t + \phi)\\ \psi_2(t) &= \sqrt{\frac{2}{T}}\cos\left[2\pi\left(f_c + \frac{1}{2T}\right)t + \phi\right]\end{aligned} \tag{10.1.30}$$

If $m = 0$, for example, the two correlator outputs are

$$\begin{aligned}r_1 &= \alpha\sqrt{\mathcal{E}_b} + n_1\\ r_2 &= n_2\end{aligned} \tag{10.1.31}$$

where n_1 and n_2 are the additive noise components at the outputs of the two correlators. Hence, the probability of error is simply the probability that $r_2 > r_1$. Since the signals are orthogonal, the probability of error for a fixed value of α has the familiar form

$$P_b(\alpha) = Q\left(\sqrt{\frac{\alpha^2\mathcal{E}_b}{N_0}}\right) \tag{10.1.32}$$

As in the case of antipodal signals, the average probability of error over all values of α is determined by evaluating the integral in Equation (10.1.25). Thus, we obtain

$$P_b = \frac{1}{2}\left[1 + \sqrt{\frac{\bar{\rho}_b}{2 + \bar{\rho}_b}}\right] \tag{10.1.33}$$

where $\bar{\rho}_b$ is the average SNR/bit defined by Equation (10.1.27).

Figure 10.7 illustrates the average probability of error for binary antipodal and orthogonal signals. The striking aspects of these graphs is the slow decay of the probability of error as a function of SNR. In fact, for large values of $\bar{\rho}_b$, the probability of error for binary signals is

$$\begin{aligned}P_b &\approx \frac{1}{4\bar{\rho}_b}, \quad \text{antipodal signals}\\ P_b &\approx \frac{1}{2\bar{\rho}_b}, \quad \text{orthogonal signals}\end{aligned} \tag{10.1.34}$$

Hence the probability of error in both cases decreases only inversely as the SNR. This is in contrast to the exponential decrease in the case of the AWGN channel. We also note that the difference in SNR between antipodal signals (binary PSK) and orthogonal signals (binary FSK) is 3 dB.

Two other types of signal modulation are DPSK and noncoherent FSK. For completeness, we state that the average probability of error for these signals (see

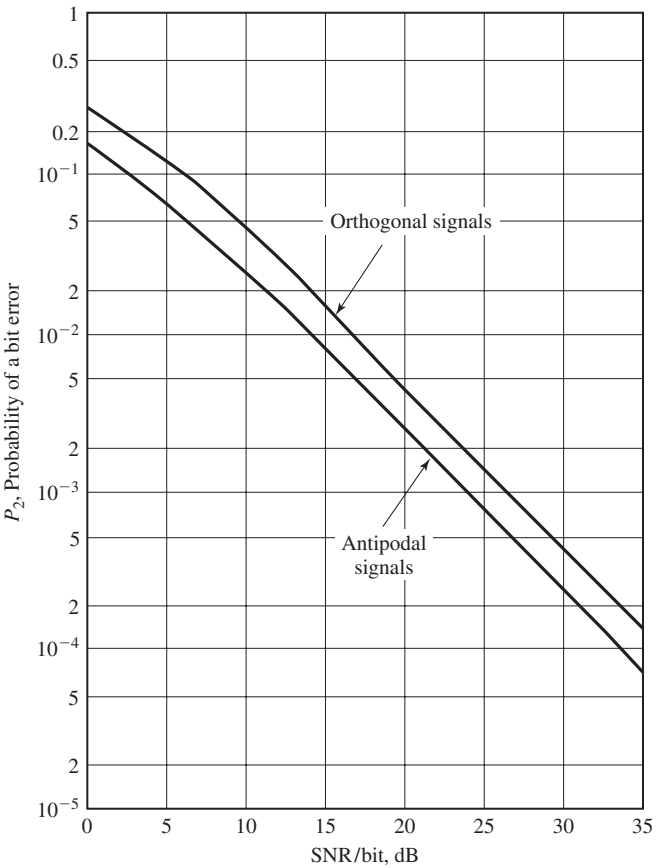

Figure 10.7 Performance of binary signaling on a Rayleigh fading channel.

Problem 10.3) is

$$P_b = \frac{1}{2(1 + \bar{\rho}_{b)}}, \quad DPSK \tag{10.1.35}$$

$$P_b = \frac{1}{2 + \bar{\rho}_b}, \quad \text{noncoherent FSK} \tag{10.1.36}$$

10.1.4 Performance Improvement Through Signal Diversity

The basic problem in digital communication through a fading channel is that a large number of errors occur when the channel attenuation is large; i.e., when the channel is in a deep fade. If we can supply to the receiver two or more replicas of the same information signal transmitted through independently fading channels, the probability that all the signal components will fade simultaneously is reduced considerably. If p

is the probability that any one signal will fade below some critical value, than p^D is the probability that all D independently fading replicas of the same signal will fade below the critical value. There are several ways that we can provide the receiver with D independently fading replicas of the same information-bearing signal.

One method for achieving D independently fading versions of the same information-bearing signal is to transmit the same information on D OFDM carrier frequencies, where the separation between successive carriers equals or exceeds the coherence bandwidth B_{cb} of the channel. This method is called *frequency diversity*.

A second method for achieving D independently fading versions of the same information-bearing signal is to transmit the same information in D different time slots, where the time separation between successive time slots equals or exceeds the coherence time T_{ct} of the channel. This method is called *time diversity*.

Another commonly used method for achieving diversity is via use of multiple receiving antennas, but only one transmitting antenna. The receiving antennas must be spaced sufficiently far apart so that the multipath components in the signal have significantly different propagation paths, as illustrated in Figure 10.8. Usually, a separation of a few wavelengths is required between a pair of receiving antennas in order to obtain signals that fade independently.

Other diversity transmission and reception techniques that are used in practice, are angle-of-arrival diversity and polarization diversity.

Given that the information is transmitted to the receiver via D independently fading channels, there are several ways that the receiver may extract the transmitted information from the received signal. The simplest method is for the receiver to monitor the received power level in the D received signals and to select for demodulation and detection the strongest signal. In general, this approach results in frequent switching from one signal to another. A slight modification that leads to a simpler implementation is to use a signal for demodulation and detection as long as the received power level in that signal is above a preset threshold. When the signal falls below the threshold, a switch is made to the channel which has the largest received power level. This method of signal selection is called *selection diversity*.

For better performance, we may use one of several more complex methods for combining the independently fading received signals as illustrated in Figure 10.9. One

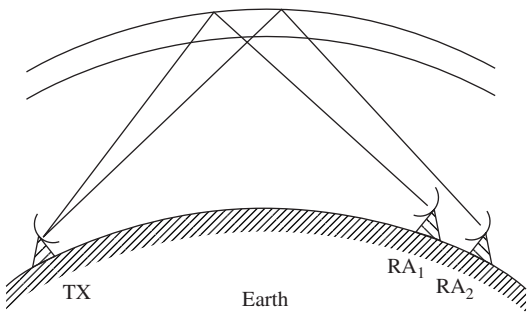

Figure 10.8 Illustration of diversity reception using two receiving antennas.

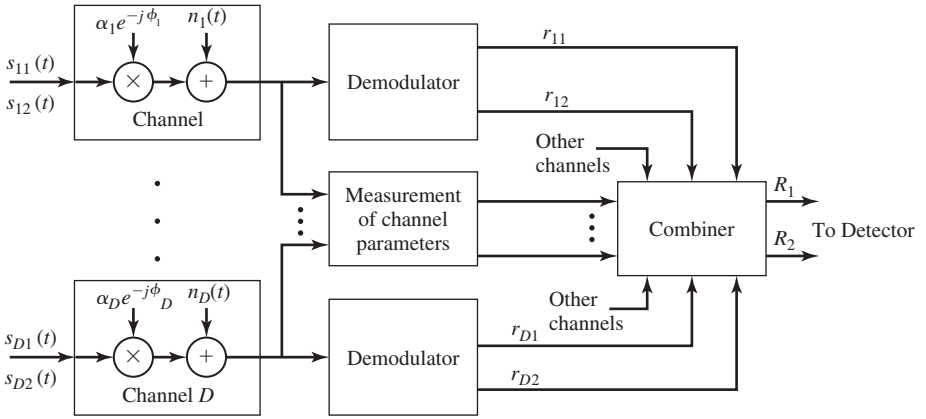

$$\text{Equal gain combiner :} \quad R_m = \sum_{k=1}^{D} r_{km} e^{j\phi_k},\ m = 1, 2$$

$$\text{Maximal ratio combiner:} \quad R_m = \sum_{k=1}^{D} \alpha_k r_{km} e^{j\phi_k},\ m = 1, 2$$

$$\text{Square low combiner:} \quad R_m = \sum_{k=1}^{D} |r_{km}|^2,\ m = 1, 2$$

Figure 10.9 Model of binary digital communication system with D-order diversity.

that is appropriate for coherent demodulation and detection requires that the receiver estimate and correct for the different phase offsets on each of the D received signals after demodulation. Then, the phase-corrected signals at the outputs of the D demodulators are summed and fed to the detector. This type of signal combining is called *equal-gain combining*. If, in addition, the received signal power level is estimated for each of the D received signals, and the phase-corrected demodulator outputs are weighted in direct proportion of the received signal strength (square-root of power level) and then fed to the detector, the combiner is called a *maximal-ratio combiner*. On the other hand, if orthogonal signals are used for transmitting the information through D independently fading channels, the receiver may employ noncoherent demodulation. In such a case the outputs from the D demodulators may be squared, summed, and then fed to detector. This combiner is called a *square-law combiner*.

All these types of combining methods lead to performance characteristics that result in a probability of error which behaves as $K_D/\bar{\rho}^D$ where K_D is a constant that depends on D, and $\bar{\rho}$ is the average SNR/diversity channel. Thus, we achieve an exponential decrease in the error probability. Without providing a detailed derivation, we simply state that for antipodal signals with maximal ratio combining, the probability

of error has the general form

$$P_b \approx \frac{K_D}{(4\bar{\rho})^D}, \quad \bar{\rho}_b \gg 1 \tag{10.1.37}$$

where K_D is defined as

$$K_D = \frac{(2D-1)!}{D!(D-1)!} \tag{10.1.38}$$

For binary orthogonal signals with square-law combining, the probability of error has the asymptotic form

$$P_b \approx \frac{K_D}{\bar{\rho}^D}, \quad \bar{\rho} \gg 1 \tag{10.1.39}$$

Finally, for binary DPSK with equal gain combining, the probability of error has the asymptotic form

$$P_b \approx \frac{K_D}{(2\bar{\rho})^D}, \quad \bar{\rho} \gg 1 \tag{10.1.40}$$

These error probabilities are plotted in Figure 10.10 for $D = 1, 2, 4$ as a function of the SNR/bit $\bar{\rho}_b = D\bar{\rho}$. It is apparent that a large reduction in SNR/bit is achieved in having $D = 2$ (dual diversity) compared to no diversity. A further reduction in SNR is achieved by increasing the order of diversity to $D = 4$, although the additional gain from $D = 2$ to $D = 4$ is smaller than going from $D = 1$ to $D = 2$. Beyond $D = 4$, the additional reduction in SNR is significantly smaller.

These performance results illustrate that efficient use of transmitter power in a Rayleigh fading channel can be achieved by using some form of diversity to provide the receiver with several independently fading signals all carrying the same information. The types of diversity that we described (time or frequency) are a form of channel coding usually called *repetition coding* where the code rate is $1/D$. Thus, if each information bit is transmitted twice in two widely separated time slots or in two widely separated frequency bands, we have a dual diversity ($D = 2$) system obtained with a repetition code of rate $R_c = 1/2$. However, in general, a nontrivial code of rate $1/2$ will yield significantly better performance if the coded bits are interleaved prior to transmission, as described in Chapter 9, so that the fading on each bit of a code word is statistically independent. In particular, a binary linear (n, k) code with minimum Hamming distance $d_{\min}$ results in a performance that is equivalent to a repetition code of diversity $d_{\min}$ when soft-decision decoding is used and $d_{\min}/2$ when hard-decision decoding is used. Therefore, for any code rate $1/D$, a nontrivial code can be selected which has a minimum Hamming distance $d_{\min} > D$ and, thus, provides a larger order of diversity than the corresponding repetition code of the same rate.

Example 10.1.7

Compare the error-rate performance of binary orthogonal FSK with dual diversity with the performance of the rate $1/2$, $d_{\min} = 8$, extended Golay (24, 12) code in which binary

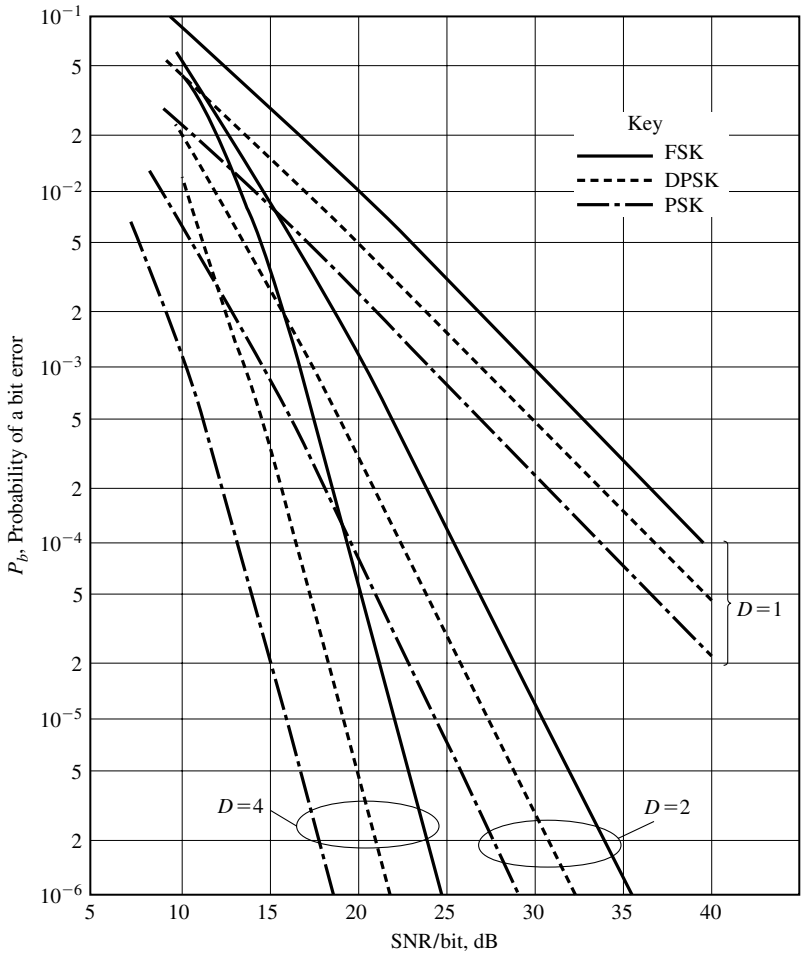

Figure 10.10 Performance of binary signals with diversity.

orthogonal FSK is used to transmit each code bit. The channel is a Rayleigh fading channel and the receiver employs square-law combining and detection for both types of signals.

Solution Let us assume that signal diversity is obtained by interleaving the coded bits so that we have statistically independent fading among the coded bits for both signals. Note that, the repetition code and the Golay (24, 12) code, are rate 1/2 codes. For the repetition code, we combine the square-law detected FSK signals in the two (interleaved) signal intervals. Hence, if a zero is transmitted, the two metrics at the combiner output corresponding to a 0 and a 1, respectively, are

$$r_0 = |\alpha_1\sqrt{\mathcal{E}}\,e^{j\phi_1} + n_{01}|^2 + |\alpha_2\sqrt{\mathcal{E}}\,e^{j\phi_2} + n_{02}|^2$$

$$r_1 = |n_{11}|^2 + |n_{12}|^2$$

where the $\{n_{ij}\}$ are statistically i.i.d. complex-valued, zero-mean Gaussian random variables. The probability of error is simply the probability that $r_2 > r_1$, and is given as

$$P_b \approx \frac{K_2}{\bar{\rho}^2} = \frac{3}{(\bar{\rho}_b/2)^2}, \qquad \bar{\rho} \gg 1$$

where the average SNR/bit is $\bar{\rho}_b$. In the Golay code, there are $2^{12} = 4096$ code words, so that there are 4096 metrics at the output of the square-law combiner. To compute the probability of error, we may assume that the all-zero code word is transmitted. Then the combiner output corresponding to the all-zero code word is the metric

$$r_0 = \sum_{k=1}^{24} |\alpha_k \sqrt{\mathcal{E}}\, e^{j\phi_k} + n_{0k}|^2$$

In the Golay (24, 12) code, there are 759 code words having distance $d_{\min} = 8$ from the all-zero code words. Since any one of these code words differs in 8 bits from the all-zero code word and is identical with the all-zero word in 16 bits, the combiner output corresponding to any one of these 759 code words is statistically equivalent to the metric

$$r_1 = \sum_{k=1}^{8} |n_{1k}|^2 + \sum_{k=9}^{24} |\alpha_k \sqrt{\mathcal{E}}\, e^{j\phi_k} + n_{0k}|^2$$

Hence, the difference between r_0 and r_1 is

$$r_0 - r_1 = \sum_{k=1}^{8} [|\alpha_k \sqrt{\mathcal{E}}\, e^{j\phi_k} + n_{0k}|^2 - |n_{1k}|^2]$$

We observe that this difference is a function of summing the received signal over eight independently fading bits and, consequently, the code provides an order of diversity of $d_{\min} = 8$. This implies that the error rate for the Golay code decays inversely as $\bar{\rho}^8$; i.e., the bit-error rate is

$$P_2 \approx \frac{K}{\bar{\rho}^8} = \frac{K}{(\bar{\rho}_b/2)^8}$$

where K is a constant independent of SNR, $\bar{\rho}_b = \bar{\rho}/R_c$ is the SNR/bit and R_c is the code rate. Figure 10.11 illustrates the error probability for the two types of signals. Note that the Golay code outperforms the repetition code by over 8 dB at a bit-error probability of 10^{-4}. The difference is even greater at lower error rates. In conclusion, a nontrivial code with interleaving generally provides more signal diversity than a repetition code of the same code rate.

10.1.5 Modulation and Demodulation on Frequency Selective Channels—The RAKE Demodulator

Let us consider the case in which the available channel bandwidth W exceeds the coherence bandwidth B_{cb} of the channel, and we transmit digital information at a symbol rate $1/T$ by modulating a single carrier frequency. We assume that the symbol duration T satisfies the condition $T \ll T_{ct}$. Consequently, the channel characteristics change very slowly in time, so that the channel is slowly fading, but it is frequency selective because $W \gg B_{cb}$. Furthermore, we assume that $T \gg T_m$ so that ISI is negligible.

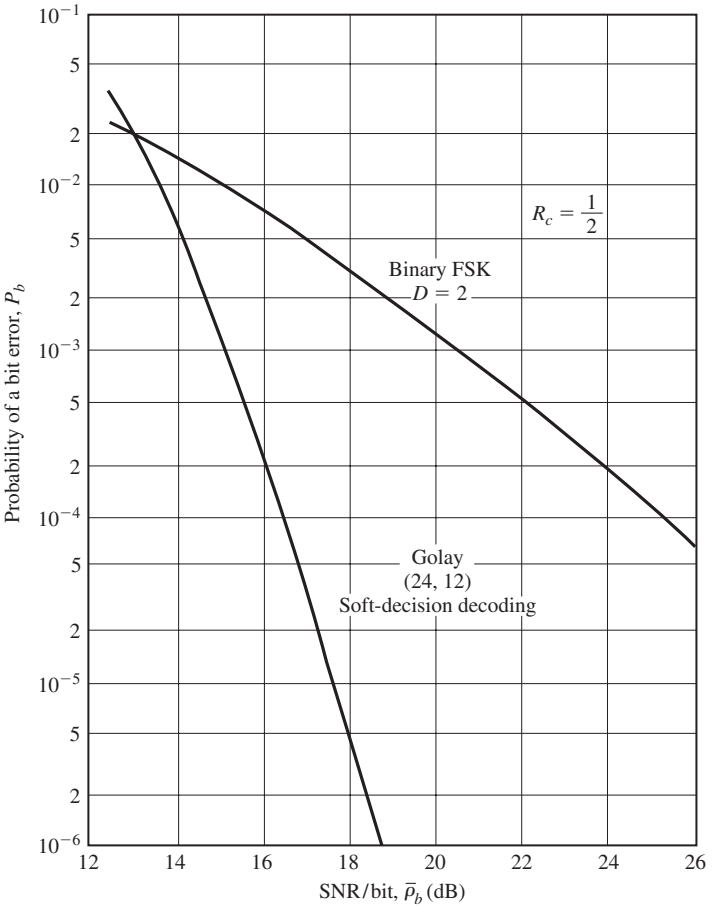

Figure 10.11 Comparison of performance of repetition code with Golay (24, 12) code.

Since W is the bandwidth of the bandpass signal, the bandwidth occupancy of the equivalent lowpass signal is $W/2$. Hence, we employ a band-limited lowpass signal $s(t)$. Using the channel model for the frequency, selective channel shown in Figure 10.4, we may express the received signal as

$$r(t) = \sum_{n=1}^{L} c_n(t)s(t - n/W) + n(t) \tag{10.1.41}$$

where $n(t)$ represents the AWGN. Therefore, the frequency-selective channel provides the receiver with up to L replicas of the transmitted signal, where each signal component is multiplied by a corresponding channel tap weight $c_n(t)$, $n = 1, 2, \ldots, L$. Based on

the slow fading assumption, the channel coefficients are considered as constant over the duration of one or more symbol intervals.

Since there are up to L replicas of the transmitted signal $s(t)$ in $r(t)$, a receiver that processes the received signal in an optimum manner will achieve the performance that is equivalent to that of a communication system with diversity equal to the number of received (resolvable) signal components.

Let us consider binary signaling over the channel. Suppose we have two equal energy signals $s_1(t)$ and $s_2(t)$, which are orthogonal, with a time duration $T \gg T_m$. Since the ISI is negligible, the optimum receiver consists of two correlators or two matched filters that are matched to the received signals. Let us use the correlator structure that is illustrated in Figure 10.12. The received signal is passed through a tapped

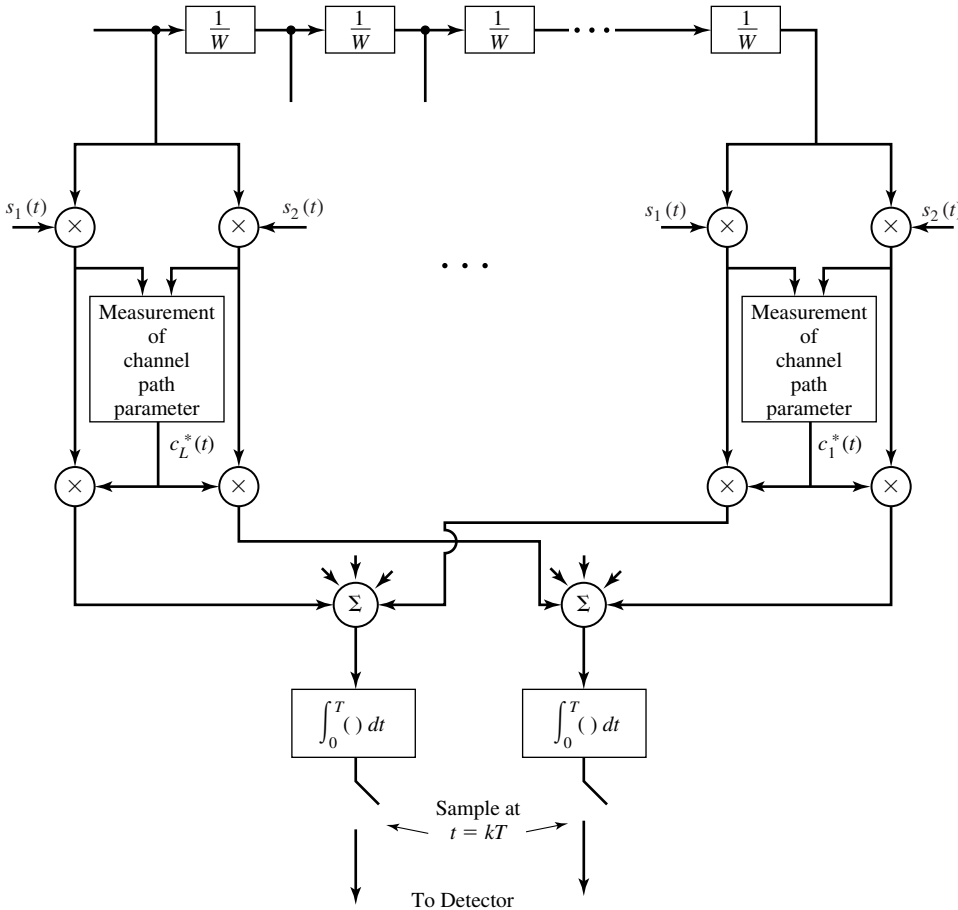

Figure 10.12 RAKE demodulator for signal transmitted through a frequency selective channel.

delay-line filter with tap spacing of $1/W$, as in the channel model. The number of taps is selected to match the total number of resolvable signal components. At each tap, the signal is multiplied with each of the two possible transmitted signals $s_1(t)$ and $s_2(t)$, and, then, each multiplier output is phase corrected and weighted by multiplication with $c_n^*(t)$, $n = 1, 2, \ldots, L$. Then, the corresponding phase-aligned and weighted signal components are integrated over the duration of the symbol interval T and the two integrator outputs are sampled periodically every T seconds. Their outputs are then sent to the detector. Thus, we have crosscorrelated the received signal with each of the two possible transmitted signals at all possible delays introduced by the channel. Note that the multiplication of the signal at each tap with the corresponding tap coefficient $c_n^*(t)$ results in weighting the signal components by the corresponding signal strengths. Hence, the combining of the phase-corrected and weighted signal components corresponds to maximal ratio combining.

In order to perform maximal ratio combining, it is necessary to estimate the channel-tap coefficients $c_n(t)$ from the received signal. Since these coefficients are time varying, it is necessary for the estimator to be adaptive; i.e., to be able to track the time variations.

The demodulator structure shown in Figure 10.12 is called a *RAKE demodulator*. Because this demodulator has equally spaced taps with tap coefficients that essentially collect all the signal components in the received signal, its operation has been likened to that of an ordinary garden rake.

Assuming that there are L signal components in the received signal, with corresponding signal strengths that are distinct and Rayleigh distributed, the probability of error for binary signals is well approximated as

$$P_b = K_L \prod_{k=1}^{L} \frac{1}{[2\bar{\rho}_k(1-\gamma_r)]} \tag{10.1.42}$$

where $\bar{\rho}_k$ is the average SNR for the kth-signal component; i.e.,

$$\bar{\rho}_k = \frac{\mathcal{E}_b}{N_0} E\left(\alpha_k^2\right) \tag{10.1.43}$$

where $\alpha_k = |c_k|$ is the amplitude of the kth-tap coefficient, $\gamma_r = -1$ for antipodal signals and $\gamma_r = 0$ for orthogonal signals, and K_L is the constant defined in Equation (10.1.38). In the special case where all the signal components have the same strength, the error probability in Equation (10.1.42) reduces to that given by Equation (10.1.37) with $D = L$.

10.1.6 Multiple Antenna Systems and Space-Time Codes

The use of two or more antennas at the receiving terminal of a digital communication system is a commonly employed method for achieving spatial diversity to mitigate the effects of signal fading. Typically, the receiving antennas must be separated by one or more wavelengths to ensure that the received signal undergoes statistically independent fading. Spatial receiver diversity is especially attractive because the signal diversity is achieved without expanding the signal transmission bandwidth.

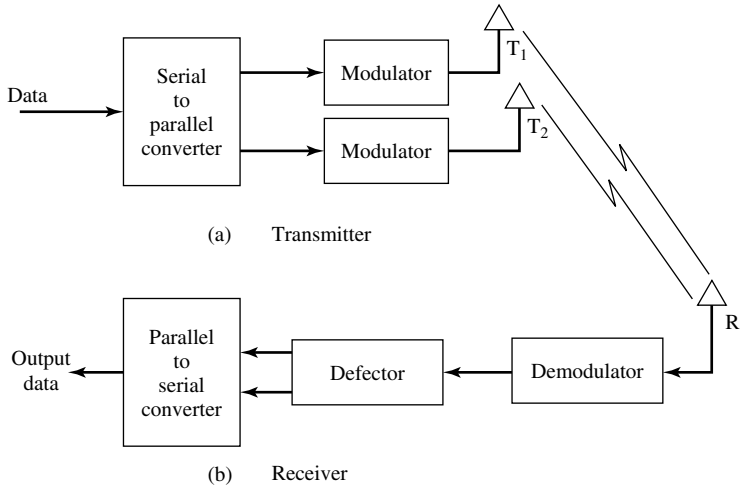

Figure 10.13 Communication system employing two transmit antennas and one receive antenna.

Spatial diversity can also be achieved by using multiple antennas at the transmitter terminal of the communication system. For example, suppose we employ two antennas at the transmitter (T1 and T2) and one antenna at the receiver, as shown in Figure 10.13. Two information symbols are transmitted in each symbol interval. In the kth-symbol interval, antenna T1 transmits the signal $s_{1k}g_T(t)$ and antenna T2 simultaneously transmits the signal $s_{2k}g_T(t)$, where $g_T(t)$ is some basic signal pulse and s_{1k} and s_{2k} are symbols selected from some signal constellation; e.g., QAM or PSK. The signal at the receiving antenna may be expressed as

$$r(t) = c_1 s_{1k} g_T(t) + c_2 s_{2k} g_T(t) + n(t) \tag{10.1.44}$$

where the fading channel is assumed to be slowly fading and frequency nonselective with complex valued channel coefficients c_1 and c_2, and $n(t)$ denotes the additive noise. The receiver processes the received signal by passing it through a filter matched to $g_T(t)$. Hence, at the sampling instant, the matched-filter output may be expressed as

$$r_k = c_1 s_{1k} + c_2 s_{2k} + n_k \tag{10.1.45}$$

In the following symbol interval, T1 transmits the signal $s_{2k}^* g_T(t)$ and T2 transmits $-s_{1k}^* g_T(t)$ where the asterisk denotes complex conjugate. Hence, the output of the matched filter may be expressed as

$$r_{k+1} = c_1 s_{2k}^* - c_2 s_{1k}^* + n_{k+1} \tag{10.1.46}$$

It is assumed that the receiver has knowledge of the channel coefficients c_1 and c_2, which is obtained by periodically transmitting pilot signals through the channel and measuring the channel coefficients c_1 and c_2. Thus, it is possible for the receiver to recover s_{1k} and s_{2k} and, thus, achieve dual diversity. The recovery of s_{1k} and s_{2k} from

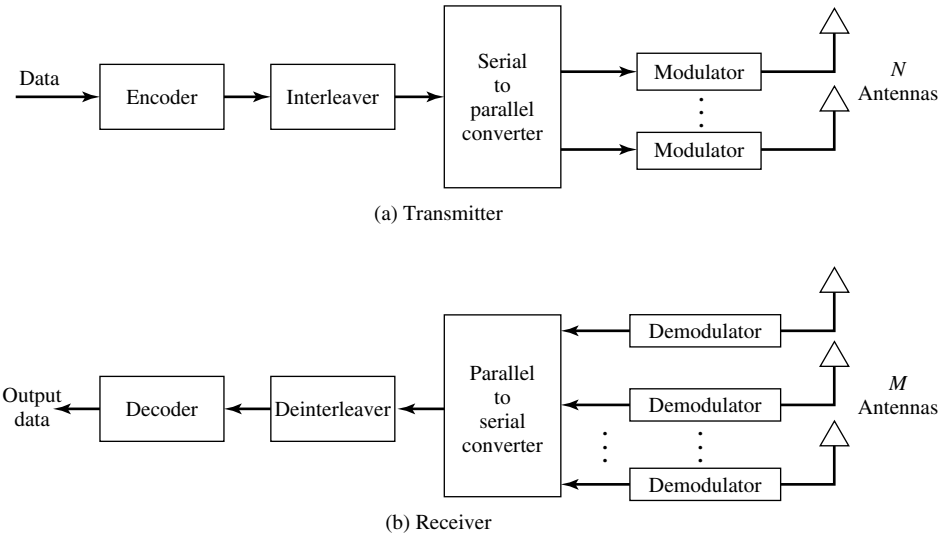

Figure 10.14 A digital communication system with multiple transmit and receive antennas.

r_k and r_{k+1} is left as an exercise for the reader. The scheme for achieving dual transmit diversity is especially suitable when the receiving terminal is a small mobile platform where it may be difficult more than one receiving antenna on the platform.

In addition to providing signal diversity, multiple transmit antennas can be used to create multiple spatial channels for the purpose of increasing the data transmission rate. In particular, suppose that we employ N transmit antennas and M receive antennas, where each of the N transmit antennas is used to transmit a different symbol in every symbol interval. Figure 10.14 illustrates the block diagram of a digital communication system that employs N transmit antennas and N receive antennas. The system shown in this figure includes an encoder and an interleaver at the transmitter and a deinterleaver and a decoder at the receiver. In the system all signals from the N transmit antennas are transmitted synchronously through the common channel. Thus, we achieve an N-fold increase in data rate compared to a system that uses a single transmit antenna. Assuming that the channel is frequency nonselective and slowly fading, so that the channel coefficients can be accurately measured, we can achieve Mth-order spatial diversity by using M receive antennas, where $M \geq N$. Additional diversity, equal to the minimum distance of the code, can be achieved by encoding the data, provided that we employ a sufficiently long interleaver to ensure statistically independent channel fading.

Example 10.1.8

Consider a communication system that employs two transmit and two receive antennas. The encoder implements a rate $1/2$ convolutional code with free distance $d_{\text{free}} = 6$. The interleaver is sufficiently long to assure that successive code symbols are separated in time

by at least the coherence time of the channel. The channel is slowly fading and frequency nonselective. The decoder employs the Viterbi algorithm to recover the data.

1. Express mathematically the signal that is transmitted through the channel by the two antennas, the signal received at each of the received antennas, and the signal at the output of the demodulator (input to the decoder).
2. What is the order of diversity achieved by the receiver if the decoder performs soft-decision decoding?
3. What is the order of diversity achieved by the receiver if the decoder performs hard-decision decoding?

Solution

1. The signal at the input to the channel at the kth-symbol interval is

$$x(t) = s_{1k}g_T(t) + s_{2k}g_T(t), \qquad 0 \le t \le T$$

The signal received at the two receive antennas are

$$r_1(t) = c_{11}s_{1k}g_T(t) + c_{12}s_{2k}g_T(t) + n_1(t)$$
$$r_2(t) = c_{21}s_{1k}g_T(t) + c_{22}s_{2k}g_T(t) + n_2(t)$$

where the $\{c_{ij}\}$ are the channel coefficients, s_{1k} and s_{2k} are the channel symbols and $n_1(t)$ and $n_2(t)$ are the additive noise noise terms at the input to the receiver. The demodulator (matched filter) outputs are

$$r_1 = c_{11}s_{1k} + c_{12}s_{2k} + n_1$$
$$r_2 = c_{21}s_{1k} + c_{22}s_{2k} + n_2$$

These two signals are fed to the decoder.

2. With ideal interleaving, all the coded symbols fade independently so the received signal at each antenna provides a diversity order equal to $d_{\text{free}} = 6$. If the decoder is a soft-decision decoder; the total order of diversity for the two antennas is $2d_{\text{free}} = 12$.
3. With hard-decision decoding, the order of signal diversity from each antenna is $d_{\text{free}}/2$. Hence, the total order of diversity for the two antennas is reduced to $d_{\text{free}} = 6$.

An alternative approach to coding for multiple antenna systems is to employ a new class of codes, called *space-time codes*. A space-time code may be either a block code or a trellis code that is especially designed for multiple transmit and receive antennas to achieve diversity and an increase in data rate.

We consider a trellis code to illustrate the encoding process. A block diagram of the transmitter and the receiver is illustrated in Figure 10.15 for the case of two transmit and receive antennas. We assume that the data is binary and a signal constellation of 2^k signal points is selected. Thus, any k-input data bits are mapped into one of 2^k signal points. As an example, suppose that the modulation is 4-PSK and the encoder is represented by the 4-state trellis shown in Figure 10.16. This trellis generates a rate $\frac{1}{2}$ code, where each input symbol, represented by the possible phase values 0, 1, 2, 3 is encoded into two output symbols, as specified by the trellis code. Each of the two output symbols is passed to (identical) interleavers. The symbol (phase) sequence at the output of each interleaver modulates a basic pulse shape $g_T(t)$ and the

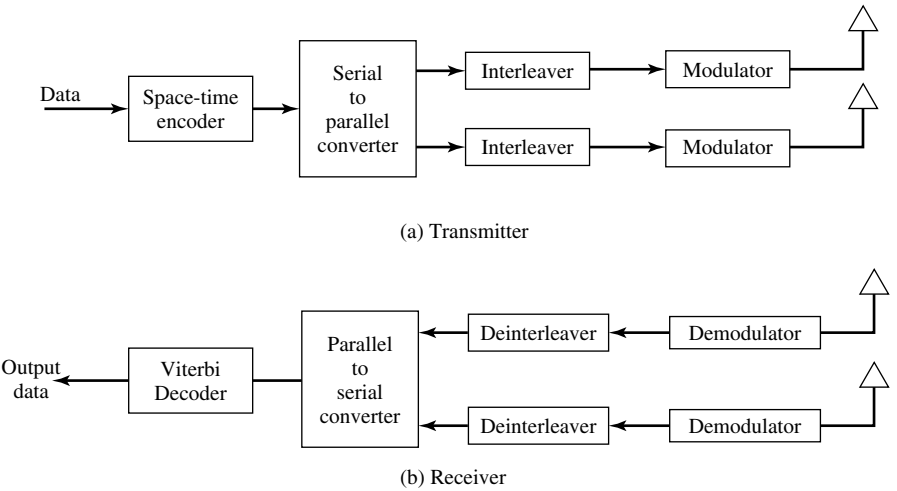

Figure 10.15 Block diagram of communication system employing a space-time code for two transmit and two receive antennas.

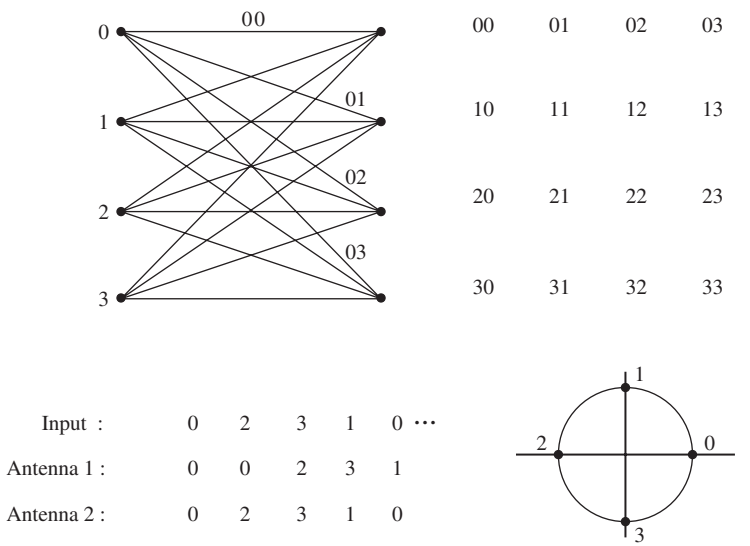

Figure 10.16 4-PSK, 4-state, space-time code.

two symbols are transmitted synchronously through the channel. At the receiver, the signals received at the antennas are passed through matched filters, deinterleaved, and fed to the trellis (Viterbi) decoder. The 4-state trellis code can be shown to provide dual diversity and the use of two antennas at the receiver results in fourth-order diversity for the communication system.

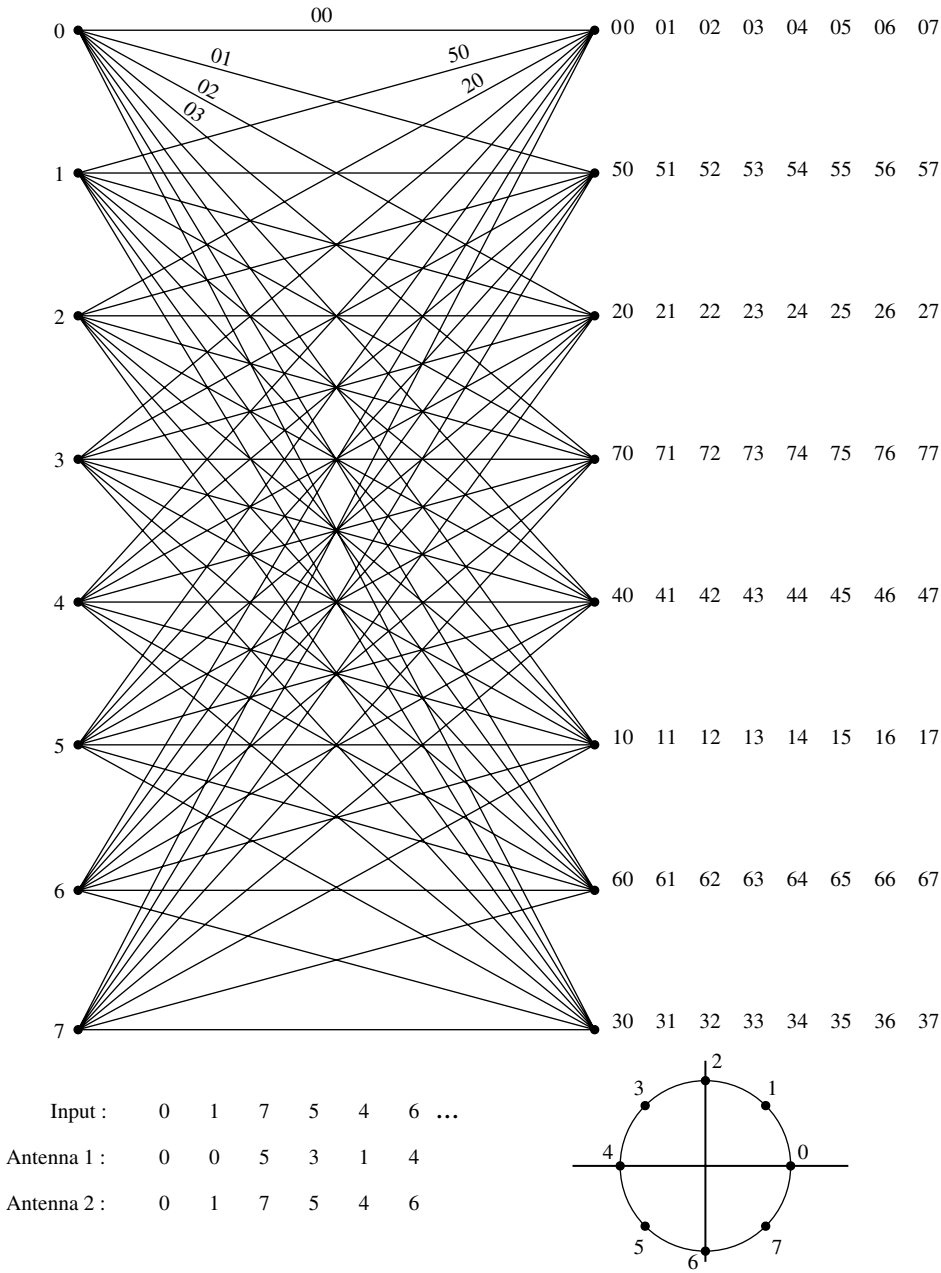

Figure 10.17 8-PSK, 8-state, space-time code.

As a second example, we consider a rate 1/2, 8-state trellis code which is used with 8-PSK modulation, as shown in Figure 10.17. In this case, we transmit 3 bits/symbol, so that the throughput is 50% higher compared with the rate $\frac{1}{2}$, 4-state trellis code. With two transmit and two receive antennas, the code also results in fourth-order diversity.

For the sake of brevity, we will not discuss methods for designing space-time codes. For the interested reader, we cite the papers by Tarokh, et al. (1998, 1999) which describe the design of trellis codes and block codes.

10.2 CONTINUOUS CARRIER-PHASE MODULATION

The radio spectrum is a precious commodity that is shared by many users. For example, in the 900 MHz- and 1800 MHz-frequency bands used for digital cellular communications, the available licenses to use this spectrum are sold by the government licensing authorities—such as the FCC in the U.S.—to the cellular telephone operators, by means of an auction. In other words, the licenses to use certain parts of the spectrum are sold to the highest bidder. Therefore, it is important that the modulation used to transmit information over these radio channels be bandwidth efficient, so that more subscribers can be accommodated in any given frequency band.

In the case of FSK and PSK modulation, the bandwidth of the transmitted signal can be narrowed further by imposing the condition that the carrier phase of the transmitted signal be continuous from one signal interval to the next. This is in contrast to conventional FSK and PSK, where the carrier phase may change instantaneously at the beginning of each symbol interval.

In Sections 10.2.1 and 10.2.2, we describe both continuous-phase FSK and, more generally, continuous-phase modulation. After describing the characteristics of these modulations, we present their spectral characteristics and describe their demodulation and detection. We will observe that the inherent memory provided by the phase continuity of the signal not only results in a narrower spectrum, but it also allows us to employ a demodulator that exploits this memory. We begin by describing continuous-phase FSK.

10.2.1 Continuous-Phase FSK (CPFSK)

Ordinary FSK signals may be generated by having $M = 2^k$ separate oscillators tuned to the desired frequencies $f_c + m\Delta f \equiv f_m$, and selecting one of the M frequencies according to the particular k-bit symbol that is to be transmitted in a signal interval. However, such abrupt switching from one oscillator output to another in successive signaling intervals results in relatively large spectral sidelobes outside of the main spectral band of the signal, which decay slowly with frequency separation. Consequently, this method is wasteful of bandwidth.

To avoid the use of signals having large spectral sidelobes, we may use the information-bearing signal to frequency-modulate a single carrier whose frequency is changed in a continuous manner. The resulting frequency-modulated signal is phase continuous and, hence, it is called *continuous-phase* FSK (CPFSK).

In order to represent a CPFSK signal, we begin with a PAM signal

$$v(t) = \sum_n a_n g_T(t - nT) \tag{10.2.1}$$

where the amplitudes are obtained by mapping k-bit blocks of binary digits from the information sequence into the amplitude levels $\pm 1, \pm 3, \ldots, \pm(M-1)$, and $g_T(t)$ is a rectangular pulse of amplitude $1/2T$ and duration T. The signal $v(t)$ is used to frequency modulate the carrier. Consequently, the frequency-modulated carrier is

$$u(t) = \sqrt{\frac{2\mathcal{E}_s}{T}} \cos\left[2\pi f_c t + 4\pi T f_d \int_{-\infty}^{t} v(\tau)\, d\tau + \phi_0\right] \tag{10.2.2}$$

where f_d is the *peak-frequency deviation* and ϕ_0 is an arbitrary initial phase of the carrier. Note that the instantaneous frequency of the carrier is $f_c + 2T f_d v(t)$.

We observe that, although $v(t)$ contains discontinuities, the integral of $v(t)$ is continuous. We may denote the phase of the carrier as

$$\theta(t; \mathbf{a}) = 4\pi T f_d \int_{-\infty}^{t} v(\tau)\, d\tau \tag{10.2.3}$$

where $\mathbf{a}$ denotes the sequence of signal amplitudes. Since $\theta(t; \mathbf{a})$ is a continuous function of t, we have a continuous-phase signal.

The phase of the carrier in the interval, $nT \le t \le (n+1)T$, is determined by the integral in Equation (10.2.3). Thus,

$$\begin{aligned}\theta(t; \mathbf{a}) &= 2\pi f_d T \sum_{k=-\infty}^{n-1} a_k + 2\pi(t - nT) f_d a_n \\ &= \theta_n + 2\pi h a_n q(t - nT)\end{aligned} \tag{10.2.4}$$

where, h, θ_n and $q(t)$ are defined as

$$h = 2 f_d T \tag{10.2.5}$$

$$\theta_n = \pi h \sum_{k=-\infty}^{n-1} a_k \tag{10.2.6}$$

$$q(t) = \begin{cases} 0, & t < 0 \\ t/2T, & 0 \le t \le T \\ \frac{1}{2}, & t > T \end{cases} \tag{10.2.7}$$

The parameter h is called the *modulation index*. We observe that θ_n represents the phase accumulation (memory) from all symbols up to time $(n-1)T$. The signal $q(t)$ is simply the integral of the rectangular pulse, as illustrated in Figure 10.18.

It is instructive to sketch the set of all phase trajectories $\theta(t; \mathbf{a})$ generated by all possible values of the information sequence $\{a_n\}$. For example, with binary symbols, $a_n = \pm 1$, the set of phase trajectories beginning at time $t = 0$ are shown in Figure 10.19.

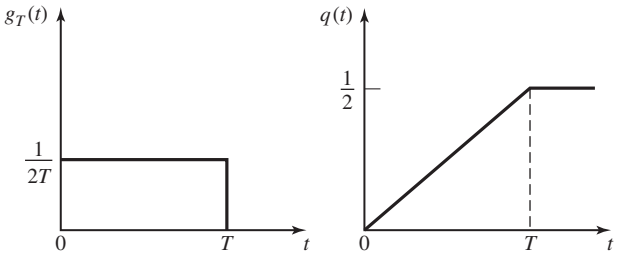

Figure 10.18 The signal pulse $g_T(t)$ and its integral $q(t)$.

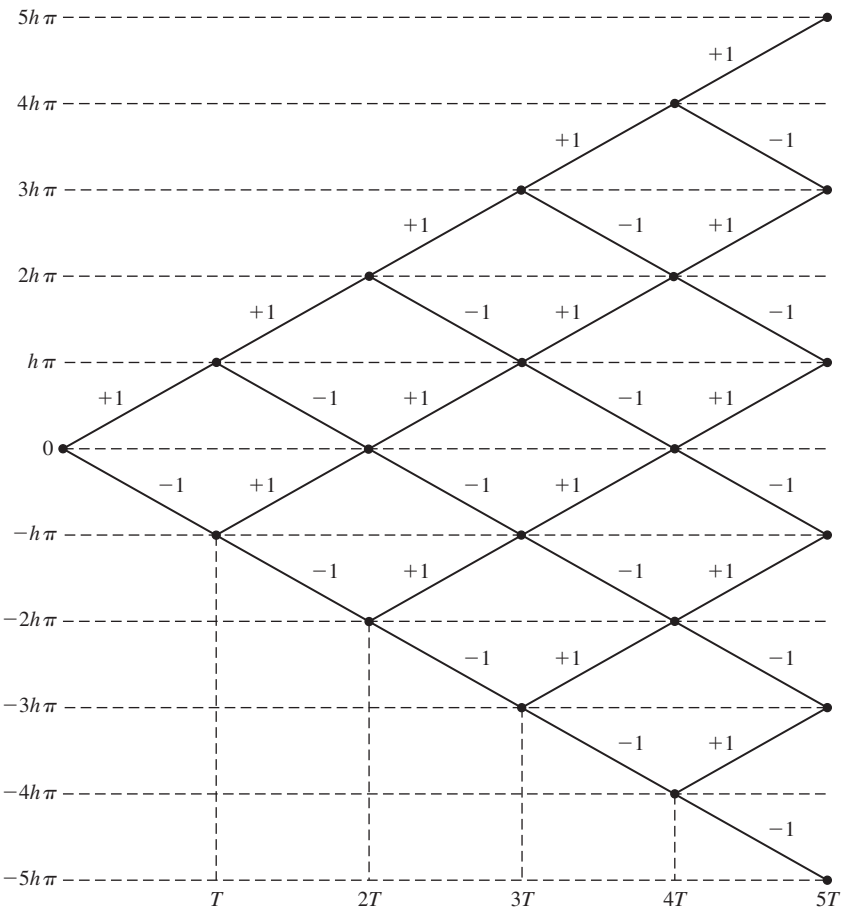

Figure 10.19 Phase trajectory for binary CPFSK.

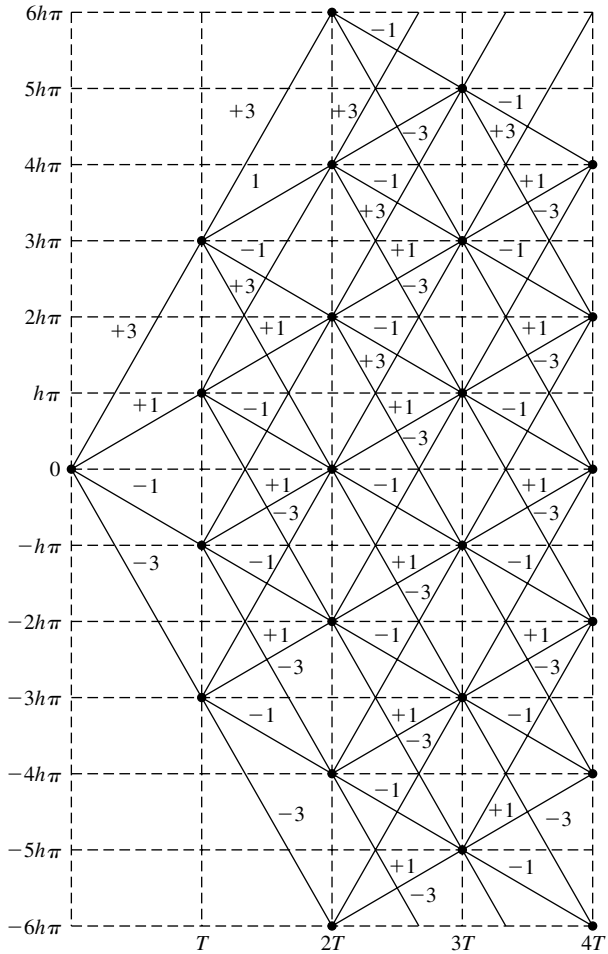

Figure 10.20 Phase trajectory for quaternary CPFSK.

For comparison, the phase trajectories for quaternary CPFSK ($a_n = \pm 1, \pm 3$) are illustrated in Figure 10.20. These phase diagrams are called *phase trees*. We observe that the phase trees are piecewise linear as a consequence of the fact that the pulse $g_T(t)$ is rectangular. Smoother phase trajectories and phase trees may be obtained by using pulses that do not contain discontinuities.

The phase trees shown in these figures grow with time. However, the phase of the carrier is unique only in the range $\theta = 0$ to $\theta = 2\pi$, or equivalently, from $\theta = -\pi$ to $\theta = \pi$. When the phase trajectories are plotted modulo 2π, say in the range $(-\pi, \pi)$, the phase tree collapses into a structure called a *phase trellis*. One way to view the phase trellis as a function of time is to plot the two quadrature components $x_c(t; \mathbf{a}) = \cos\theta(t; \mathbf{a})$ and $x_s(t; \mathbf{a}) = \sin\theta(t; \mathbf{a})$ as (x, y) coordinates and to let time vary in a third dimension.

Since $x_c^2 + x_s^2 = 1$ at any time instant, the three-dimensional plot generated by $x_c(t; \mathbf{a})$ and $x_s(t; \mathbf{a})$ appears as a trajectory on the surface of a cylinder of unit radius.

Simpler representations for the phase trajectories can be obtained by displaying only the terminal values of the signal phase at the time instants $t = nT$. In this case, we restrict the modulation index h to be rational. In particular, let us assume that $h = m/p$, where m and p are relatively prime integers. Then, at the time instants $t = nT$, the terminal phase states for m even are

$$\Theta_s = \left\{0, \quad \frac{\pi m}{p}, \quad \frac{2\pi m}{p}, \ldots, \frac{(p-1)\pi m}{p}\right\} \tag{10.2.8}$$

and for m odd are

$$\Theta_s = \left\{0, \quad \frac{\pi m}{p}, \quad \frac{2\pi m}{p}, \ldots, \frac{(2p-1)\pi m}{p}\right\} \tag{10.2.9}$$

Hence, there are p terminal phase states when m is even and $2p$ terminal phase states when m is odd. For example, binary CPFSK with $h = 1/2$ has four terminal phase states. The *state trellis* for this signal is illustrated in Figure 10.21. We emphasize that the phase transitions from one state to another are not true phase trajectories. They represent phase transitions to the terminal states at the time instants $t = nT$.

An alternative representation to the state trellis is the *state diagram,* which also illustrates the state transitions at the time instants $t = nT$. This is an even more compact representation of the CPFSK signal. Only the possible terminal phase states and their transitions are displayed in the state diagram. Time does not appear explicitly as a variable. For example, the state diagram for the CPFSK signal with $h = 1/2$ is shown in Figure 10.22.

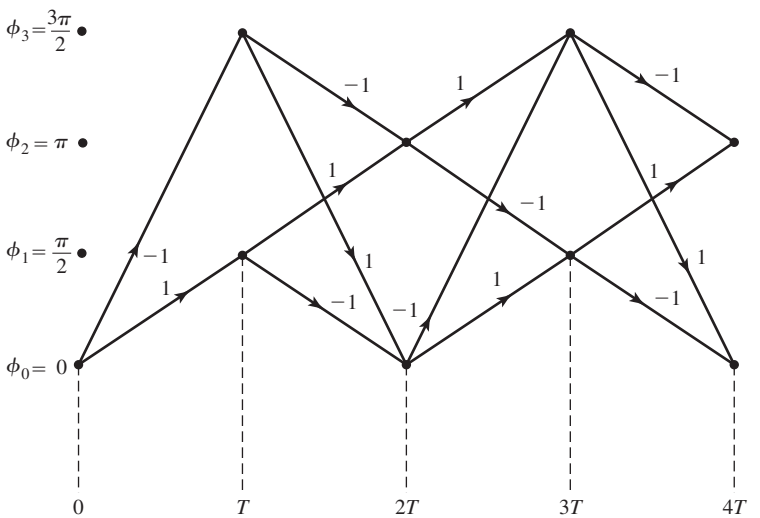

Figure 10.21 State trellis for binary CPFSK with $h = 1/2$.

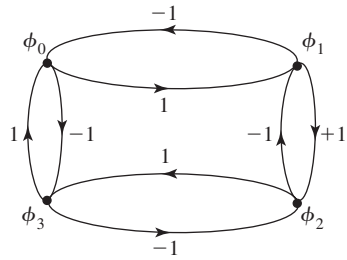

Figure 10.22 State diagram for binary CPFSK with $h = 1/2$.

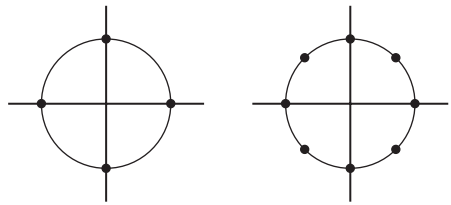

Figure 10.23 Signal-space diagrams for binary FSK with (a) $h = 1/2$ and (b) $h = 1/4$.

We should emphasize that a CPFSK signal cannot be represented by discrete points in signal space as in the case of PAM, PSK, and QAM, because the phase of the carrier is time-variant. Instead, the constant amplitude CPFSK signal may be represented in two-dimensional space by a circle, where points on the circle represent the combined amplitude and phase trajectory of the carrier as a function of time. For example, Figure 10.23 illustrates the signal space diagrams for binary CPFSK with $h = 1/2$ and $h = 1/4$. The four dots at $\theta = 0, \pi/2, \pi, 3\pi/2$ and $\theta = 0, \pm\pi/4, \pm\pi/2, \pm 3\pi/M, \pi$ for $h = 1/2$ and $h = 1/4$, respectively, represent the terminal phase states previously shown in the state diagram.

Minimum-Shift Keying (MSK). MSK is a special form of binary CPFSK in which the modulation index $h = 1/2$. Thus, the phase of the carrier for the MSK signal is

$$\begin{aligned}\theta(t; \mathbf{a}) &= \frac{\pi}{2} \sum_{k=-\infty}^{n-1} a_k + \pi a_n q(t - nT_b) \\ &= \theta_n + \frac{\pi}{2}\left(\frac{t - nT_b}{T_b}\right) a_n, \quad nT_b \le t \le (n+1)T_b \end{aligned} \tag{10.2.10}$$

which follows from Equation (10.2.4). The corresponding carrier-modulated signal is

$$\begin{aligned} u(t) &= \sqrt{\frac{2\mathcal{E}_b}{T_b}} \cos[2\pi f_c t + \theta_n + \pi(t - nT_b)a_n/2T_b] \\ &= \sqrt{\frac{2\mathcal{E}_b}{T_b}} \cos\left[2\pi\left(f_c + \frac{1}{4T_b}a_n\right)t - \frac{n\pi}{2}a_n + \theta_n\right] \end{aligned} \tag{10.2.11}$$

The expression in Equation (10.2.11) indicates that the MSK (binary CPFSK) signal is basically a sinusoid consisting of one of two possible frequencies in the interval $nT_b \le t \le (n+1)T_b$, namely,

$$\begin{aligned} f_1 &= f_c - \frac{1}{4T_b} \\ f_2 &= f_c + \frac{1}{4T_b} \end{aligned} \tag{10.2.12}$$

Hence, the two sinusoidal signals may be expressed as

$$u_i(t) = \sqrt{\frac{2\mathcal{E}_b}{T_b}} \cos\left[2\pi f_i t + \theta_n + \frac{n\pi}{2}(-1)^{i-1}\right], \qquad i = 1, 2 \tag{10.2.13}$$

The frequency separation is $\Delta f = f_2 - f_1 = 1/2T_b$. Recall that this is the minimum-frequency separation for orthogonality of the two sinusoids, provided the signals are detected coherently. This explains why binary CPFSK with $h = 1/2$ is called *minimum-shift keying* (MSK). Note that the phase of the carrier in the nth signaling interval is the phase state of the signal that results in phase continuity between adjacent intervals.

It is interesting to demonstrate that MSK is also a form of four-phase PSK. To prove this point, let us begin with a four-phase PSK signal which has the form

$$\begin{aligned} u(t) = \sqrt{\frac{2\mathcal{E}_b}{T_b}} \Bigg\{ &\left[\sum_{n=-\infty}^{\infty} a_{2n} g_T(t - 2nT_b)\right] \cos 2\pi f_c t \\ &+ \left[\sum_{n=-\infty}^{\infty} a_{2n+1} g_T(t - 2nT_b - T_b)\right] \sin 2\pi f_c t \Bigg\} \end{aligned} \tag{10.2.14}$$

where $g_T(t)$ is a sinusoidal pulse defined as

$$g_T(t) = \begin{cases} \sin \frac{\pi t}{2T_b}, & 0 \le t \le 2T_b \\ 0, & \text{otherwise} \end{cases} \tag{10.2.15}$$

and illustrated in Figure 10.24. First, we observe that the four-phase PSK signal consists of two quadrature carriers, $\cos 2\pi f_c t$ and $\sin 2\pi f_c t$, which are amplitude modulated at a rate of one bit/$2T_b$ interval. The even-numbered information bits $\{a_{2n}\}$ are transmitted

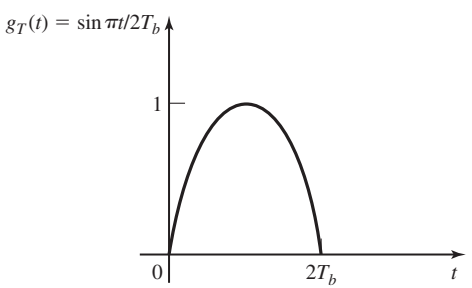

Figure 10.24 Sinusoidal pulse shape.

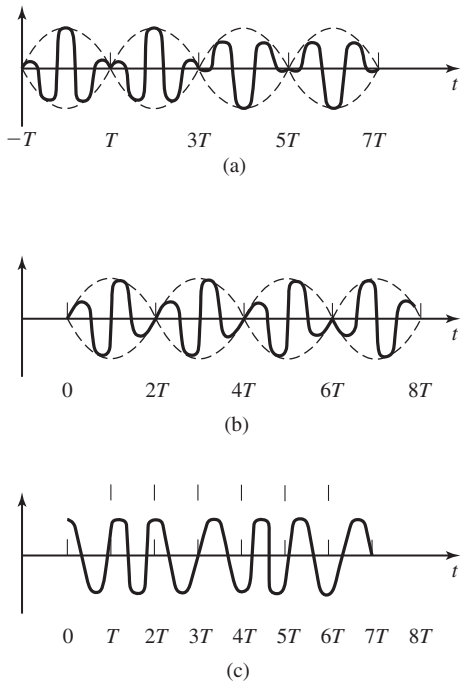

Figure 10.25 Representation of MSK signal as a form of two staggered binary PSK signals, each with a sinusoidal envelope. (a) In-phase signal components, (b) quadrature signal component, and (c) MSK signal $(a + b)$.

by modulating the cosine carrier, while the odd-numbered information bits $\{a_{2n+1}\}$ are transmitted by amplitude modulating the sine carrier. Note that the modulation of the two quadrature carriers is staggered in time by T_b and that the transmission rate for each carrier is $1/2T_b$. This type of four-phase modulation is called *offset quadrature PSK* (OQPSK) or *staggered quadrature PSK* (SQPSK).

Figure 10.25 illustrates the SQPSK signal in terms of the two staggered quadrature-modulated binary PSK signal. The corresponding sum of the two quadrature signals is a constant-amplitude, continuous-phase FSK signal, as shown in Figure 10.25.

It is also interesting to compare the waveforms for MSK with the waveforms for staggered QPSK in which the pulse $g_T(t)$ is rectangular for $0 \le t \le 2T_b$, and with conventional quadrature PSK (QPSK) in which the baseband pulse is rectangular in the interval $0 \le t \le 2T_b$. We emphasize that all three of these modulation methods result in identical data rates. The MSK signal is phase continuous. The SQPSK signal with a rectangular baseband pulse is basically two binary PSK signals for which the phase transitions are staggered in time by T_b seconds. Consequently, this signal contains phase jumps of $\pm 90^\circ$ that may occur as often as every T_b seconds. On the other hand, in conventional QPSK with constant envelope, one or both of the information symbols may cause phase transitions as often as every $2T_b$ seconds. These phase jumps may be $\pm 180^\circ$ or $\pm 90^\circ$. An illustration of these three types of four-phase PSK signals is shown in Figure 10.26.

From the description given above, it is clear that CPFSK is a modulation method with memory because the [illegible] of the continuous-phase carrier

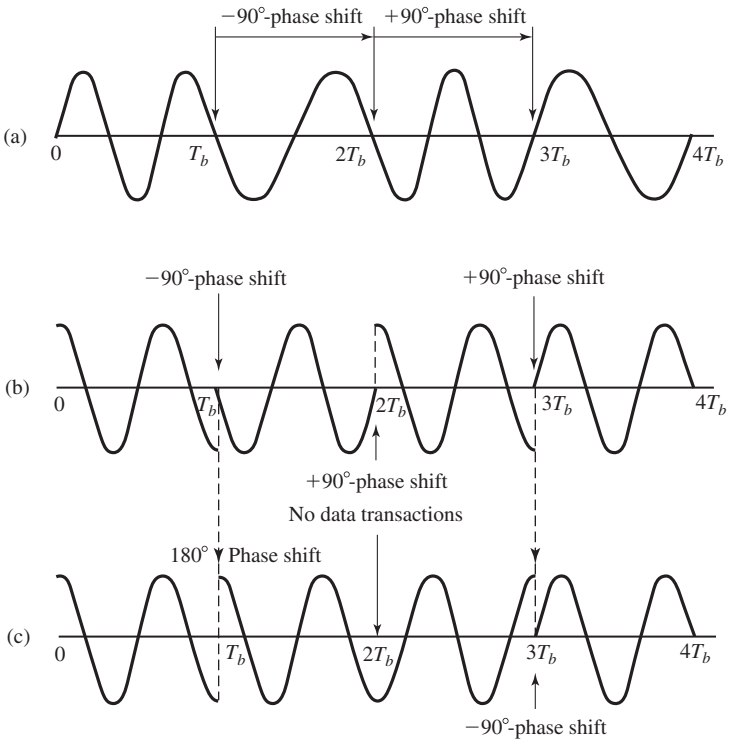

Figure 10.26 Signal waveforms for (a) MSK, (b) offset QPSK (rectangular pulse), and (c) conventional QPSK (rectangular pulse). (From Gronemeyer and McBride; © 1976 IEEE.)

phase from one symbol interval to the next. As a consequence of the continuous phase characteristics, the power spectra of CPFSK signals are narrower than the corresponding FSK signals in which the phase is allowed to change abruptly at the beginning of each symbol interval. The spectral characteristics of CPFSK signals are given in Section 10.2.3. The demodulation and detection of CPFSK are described in Section 10.2.4, which deals with the demodulation and detection of the more general class of continuous-phase modulated signals.

10.2.2 Continuous-Phase Modulation (CPM)

When the phase of the carrier is expressed in the form of Equation (10.2.4), CPFSK becomes a special case of a general class of continuous-phase modulated (CPM) signals in which the carrier phase is

$$\theta(t; \mathbf{a}) = 2\pi \sum_{k=-\infty}^{n} a_k h_k q(t - kT), \qquad nT \le t \le (n+1)T \tag{10.2.16}$$

where $\{a_k\}$ is the sequence of M-ary information symbols with possible values $\pm 1, \pm 3, \ldots, \pm(M-1)$, $\{h_k\}$ is a sequence of modulation indices, and $q(t)$ is some arbitrary normalized waveform. Recall that for CPFSK, $q(t) = t/2T$ for $0 \le t \le T$, $q(t) = 0$ for $t < 0$, and $q(t) = 1/2$ for $t > T$.

When $h_k = h$ for all k, the modulation index is fixed for all symbols. When the modulation index varies from one symbol to another, the CPM signal is called *multi-h*. In such a case the $\{h_k\}$ are usually selected to vary in a cyclic pattern through the set of indices.

The waveform $q(t)$ is the integral of a pulse $g_T(t)$ of arbitrary shape; i.e.,

$$q(t) = \int_0^t g_T(\tau)\, d\tau \tag{10.2.17}$$

If $g_T(t) = 0$ for $t > T$, the CPM signal is called a *full-response CPM signal*. If the signal pulse $g_T(t)$ is nonzero for $t > T$, the modulated signal is called *partial-response CPM*. In Figure 10.27 we illustrate several pulse shapes for $g_T(t)$ and the corresponding $q(t)$. It is apparent that there is an infinite number of CPM signals that can be obtained by selecting different pulse shapes for $g_T(t)$ and by varying the modulation index h and the number of symbols M.

The primary reason for extending the duration of the pulse $g(t)$ beyond the time interval $0 \le t \le T$ is to further reduce the bandwidth of the transmitted signal, as it is demonstrated in Section 10.2.3. We note that, when the duration of the pulse $g_T(t)$ extends over the time interval $0 \le t \le LT$, where $L > 1$, additional memory is introduced in the CPM signals and, hence, the number of phase states increases.

Three popular pulse shapes are given in Table 10.2. LREC denotes a rectangular pulse of duration LT, where L is a positive integer. In this case, $L = 1$ results in a CPFSK signal, with the pulse as shown in Figure 10.27(a). The LREC pulse for $L = 2$ is shown in Figure 10.27(c). LRC denotes a raised cosine pulse of duration LT. The LRC pulses corresponding to $L = 1$ and $L = 2$ are shown in Figure 10.27(b) and (d), respectively.

TABLE 10.2 SOME COMMONLY USED CPM PULSE SHAPES

LREC

$$g(t) = \begin{cases} \frac{1}{2LT} & (0 \le t \le LT) \\ 0, & \text{otherwise} \end{cases}$$

LRC

$$g(t) = \begin{cases} \frac{1}{2LT}\left(1 - \cos\frac{2\pi t}{LT}\right) & (0 \le t \le LT) \\ 0, & \text{otherwise} \end{cases}$$

GMSK

$$g(t) = \left\{ Q\left[2\pi B\left(t - \frac{T}{2}\right)\Big/(\ln 2)^{1/2}\right] - Q\left[2\pi B\left(t + \frac{T}{2}\right)\Big/(\ln 2)^{1/2}\right] \right\}$$

$$Q(t) = \frac{1}{2\pi}\int_t^\infty e^{-x^2/2}\, dx$$

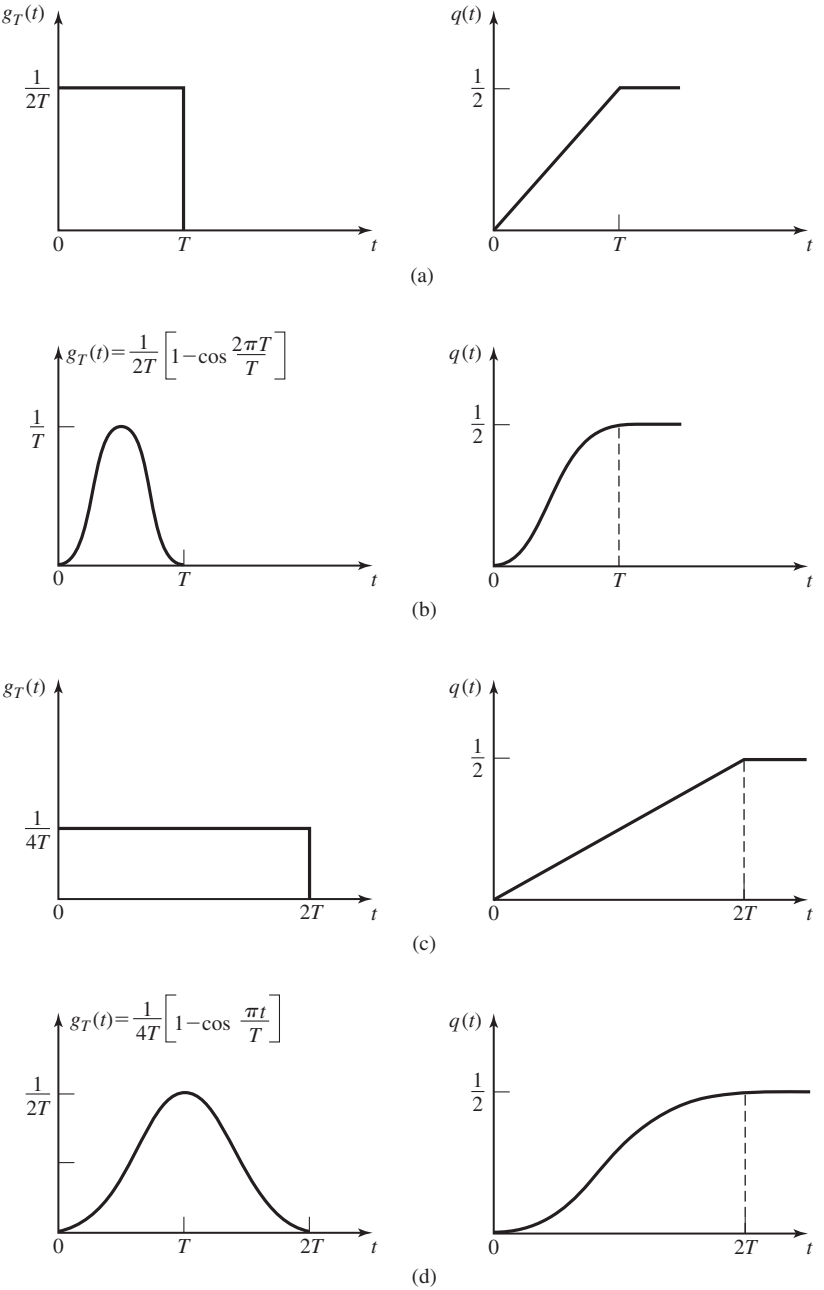

Figure 10.27 Pulse shapes for full-response (a, b) and partial response (c, d) CPM.

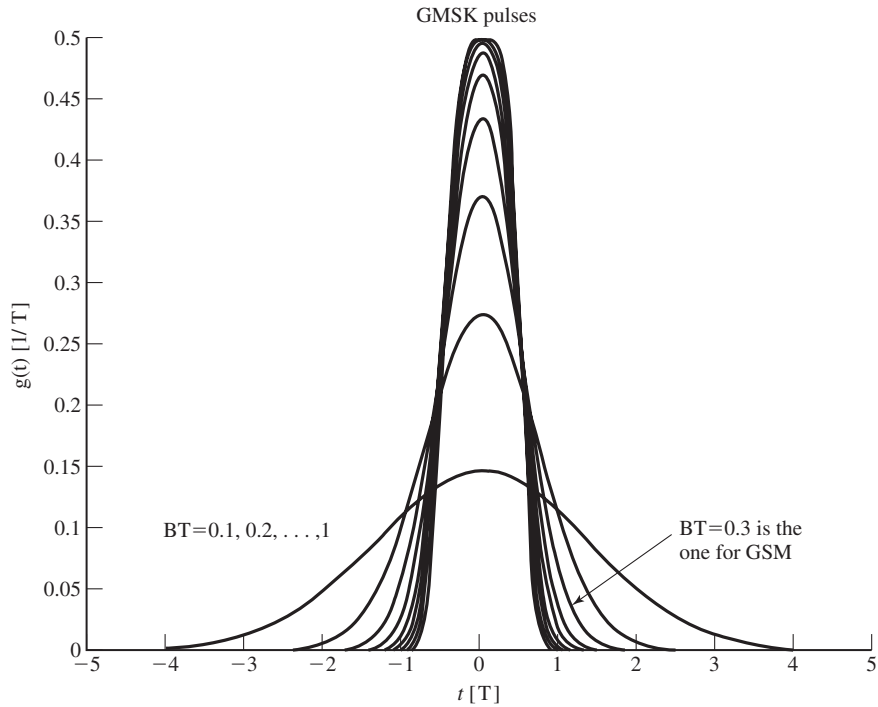

Figure 10.27 (*continued*) (e) GMSK pulse shape.

The third pulse given in Table 10.2 is called a Gaussian minimum-shift keying (GMSK) pulse with bandwidth parameter B, which represents the -3-dB bandwidth of the Gaussian pulse. Figure 10.27(e) illustrates a set of GMSK pulses with time-bandwidth products BT ranging from 0.1–1. We observe that the pulse duration increases as the bandwidth of the pulse decreases, as expected. In practical applications, the pulse is usually truncated to some specified fixed duration. GMSK with $BT = 0.3$. is used in the European digital cellular communication system, called GSM. From Figure 10.27(e) we observe that when $BT = 0.3$, the GMSK pulse may be truncated at $|t| = 1.5T$ with a relatively small error incurred for $t > 1.5T$.

In general, CPM signals cannot be represented by discrete points in signal space as in the case of PAM, PSK, and QAM, because the phase of the carrier is time-variant. As we observed in the case of CPFSK, we may employ phase trajectories (or phase trees) to illustrate the signal phase as a function of time. Alternatively, we may use a state trellis or a state diagram to illustrate the terminal phase states and the phase transitions from one state to another. Finally, as in the case of CPFSK, we may represent a CPM signal in signal space by a circle, where the points on the circle correspond to the combined amplitude and phase of the carrier as a function of time. The terminal phase states are usually identified as discrete points on the circle. For example, Figure 10.28 illustrates the signal space diagrams for binary CPFSK with $h = 1/4, 1/3$, and $2/3$. Note that the

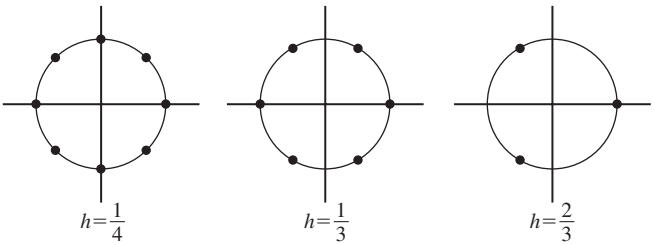

Figure 10.28 Signal-space diagram for CPFSK.

length of the phase trajectory (lengths of the arc) between two terminal phase states increases with an increase in h. An increase in h also results in an increase of the signal bandwidth, as shown in Section 10.2.3.

10.2.3 Spectral Characteristics of CPFSK and CPM Signals

In this section, we consider the spectral characteristics of CPFSK and CPM signals and present some results on their power-spectral density. The derivation of these results may be found in more advanced digital communication textbooks; e.g., Anderson et al. (1986) and Proakis (2001).

A CPM signal may be expressed in the general form

$$\begin{aligned} u(t;\mathbf{a}) &= \sqrt{\frac{2\mathcal{E}_s}{T}}\cos[2\pi f_c t + \theta(t;\mathbf{a})] \\ &= \text{Re}\left\{\sqrt{\frac{2\mathcal{E}_s}{T}}\, e^{j[2\pi f_c t+\theta(t;\mathbf{a})]}\right\} \end{aligned} \tag{10.2.18}$$

where the carrier phase $\theta(t;\mathbf{a})$ is given by Equation (10.2.16). Since the complex exponential $e^{j2\pi f_c t}$ serves as a frequency translation of the complex-valued baseband signal

$$v(t) = \sqrt{\frac{2\mathcal{E}_s}{T}}\, e^{j\theta(t;\mathbf{a})} \tag{10.2.19}$$

it is sufficient to focus our attention on the spectral characteristics of the information-bearing signal $v(t)$.

Unlike the computation of the power-spectral density for linear modulation methods such as PAM, PSK, and QAM, which was relatively straightforward, the computation of the power-density spectrum of a CPM signal is much more tedious and involved. The difficulties are due to the memory in the continuous-phase signal and to the exponential relationship between $v(t)$ and $\theta(t;\mathbf{a})$. Nevertheless, the general procedure used in the derivation for the power-density spectrum of PAM, given in Section 8.2, may be followed.

The general procedure begins with the computation of the autocorrelation function of the random process $V(t)$, denoted as $R_V(t+\tau, t)$. As in the case of linear modulation methods, the random process $V(t)$ is cyclostationary and, hence, the autocorrelation function is periodic with period T; i.e., $R_V(t + T + \tau, t + T) = R_V(t + \tau, t)$. By averaging $R_V(t + \tau, t)$ over a single period, we eliminate the time dependence t and, thus, we obtain the average autocorrelation function

$$\bar{R}_V(\tau) = \frac{1}{T}\int_0^T R_V(t + \tau, t)\, dt \tag{10.2.20}$$

Finally, we compute the Fourier transform of $\bar{R}_V(\tau)$ to obtain the power-spectral density $\mathcal{S}_V(f)$ of the signal. The power-spectral density of the real-valued signal $u(t; \mathbf{a})$ is then found by translating $\mathcal{S}_V(f)$ in frequency by the carrier f_c. Thus, we obtain

$$\mathcal{S}_U(f) = \frac{1}{4}[\mathcal{S}_V(f - f_c) + \mathcal{S}_V(f + f_c)] \tag{10.2.21}$$

In the case of the CPFSK signal, this procedure yields the following expression for the power-spectral density

$$\mathcal{S}_V(f) = T\left[\frac{1}{M}\sum_{n=1}^{M} A_n^2(f) + \frac{2}{M^2}\sum_{n=1}^{M}\sum_{m=1}^{M} B_{nm}(f)A_n(f)A_m(f)\right] \tag{10.2.22}$$

where

$$\begin{aligned} A_n(f) &= \frac{\sin\pi[fT - (2n - 1 - M)h/2]}{\pi[fT - (2n - 1 - M)h/2]} \\ &= \operatorname{sinc}\left(fT - \frac{h(2n - 1 - M)}{2}\right) \end{aligned} \tag{10.2.23}$$

$$B_{nm}(f) = \frac{\cos(2\pi fT - \alpha_{nm}) - \beta\cos\alpha_{nm}}{1 + \beta^2 - 2\beta\cos 2\pi fT} \tag{10.2.24}$$

$$\alpha_{nm} = \pi h(m + n - 1 - M) \tag{10.2.25}$$

$$\beta = \frac{\sin M\pi h}{M\sin\pi h} \tag{10.2.26}$$

The power-spectral density of CPFSK for $M = 2$ is plotted in Figure 10.29 as function of the normalized frequency fT, with the modulation index $h = 2f_dT$ as a parameter. Note that only one-half of the spectrum is shown in these graphs, because the spectrum is symmetric in frequency. The origin $fT = 0$ corresponds to the carrier frequency f_c in the spectrum of the real-valued signal.

These graphs show that the spectrum of the CPFSK signal is relatively smooth and well-confined for $h < 1$. As h approaches unity, the spectra become very peaked and, for $h = 1$, where $|\beta| = 1$, we find that impulses occur at M frequencies. When

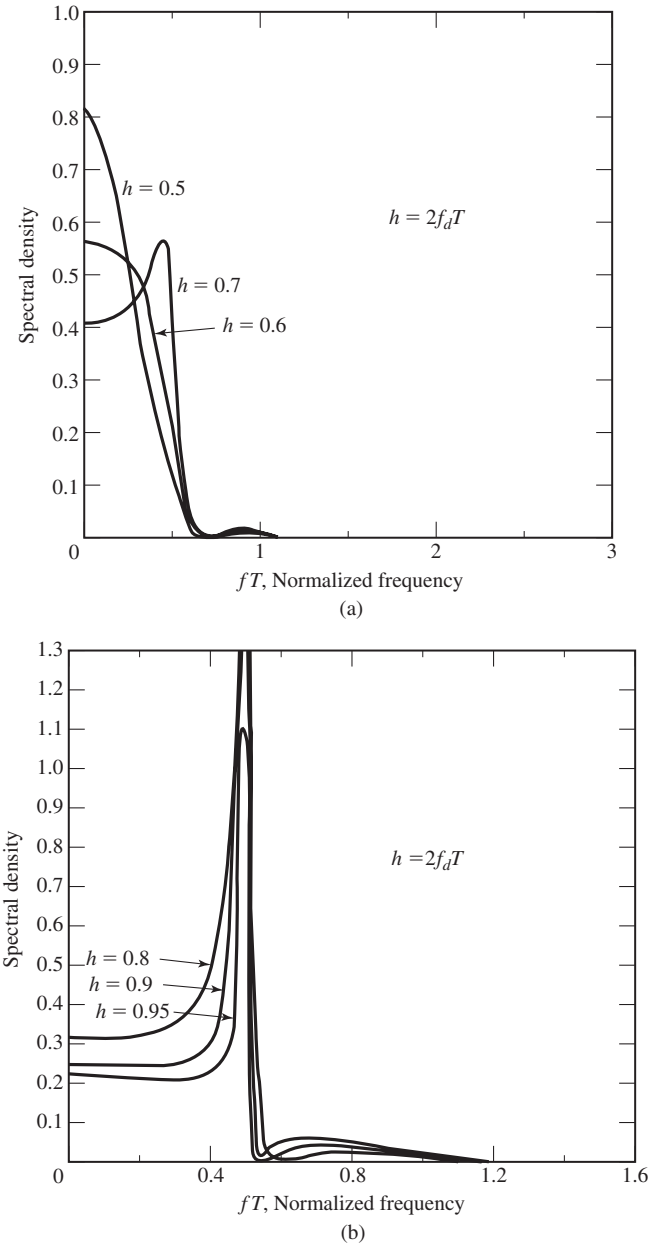

Figure 10.29 Power-density spectrum of binary CPFSK. (From *Digital Communications,* 2nd Ed., by J. G. Proakis; © 1989 McGraw-Hill. Reprinted with permission of the publisher.)

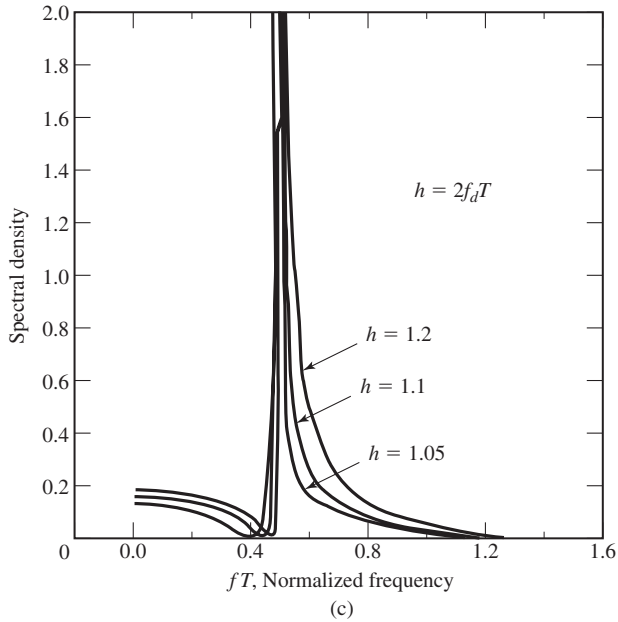

(c)

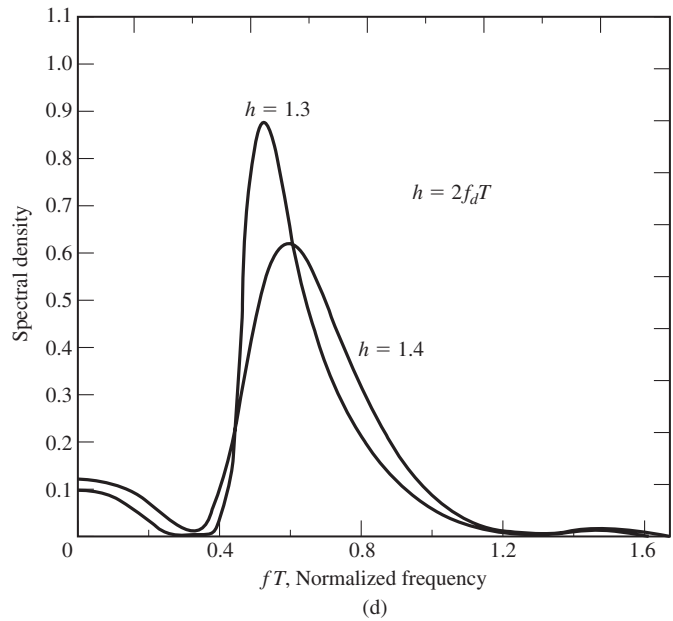

(d)

Figure 10.29 (*continued*)

$h > 1$, the spectrum becomes much broader. In communication systems that employ CPFSK, the modulation index is selected to conserve bandwidth, so that $h < 1$.

The special case of binary CPFSK with $h = 1/2$ (or $f_d = 1/4T_b$) and $\beta = 0$, corresponds to MSK. In this case, the power-spectral density obtained from Equation (10.2.22) through Equation (10.2.26) is

$$\mathcal{S}_V(f) = \frac{32\mathcal{E}_s}{\pi^2}\left[\frac{\cos 2\pi fT}{1 - 16f^2T^2}\right]^2 \tag{10.2.27}$$

In contrast, the power-density spectrum of SQPSK with a rectangular pulse $g_T(t)$ of duration $T = 2T_b$ is

$$\mathcal{S}_V(f) = 4\mathcal{E}_s\left(\frac{\sin 2\pi fT_b}{2\pi fT_b}\right)^2 \tag{10.2.28}$$

The power-density spectra in Equations (10.2.27) and (10.2.28) are illustrated in Figure 10.30. Note that the main lobe of MSK is 50% wider than that of SQPSK. However, the sidelobes of MSK fall off considerably faster. As a consequence, MSK is significantly more bandwidth efficient than SQPSK.

In the more general case of CPM signals, the use of smooth pulses such as raised cosine pulses (LRC) of the form given in Table 10.2, where $L = 1$ for full response and $L > 1$ for partial response, result in smaller bandwidth occupancy and, hence, in greater bandwidth efficiency than the use of rectangular pulses. For example, Figure 10.31

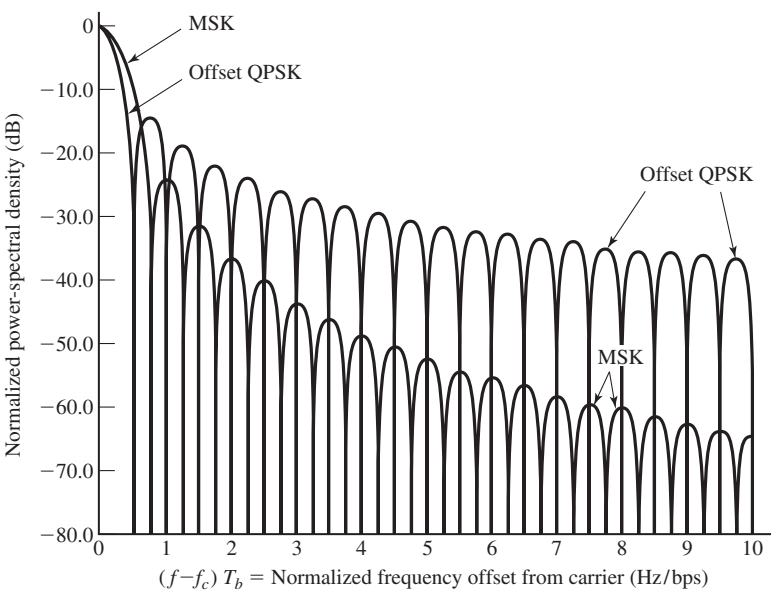

Figure 10.30 Power-density spectra of MSK and QPSK. (From Gronemeyer and McBride; © 1976 IEEE.)

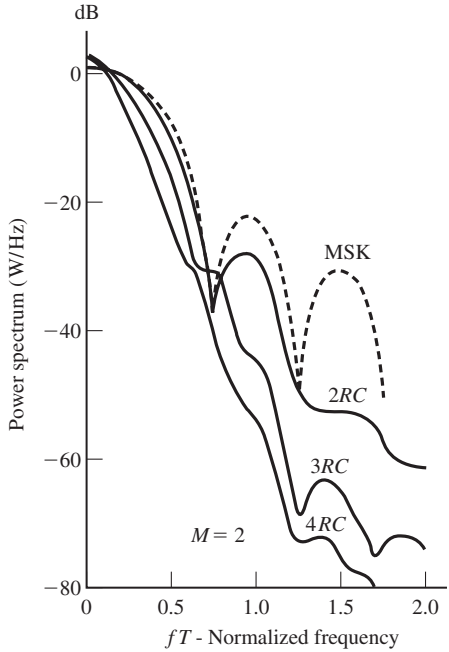

Figure 10.31 Power-spectral density for binary CPM with $h = 1/2$ and different pulse shapes (From Aulin et al.; © 1981 IEEE.)

illustrates the power-spectral density for binary CPM with different partial-response raised cosine (LRC) pulses and $h = 1/2$. For comparison, the spectrum of binary CPFSK with $h = 1/2$ (MSK) is also shown. We note that, as L increases, the pulse $g_T(t)$ becomes smoother and the corresponding spectral occupancy of the signal is reduced.

The effect of varying the modulation index in a CPM signal is illustrated in Figure 10.32 for the case of $M = 4$ and a raised cosine pulse of the form given with $L = 3$. Note that these spectral characteristics are similar to the ones for CPFSK, except that the power spectra for CPM are narrower due to the smoother raised cosine pulse shape.

10.2.4 Demodulation and Detection of CPM Signals

The transmitted CPM signal may be expressed as

$$u(t) = \sqrt{\frac{2\mathcal{E}_s}{T}} \cos[2\pi f_c t + \theta(t; \mathbf{a})] \tag{10.2.29}$$

where $\theta(t; \mathbf{a})$ is the carrier phase. The filtered received signal for an additive Gaussian noise channel is

$$r(t) = u(t) + n(t) \tag{10.2.30}$$

where

$$n(t) = n_c(t) \cos 2\pi f_c t - n_s(t) \sin 2\pi f_c t \tag{10.2.31}$$

The optimum receiver for this signal consists of a correlator followed by a ML

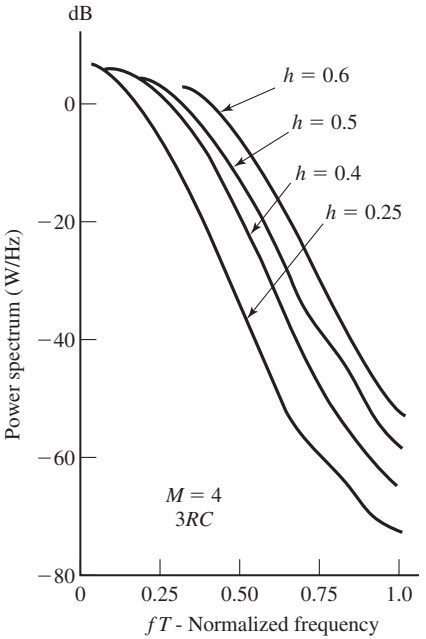

Figure 10.32 Power-spectral density for $M = 4$ CPM for $3RC$ different modulation indices (From Aulin et al.; © 1981 IEEE.)

sequence detector that searches the paths through the state trellis for the minimum Euclidean distance path. The Viterbi algorithm is an efficient method for performing this search. Let us establish the general state trellis structure for CPM and then describe the metric computations.

The carrier phase for a CPM signal having a fixed modulation index h may be expressed as

$$\begin{aligned}\theta(t;\mathbf{a}) &= 2\pi h \sum_{k=-\infty}^{n} a_k q(t-kT), \qquad nT \le t \le (n+1)T \\ &= \pi h \sum_{k=-\infty}^{n-L} a_k + 2\pi h \sum_{k=n-L+1}^{n} a_k q(t-kT) \\ &= \theta_n + \phi(t;\mathbf{a}), \qquad nT \le t \le (n+1)T \end{aligned} \tag{10.2.32}$$

where, by definition,

$$\theta_n = \pi h \sum_{k=-\infty}^{n-L} a_k \tag{10.2.33}$$

$$\phi(t;\mathbf{a}) = 2\pi h \sum_{k=n-L+1}^{n} a_k q(t-kT) \tag{10.2.34}$$

and $q(t) = 0$ for $t < 0$, $q(t) = 1/2$ for $t \geq LT$, and

$$q(t) = \int_0^t g_T(\tau)\, d\tau \tag{10.2.35}$$

where L is a positive integer. The signal pulse $g_T(t) = 0$ for $t < 0$ and $t \geq LT$. For $L = 1$ we have a full response CPM signal and for $L > 1$, we have a partial response CPM signal. Note that θ_n represents the phase of the carrier at $t = nT$ and $\phi(t; \mathbf{a})$ represents the additional phase accumulation in the interval $nT \leq t \leq (n+1)T$.

When h is rational; i.e., $h = m/p$, where m and p are relatively prime integers, the phases of the CPM signal at $t = nT$ may be represented by a trellis. The number of terminal phase states for $L = 1$ is p for m even and $2p$ for m odd, as previously indicated by Equations (10.2.8) and (10.2.9). However, for $L > 1$ we have additional phase states due to the partial-response characteristic of the signal pulse $g_T(t)$. These additional terminal phase states can be determined by expressing the phase $\phi(t; \mathbf{a})$ in Equation (10.2.34) as

$$\phi(t; \mathbf{a}) = 2\pi h \sum_{k=n-L+1}^{n-1} a_k q(t - kT) + 2\pi h a_n q(t - nT) \tag{10.2.36}$$

The first term on the right-hand side of Equation (10.2.36) is a function of the information symbols $(a_{n-1}, a_{n-2}, \ldots, a_{n-L+1})$, which is called the *correlative state vector,* and represents the phase contribution of signal pulses that have not reached their final value. The second term on the right-hand side of Equation (10.2.36) represents the phase contribution due to the most recent symbol a_n. Therefore, the state of the CPM signal at $t = nT$ may be expressed as the combined phase state θ_n and the correlative state vector $(a_{n-1}, a_{n-2}, \ldots, a_{n-L+1})$, which we denote as

$$S_n = \{\theta_n, a_{n-1}, \ldots, a_{n-L+1}\} \tag{10.2.37}$$

for the partial-response signal of length LT. Thus, the number of states is

$$N_s = \begin{cases} pM^{L-1} & m \text{ even} \\ 2pM^{L-1} & m \text{ odd} \end{cases} \tag{10.2.38}$$

when $h = m/p$.

The state transition from S_n to S_{n+1} can be determined by determining the effect of the new symbol a_n in the time interval $nT \leq t \leq (n+1)T$. In general, we have

$$S_{n+1} = \{\theta_{n+1}, a_n, a_{n-1}, \ldots, a_{n-L+2}\} \tag{10.2.39}$$

where

$$\theta_{n+1} = \theta_n + \pi h a_{n-L+1} \tag{10.2.40}$$

Example 10.2.1

Determine the terminal states of a binary signal having a modulation index $h = 3/4$ and a partial response pulse of $L = 2$. Also, sketch the state trellis.

Solution Since $p = 4$, m is odd ($m = 3$) and $M = 2$, we have $N_s = 16$ phase states. The $2p$ phase states corresponding to θ_n are

$$\Theta_s = \left\{0, \quad \pm\frac{\pi}{4}, \quad \pm\frac{\pi}{2}, \quad \pm\frac{3\pi}{4}, \quad \pi\right\}$$

For each of these phase states, there are two states that result from the memory due to the partial response signal. Hence, the sixteen states $S_n = (\theta_n, a_{n-1})$ are

$$(0, +1), (0, -1), (\pi/4, 1), (\pi/4, -1), (-\pi/4, 1), (-\pi/4, -1),$$
$$(\pi/2, 1), (\pi/2, -1), (-\pi/2, 1), (-\pi/2, -1), (3\pi/4, 1), (3\pi/4, -1),$$
$$(-3\pi/4, 1), (-3\pi/4, -1), (\pi, 1), (\pi, -1)$$

Suppose the system is in phase state $\theta_n = 3\pi/4$ and $a_{n-1} = -1$. Then $S_n = (3\pi/4, -1)$ and

$$\begin{aligned}\theta_{n+1} &= \theta_n + \pi h a_{n-1} \\ &= 3\pi/4 + (3\pi/4)(-1) = 0\end{aligned}$$

Hence, $S_{n+1} = (\theta_{n+1}, a_n) = (0, a_n)$. If $a_n = 1$, then $S_{n+1} = (0, 1)$. If $a_n = -1$, then $S_{n+1} = (0, -1)$. The state trellis is illustrated in Figure 10.33. A path through the state trellis corresponding to the data sequence $(1, -1, -1, -1, 1, 1)$ is illustrated in Figure 10.34.

Let us now focus on the demodulation and detection of CPM signals. Since all signal waveforms have the same energy, we may base decisions at the detector on correlation metrics. The crosscorrelation of the received signal $r(t)$ with each of the possible transmitted signals yields the metrics

$$\begin{aligned}C_n(\mathbf{a}, \mathbf{r}) &= \int_{-\infty}^{(n+1)T} r(t)\cos[2\pi f_c t + \theta(t; \mathbf{a})]\,dt \\ &= C_{n-1}(\mathbf{a}, \mathbf{r}) + \int_{nT}^{(n+1)T} r(t)\cos[2\pi f_c t + \theta_n + \phi(t; \mathbf{a})]\,dt \qquad (10.2.41)\end{aligned}$$

In the ML sequence detector, the term $C_{n-1}(\mathbf{a}, \mathbf{r})$ represents the metrics of the surviving sequences up to time nT. The term

$$C_n(\theta_n; \mathbf{a}, \mathbf{r}) = \int_{nT}^{(n+1)T} r(t)\cos[2\pi f_c t + \theta_n + \phi(t; \mathbf{a})]\,dt \qquad (10.2.42)$$

represents the additional increments to the correlation metrics contributed by the received signal in the time interval $nT \le t \le (n+1)T$. We observe that there are M^L possible sequences $\mathbf{a} = (a_n, a_{n-1}, \ldots, a_{n-L+1})$ of symbols and either p or $2p$ possible phase states $\{\theta_n\}$. Therefore, there are either pM^L or $2pM^L$ different values of the correlation metrics $C_n(\theta_n; \mathbf{a}, \mathbf{r})$ computed in each signal interval and each value is used to increment the metrics corresponding to the surviving sequences from the previous

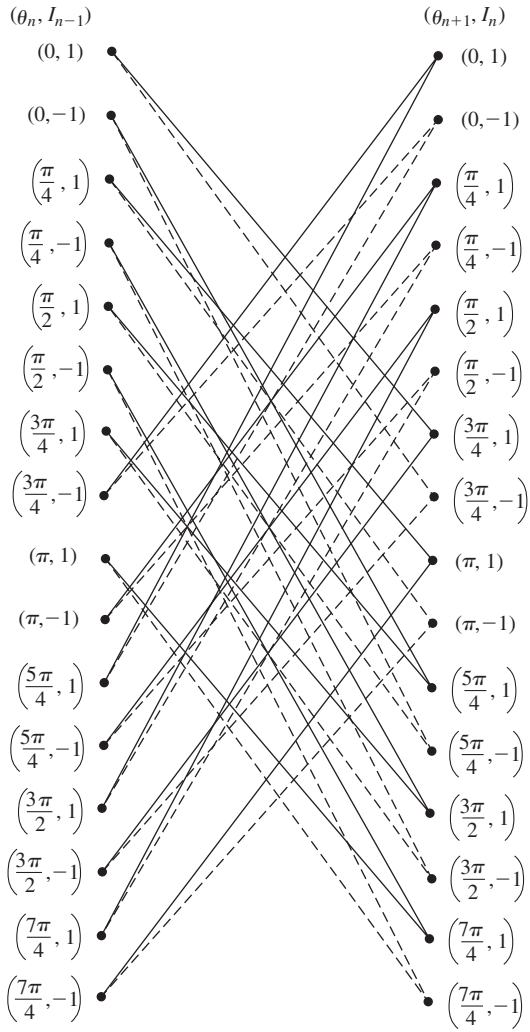

Figure 10.33 State trellis for partial-response ($L = 2$) CPM with $h = 3/4$.

signal interval. A general block diagram that illustrates the computations of $C_n(\theta_n; \mathbf{a}, \mathbf{r})$ for the Viterbi detector is shown in Figure 10.35.

In the ML sequence detector, the number of surviving sequences at each state of the Viterbi search process is either pM^{L-1} or $2pM^{L-1}$. For each surviving sequence, we have M new correlation increments $C_n(\theta_n; \mathbf{a}, \mathbf{r})$ that are added to the existing metrics to yield either pM^L or $2pM^L$ sequences with corresponding metrics. However, this number is then reduced back to either pM^{L-1} or $2pM^{L-1}$ survivors with corresponding metrics by selecting the most probable sequence of the M sequences merging at each node of the trellis and discarding the other $M - 1$ sequences.

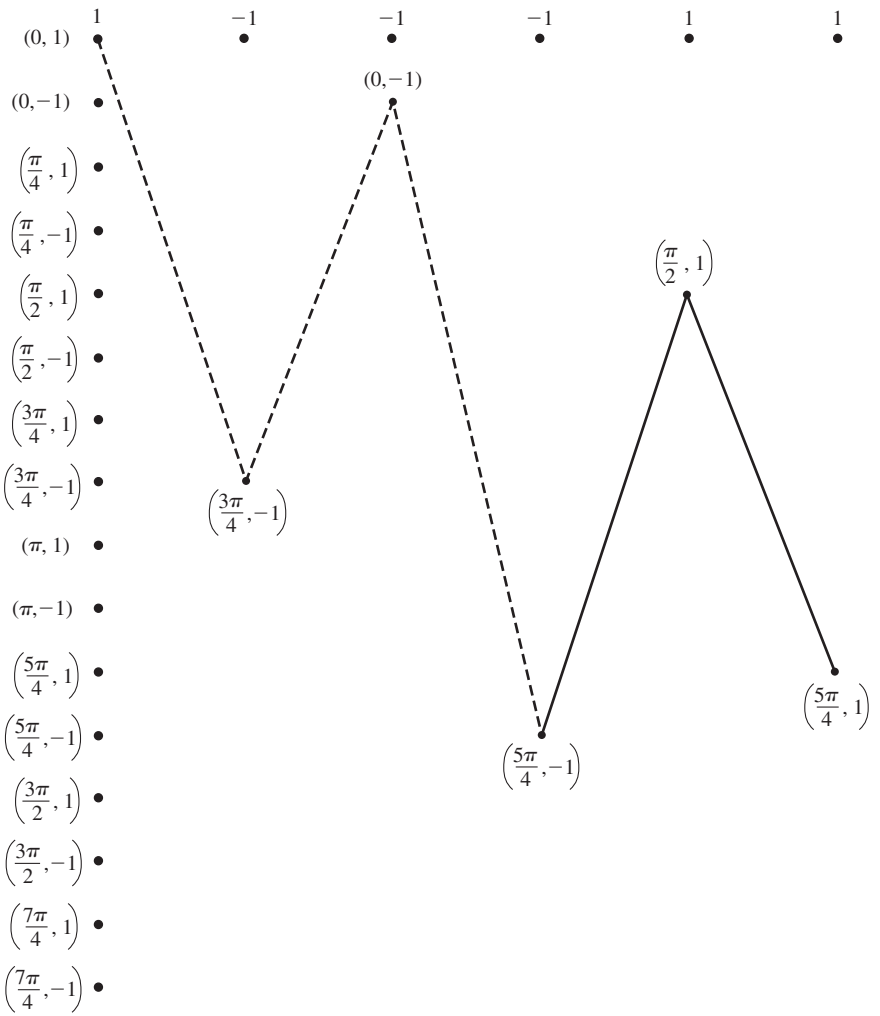

Figure 10.34 A signal path through the trellis.

Although we have described the ML sequence detector for exploiting the memory inherent in the CPM signal, it is also possible to design symbol-by-symbol detection algorithms based on the maximum a posteriori probability (MAP) criterion that also exploit the signal memory. MAP-type detection algorithms have been devised for CPM signals and can be found in the technical literature. The interested reader may refer to the paper by Gertsman and Lodge (1997) for the derivation of the MAP algorithm for CPM and the evaluation of its performance. In essence, the MAP algorithm is designed to minimize the symbol (bit) error probability and, consequently, it results in a slightly smaller symbol (bit) error probability than the ML sequence detector. More importantly,

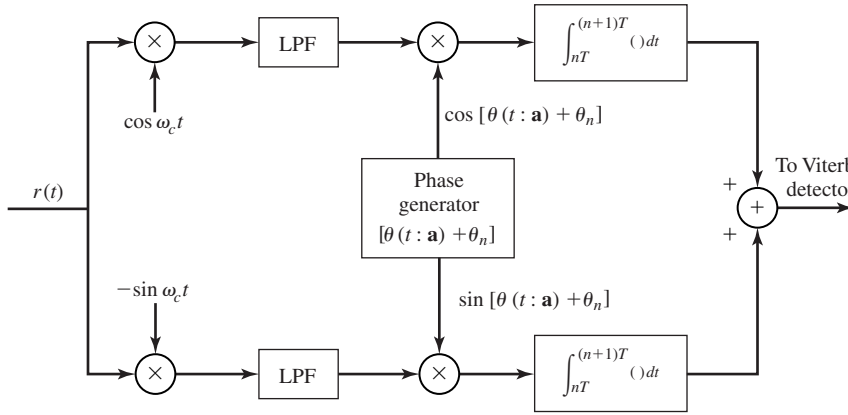

Figure 10.35 Computation of metric increments $C_n(\theta_n; \mathbf{a}, \mathbf{r})$.

in the case of coded CPM, the MAP algorithm can be employed for both signal detection and decoding, thus, making it possible to perform iterative demodulation and decoding. In such a case, the performance of the iterative MAP demodulation and decoding algorithms is significantly better than that of a conventional ML sequence detector and decoder.

10.2.5 Performance of CPM in AWGN and Rayleigh Fading Channels

In determining the probability of error for the Viterbi detector of CPM signals, we must determine the minimum Euclidean distance of paths through the trellis that separate at a node and remerge at a later time at the same node. The distance between two paths through the trellis depends on the phase difference between the paths, as we now demonstrate.

Suppose that we have two signals $u_i(t)$ and $u_j(t)$ corresponding to two phase trajectories $\theta(t; \mathbf{a}_i)$ and $\theta(t; \mathbf{a}_j)$. The sequences $\mathbf{a}_i$ and $\mathbf{a}_j$ must be different in their first symbol. Then, the Euclidean squared distance between the two signals over an interval of length NT, where $1/T$ is the symbol rate, is defined as

$$\begin{aligned} d_{ij}^2 &= \int_0^{NT} [u_i(t) - u_j(t)]^2\, dt \\ &= \int_0^{NT} u_i^2(t)\, dt + \int_0^{NT} u_j^2(t)\, dt - 2\int_0^{NT} u_i(t)u_j(t)\, dt \\ &= 2N\mathcal{E}_s - 2\left(\frac{2\mathcal{E}_s}{T}\right)\int_0^{NT} \cos[2\pi f_c t + \theta(t;\mathbf{a}_i)]\cos[2\pi f_c t + \theta(t,\mathbf{a}_j]\, dt \\ &= \frac{2\mathcal{E}_s}{T}\int_0^{NT} \{1 - \cos[\theta(t;\mathbf{a}_i) - \theta(t;\mathbf{a}_j)]\}\, dt \end{aligned} \tag{10.2.43}$$

Since the symbol energy is related to the energy/bit by the expression $\mathcal{E}_s = \mathcal{E}_b \log_2 M$, the squared Euclidean distance d_{ij}^2 may also be expressed

$$d_{ij}^2 = \frac{2\mathcal{E}_b \log_2 M}{T} \int_0^{NT} \{1 - \cos[\theta(t; \mathbf{a}_i) - \theta(t; \mathbf{a}_j)]\}\, dt \tag{10.2.44}$$

The probability of error for the Viterbi detector in an AWGN channel is dominated by the term corresponding to the minimum Euclidean distance, which is defined as

$$d_{\min}^2 = \lim_{N\to\infty} \min_{i,j} [d_{ij}^2] \tag{10.2.45}$$

Then, the symbol error probability is approximated as

$$P_M \simeq N_{\text{dmin}} Q\left(\sqrt{\frac{d_{\min}^2}{2N_0}}\right) \tag{10.2.46}$$

where N_{dmin} is the number of minimum-distance paths. We note that for conventional binary PSK with no memory, $N = 1$ and $d_{\min}^2 = d_{12}^2 = 4\mathcal{E}_b$. Hence, Equation (10.2.46) agrees with our previous result.

In general, $d_{\min}^2$ is a function of the modulation index h, the number of symbols M, and the pulse shape $g_T(t)$. The choice of the modulation index h and the pulse shape have a significant impact in determining the bandwidth occupied by the transmitted signal. The class of raised cosine (LRC) pulses are especially suitable for use in the design of bandwidth efficient CPM signals.

The value of $d_{\min}^2$ has been evaluated for a variety of CPM signals, including full response and partial response, by Aulin and Sunberg (1981, 1984). For example, Figure 10.36 illustrates the value of $d_{\min}^2$ normalized by $4\mathcal{E}_b$ as a function of the time-bandwidth product $2WT_b$, where W is the 99% in-band power bandwidth. Since MSK results in a $d_{\min}^2 = 4\mathcal{E}_b$, the MSK signal serves as a point of reference (0 dB) in this graph. Along any curve in Figure 10.36, the bandwidth W increases as the modulation index h increases and the SNR gain increases as h increases. Furthermore, the bandwidth efficiency increases with an increase in the symbol size M for fixed LRC pulse shape. We observe from this figure, that there are several decibels to be gained by using partial response signals and higher signal alphabets. The major price paid for this performance gain is the added exponentially increasing complexity in the implementation of the Viterbi detector for searching for the most probable path through the trellis. However, reduced complexity Viterbi-type detectors can be implemented with a relatively small loss in performance.

The performance results in Figure 10.36 illustrate that 3–4-dB gain relative to MSK can be easily obtained with relatively no increase in bandwidth by use of raised cosine partial response CPM and $M = 4$. Although these results are for raised cosine signal pulses, similar gains can be achieved with other partial response signal shapes. We emphasize that this gain in SNR is achieved by introducing memory into the signal modulation and exploiting this memory in the detection of the signal.

In a fading channel, the performance of CPM is no longer a function of the Euclidean distance between pairs of merging phase trajectories as described above.

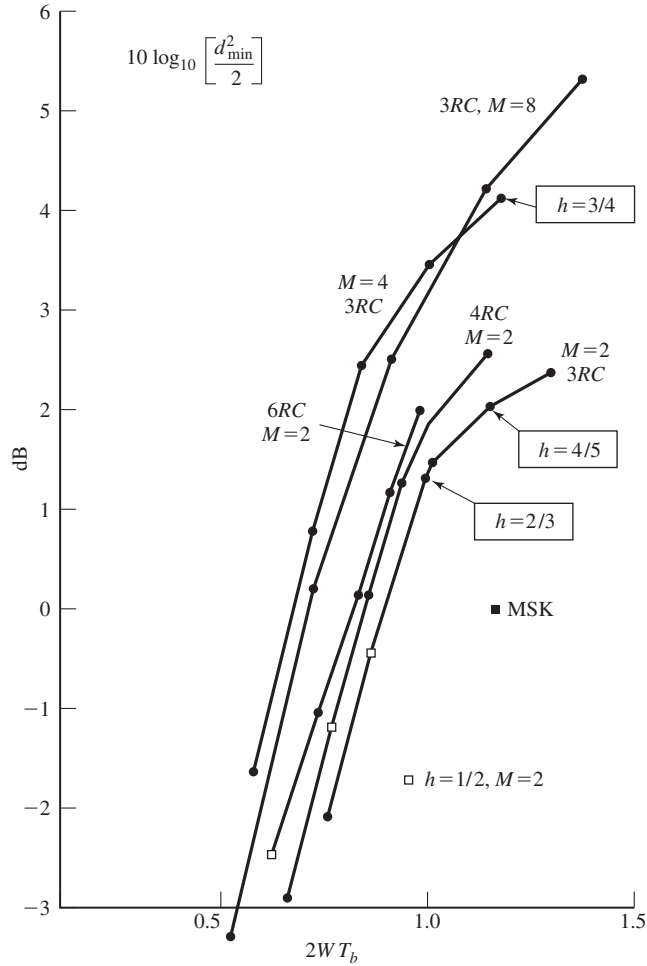

Figure 10.36 Power bandwidth trade-off for partial-response CPM signals with raised cosine pulses; W is the 99% in-band power bandwidth. (From Sundberg; © 1986 IEEE.)

In fact, uncoded CPM in a Rayleigh fading channel has performance characteristics similar to conventional uncoded PSK, in which the error probability decays inversely as the received SNR.

To improve the performance of CPM in the presence of fading, we must provide signal diversity, which is most efficiently obtained through coding and interleaving the coded symbols. Toward this goal, we may employ a linear block code or a convolutional code followed by an interleaver prior to the continuous-phase modulator. The interleaver must be sufficiently long so that any pair of coded symbols from the same code word in a block code are separated in time by an amount that exceeds the coherence time

T_{ct} of the channel. Similarly, in the case of a convolutional code, two coded symbols that fall within the constraint length of the code must be separated by the interleaver by at least T_{ct}. Thus, we achieve independent fading of the coded symbols and a level of diversity equal to d^H_{min} or d^H_{free} with soft-decision decoding and $d^H_{\text{min}}/2$ or $d^H_{\text{free}}/2$ with hard-decision decoding. Consequently, the resulting error probability decays inversely as the SNR raised to the power d^H_{min} (d^H_{free}) or $d^H_{\text{min}}/2$ ($d^H_{\text{free}}/2$) for soft-decision decoding and hard-decision decoding, respectively.

10.3 SPREAD-SPECTRUM COMMUNICATION SYSTEMS

In our treatment of signal design for digital communication over an AWGN channel, the major objective has been the efficient utilization of transmitter power and channel bandwidth. As we observed in Chapter 9, channel coding allows us to reduce the transmitter power by increasing the transmitted signal bandwidth through code redundancy and, thus, to trade off transmitter power with channel bandwidth. This is the basic methodology for the design of digital communication systems for AWGN channels.

In practice, one encounters other factors that influence the design of an efficient digital communication system. For example, in multiple-access communication when two or more transmitters use the same common channel to transmit information, the interference created by the users of the channel limits the performance achieved by the system. The system designer must take into account the existence of such interference in the design of a reliable digital communication system.

Even in this complex design problem, the basic system design parameters are transmitter power and channel bandwidth. To overcome the problems of intentional or unintentional interference, we may further increase the bandwidth of the transmitted signal, as described below, so that the bandwidth expansion factor $B_e = W/R$ is much greater than unity. This is one characteristic of a *spread-spectrum signal*. A second important characteristic is that the information signal at the modulator is spread in bandwidth by means of a code that is independent of the information sequence. This code has the property of being *pseudorandom;* i.e., it appears to be random to receivers other than the intended receiver that uses the knowledge of the code to demodulate the signal. It is this second characteristic property that distinguishes a spread-spectrum communication system from the conventional communication system that expands the transmitted signal bandwidth by means of channel code redundancy. However, we should emphasize that channel coding is an important element in the design of an efficient spread-spectrum communication system.

Spread-spectrum signals for digital communications were originally developed and used for military communications either (1) to provide resistance to jamming (antijam protection), or (2) to hide the signal by transmitting it at low power and, thus, making it difficult for an unintended listener to detect its presence in noise (low probability of intercept). However, spread-spectrum signals are now used to provide reliable communications in a variety of civilian applications, including digital cellular communications and interoffice communications.

In this section we present the basic characteristics of spread-spectrum signals and assess their performance in terms of probability of error. We concentrate our discussion on two methods for spreading the signal bandwidth, namely, by direct sequence modulation and by frequency hopping. Both methods require the use of pseudorandom code sequences whose generation is also described. Several applications of spread-spectrum signals are presented.

10.3.1 Model of a Spread-Spectrum Digital Communication System

The basic elements of a spread spectrum digital communication system are illustrated in Figure 10.37. We observe that the channel encoder and decoder and the modulator and demodulator are the basic elements of a conventional digital communication system. In addition to these elements, a spread-spectrum system employs two identical pseudorandom sequence generators, one which interfaces with the modulator at the transmitting end and the second which interfaces with the demodulator at the receiving end. These two generators produce a pseudorandom or pseudonoise (PN) binary-valued sequence, which is used to spread the transmitted signal at the modulator and to despread the received signal at the demodulator.

Time synchronization of the PN sequence generated at the receiver with the PN sequence contained in the received signal is required in order to properly despread the received spread-spectrum signal. In a practical system, synchronization is established prior to the transmission of information by transmitting a fixed PN bit pattern which is designed so that the receiver will detect it with high probability in the presence of interference. After time synchronization of the PN sequence generators is established, the transmission of information commences. In the data mode, the communication system usually tracks the timing of the incoming received signal and keeps the PN sequence generator in synchronism. The synchronization of the PN sequence generators is treated in Section 10.3.7.

Interference is introduced in the transmission of the spread-spectrum signal through the channel. The characteristics of the interference depend to a large extent on its origin. The interference may be generally categorized as being either broadband or narrowband (partial band) relative to the bandwidth of the information-bearing signal, and either continuous in time or pulsed (discontinuous) in time. For example, an

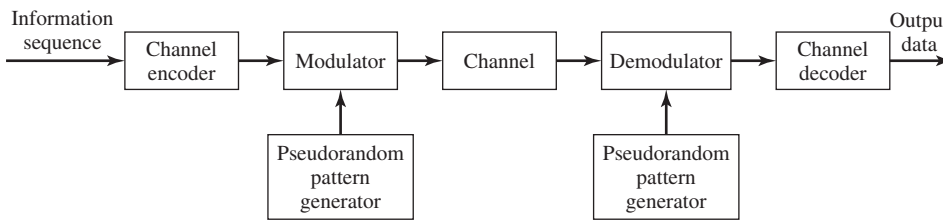

Figure 10.37 Model of spread-spectrum digital communications system.

interfering signal may consist of a high-power sinusoid in the bandwidth occupied by the information-bearing signal. Such a signal is narrowband. As a second example, the interference generated by other users in a multiple-access channel depends on the type of spread-spectrum signals that are employed by the various users to transmit their information. If all users employ broadband signals, the interference may be characterized as an equivalent broadband noise. If the users employ frequency hopping to generate spread-spectrum signals, the interference from other users may be characterized as narrowband. We shall consider these types of interference and some others in Section 10.3.6.

Our discussion will focus on the performance of spread-spectrum signals for digital communication in the presence of narrowband and broadband interference. Two types of digital modulation are considered, namely, PSK and FSK. PSK modulation is appropriate for applications where phase coherence between the transmitted signal and the received signal can be maintained over a time interval that spans several symbol (or bit) intervals. On the other hand, FSK modulation is appropriate in applications where phase coherence of the carrier cannot be maintained due to time variations in the transmission characteristics of the communications channel. For example, this may be the case in a communications link between two high-speed aircraft or between a high-speed aircraft and a ground-based terminal.

The PN sequence generated at the modulator is used in conjunction with the PSK modulation to shift the phase of the PSK signal pseudorandomly, as described below at a rate that is an integer multiple of the bit rate. The resulting modulated signal is called a *direct-sequence (DS) spread-spectrum signal*. When used in conjunction with binary or M-ary ($M > 2$) FSK, the PN sequence is used to select the frequency of the transmitted signal pseudorandomly. The resulting signal is called a *frequency-hopped (FH) spread-spectrum signal*. Although other types of spread-spectrum signals can be generated, our treatment will emphasize DS and FH spread-spectrum communication systems, which are the ones generally used in practice.

10.3.2 Direct-Sequence Spread-Spectrum Systems

Let us consider the transmission of a binary information sequence by means of binary PSK. The information rate is R bits/sec and the bit interval is $T_b = 1/R$ sec. The available channel bandwidth is B_c Hz, where $B_c \gg R$. At the modulator, the bandwidth of the information signal is expanded to $W = B_c$ Hz by shifting the phase of the carrier pseudorandomly at a rate of W times/sec according to the pattern of the PN generator. The basic method for accomplishing the spreading is shown in Figure 10.38.

The information-bearing baseband signal is denoted as $v(t)$ and is expressed as

$$v(t) = \sum_{n=-\infty}^{\infty} a_n g_T(t - nT_b) \tag{10.3.1}$$

where $\{a_n = \pm 1, -\infty < n < \infty\}$ and $g_T(t)$ is a rectangular pulse of duration T_b. This signal is multiplied by the signal from the PN sequence generator, which may be

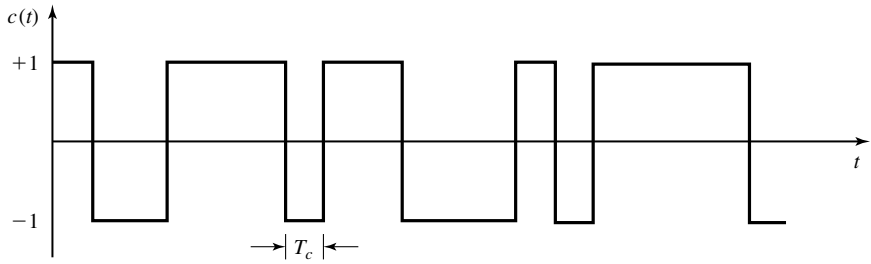

(a) PN signal

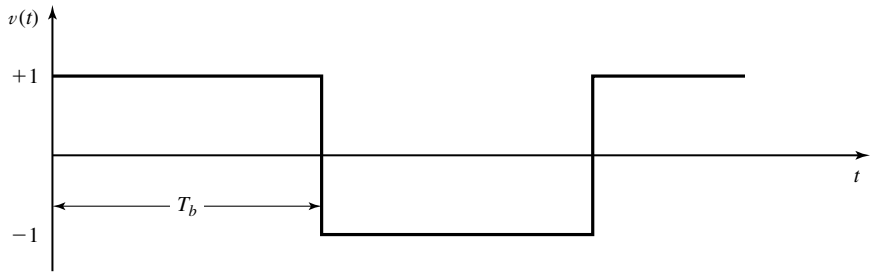

(b) Data signal

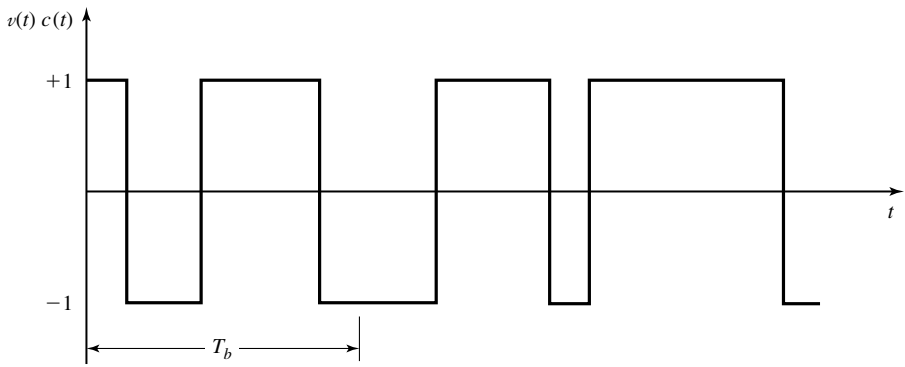

(c) Product signal

Figure 10.38 Generation of a DS spread-spectrum signal.

expressed as

$$c(t) = \sum_{n=-\infty}^{\infty} c_n p(t - nT_c) \tag{10.3.2}$$

where $\{c_n\}$ represents the binary PN code sequence of ± 1's and $p(t)$ is a rectangular pulse of duration T_c, as illustrated in Figure 10.38. This multiplication operation

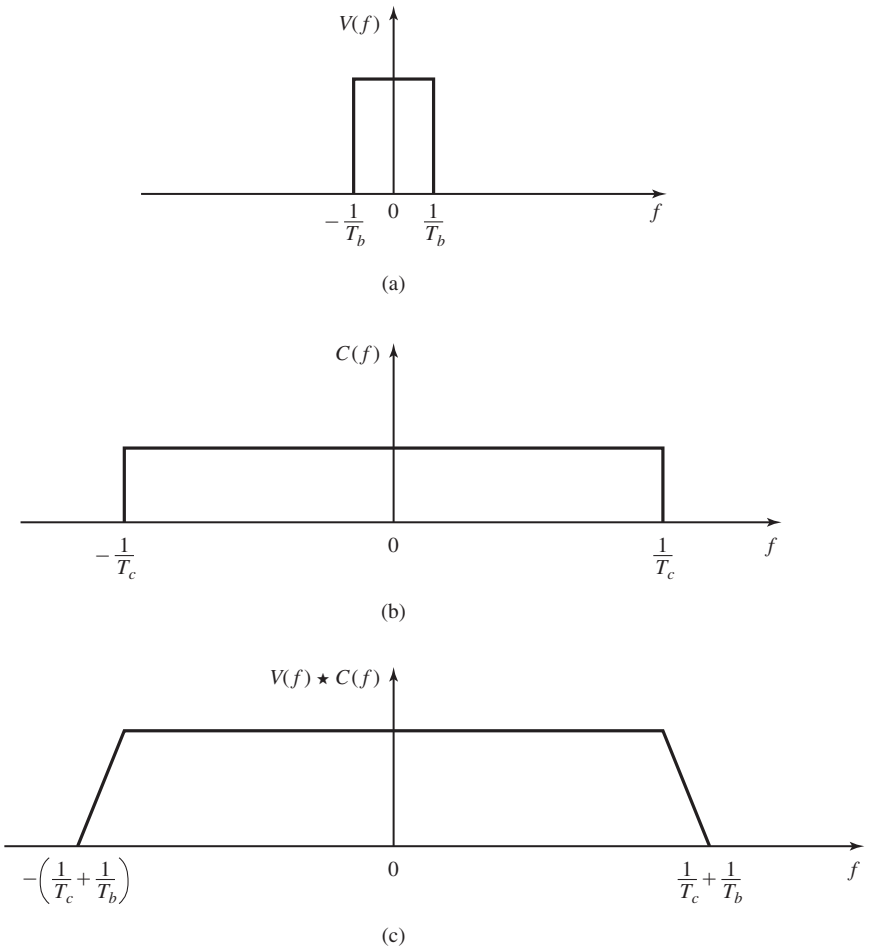

Figure 10.39 Convolution of spectra of the (a) data signal with the (b) PN code signal.

serves to spread the bandwidth of the information-bearing signal (whose bandwidth is R Hz, approximately) into the wider bandwidth occupied by PN generator signal $c(t)$ (whose bandwidth is $1/T_c$, approximately). The spectrum spreading is illustrated in Figure 10.39, which shows, in simple terms, using rectangular spectra, the convolution of the two spectra, the narrow spectrum corresponding to the information-bearing signal and the wide spectrum corresponding to the signal from the PN generator.

The product signal $v(t)c(t)$, also illustrated in Figure 10.39, is used to amplitude modulate the carrier $A_c \cos 2\pi f_c t$ and, thus, to generate the DSB-SC signal

$$u(t) = A_c v(t)c(t) \cos 2\pi f_c t \tag{10.3.3}$$

Since $v(t)c(t) = \pm 1$ for any t, it follows that the carrier-modulated transmitted signal may also be expressed as

$$u(t) = A_c \cos[2\pi f_c t + \theta(t)] \tag{10.3.4}$$

where $\theta(t) = 0$ when $v(t)c(t) = 1$ and $\theta(t) = \pi$ when $v(t)c(t) = -1$. Therefore, the transmitted signal is a binary PSK signal.

The rectangular pulse $p(t)$ is usually called a *chip* and its time duration T_c is called the *chip interval*. The reciprocal $1/T_c$ is called the *chip rate* and corresponds (approximately) to the bandwidth W of the transmitted signal. The ratio of the bit interval T_b to the chip interval T_c is usually selected to be an integer in practical spread spectrum systems. We denote this ratio as

$$L_c = \frac{T_b}{T_c} \tag{10.3.5}$$

Hence, L_c is the number of chips of the PN code sequence/information bit. Another interpretation is that L_c represents the number of possible 180° phase transitions in the transmitted signal during the bit interval T_b.

The demodulation of the signal is performed as illustrated in Figure 10.40. The received signal is first multiplied by a replica of the waveform $c(t)$ generated by the PN code sequence generator at the receiver, which is synchronized to the PN code in the received signal. This operation is called (spectrum) *despreading,* since the effect of multiplication by $c(t)$ at the receiver is to undo the spreading operation at the transmitter. Thus, we have

$$A_c v(t)c^2(t) \cos 2\pi f_c t = A_c v(t) \cos 2\pi f_c t \tag{10.3.6}$$

since $c^2(t) = 1$ for all t. The resulting signal $A_c v(t) \cos 2\pi f_c t$ occupies a bandwidth (approximately) of R Hz, which is the bandwidth of the information-bearing signal. Therefore, the demodulator for the despread signal is simply the conventional cross correlator or matched filter that was previously described in Chapter 7. Since the demodulator has a bandwidth that is identical to the bandwidth of the despread signal, the only additive noise that corrupts the signal at the demodulator is the noise that falls within the information-bandwidth of the received signal.

Effect of Despreading on a Narrowband Interference. It is interesting to investigate the effect of an interfering signal on the demodulation of the desired

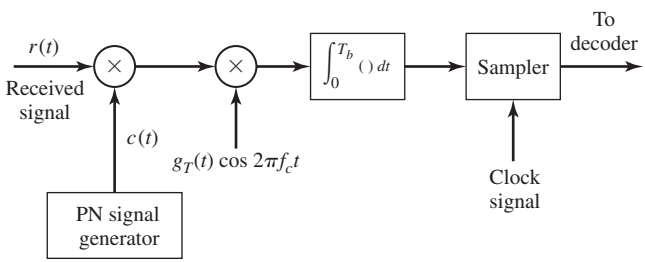

Figure 10.40 Demodulation of DS spread-spectrum signal.

information-bearing signal. Suppose that the received signal is

$$r(t) = A_c v(t)c(t)\cos 2\pi f_c t + i(t) \tag{10.3.7}$$

where $i(t)$ denotes the interference. The despreading operation at the receiver yields

$$r(t)c(t) = A_c v(t)\cos 2\pi f_c t + i(t)c(t) \tag{10.3.8}$$

The effect of multiplying the interference $i(t)$ with $c(t)$, is to spread the bandwidth of $i(t)$ to W Hz.

As an example, let us consider a sinusoidal interfering signal of the form

$$i(t) = A_I \cos 2\pi f_I t, \tag{10.3.9}$$

where f_I is a frequency within the bandwidth of the transmitted signal. Its multiplication with $c(t)$ results in a wideband interference with power-spectral density $I_0 = P_I/W$, where $P_I = A_I^2/2$ is the average power of the interference. Since the desired signal is demodulated by a matched filter (or correlator) that has a bandwidth R, the total power in the interference at the output of the demodulator is

$$I_0 R_b = P_I R_b/W = \frac{P_I}{W/R_b} = \frac{P_I}{T_b/T_c} = \frac{P_I}{L_c} \tag{10.3.10}$$

Therefore, the power in the interfering signal is reduced by an amount equal to the bandwidth expansion factor W/R. The factor $W/R = T_b/T_c = L_c$ is called the *processing gain* of the spread-spectrum system. The reduction in interference power is the basic reason for using spread-spectrum signals to transmit digital information over channels with interference.

In summary, the PN code sequence is used at the transmitter to spread the information-bearing signal into a wide bandwidth for transmission over the channel. By multiplying the received signal with a synchronized replica of the PN code signal, the desired signal is despread back to a narrow bandwidth while any interference signals are spread over a wide bandwidth. The net effect is a reduction in the interference power by the factor W/R, which is the processing gain of the spread-spectrum system.

The PN code sequence $\{c_n\}$ is assumed to be known only to the intended receiver. Any other receiver that does not have knowledge of the PN code sequence cannot demodulate the signal. Consequently, the use of a PN code sequence provides a degree of privacy (or security) that is not possible to achieve with conventional modulation. The primary cost for this security and performance gain against interference is an increase in channel bandwidth utilization and in the complexity of the communication system.

Probability of Error. To derive the probability of error for a DS spread-spectrum system, we assume that the information is transmitted via binary PSK. Within the bit interval $0 \le t \le T_b$, the transmitted signal is

$$s(t) = a_o g_T(t)c(t)\cos 2\pi f_c t, \quad 0 \le t \le T_b \tag{10.3.11}$$

where $a_o = \pm 1$ is the information symbol, the pulse $g_T(t)$ is defined as

$$g_T(t) = \begin{cases} \sqrt{\frac{2\mathcal{E}_b}{T_b}}, & 0 \le t \le T_b \\ 0, & \text{otherwise} \end{cases} \tag{10.3.12}$$

and $c(t)$ is the output of the PN code generator which, over a bit interval, is expressed as

$$c(t) = \sum_{n=0}^{L_c-1} c_n p(t - nT_c) \tag{10.3.13}$$

where L_c is the number of chips per bit, T_c is the chip interval, and $\{c_n\}$ denotes the PN code sequence. The code chip sequence $\{c_n\}$ is uncorrelated (white); i.e.,

$$E(c_n c_m) = E(c_n)E(c_m) \quad \text{for } n \neq m \tag{10.3.14}$$

and each chip is $+1$ or -1 with equal probability. These conditions imply that $E(c_n) = 0$ and $E(c_n^2) = 1$.

The received signal is assumed to be corrupted by an additive interfering signal $i(t)$. Hence,

$$r(t) = a_o g_T(t - t_d)c(t - t_d)\cos(2\pi f_c t + \phi) + i(t) \tag{10.3.15}$$

where t_d represents the propagation delay through the channel and ϕ represents the carrier-phase shift. Since the received signal $r(t)$ is the output of an ideal bandpass filter in the front end of the receiver, the interference $i(t)$ is also a bandpass signal, and may be represented as

$$i(t) = i_c(t)\cos 2\pi f_c t - i_s(t)\sin 2\pi f_c t \tag{10.3.16}$$

where $i_c(t)$ and $i_s(t)$ are the two quadrature components.

Assuming that the receiver is perfectly synchronized to the received signal, we may set $t_d = 0$ for convenience. In addition, the carrier phase is assumed to be perfectly estimated by a PLL. Then, the signal $r(t)$ is demodulated by first despreading through multiplication by $c(t)$ and then crosscorrelation with $g_T(t)\cos(2\pi f_c t + \phi)$, as shown in Figure 10.41. At the sampling instant $t = T_b$, the output of the correlator is

$$y(T_b) = \mathcal{E}_b + y_i(T_b) \tag{10.3.17}$$

where $y_i(T_b)$ represents the interference component, which has the form

$$\begin{aligned} y_i(T_b) &= \int_0^{T_b} c(t)i(t)g_T(t)\cos(2\pi f_c t + \phi)\,dt \\ &= \sum_{n=0}^{L_c-1} c_n \int_0^{T_b} p(t - nT_c)i(t)g_T(t)\cos(2\pi f_c t + \phi)\,dt \\ &= \sqrt{\frac{2\mathcal{E}_b}{T_b}} \sum_{n=0}^{L_c-1} c_n v_n \end{aligned} \tag{10.3.18}$$

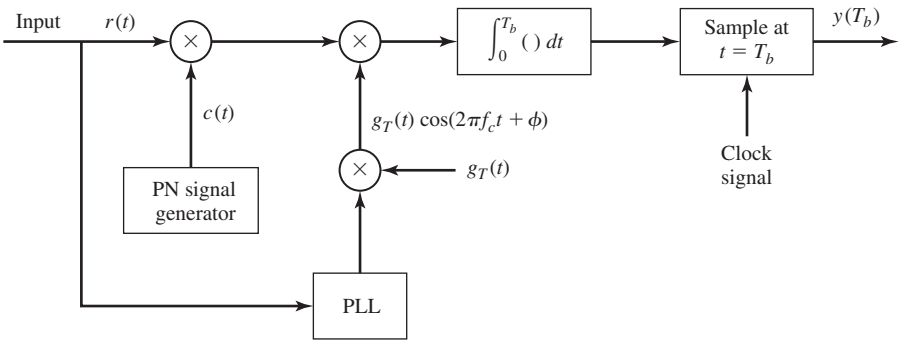

Figure 10.41 DS spread-spectrum signal demodulator.

where, by definition,

$$\nu_n = \int_{nT_c}^{(n+1)T_c} i(t)\cos(2\pi f_c t + \phi)\,dt \tag{10.3.19}$$

The probability of error depends on the statistical characteristics of the interference component. Clearly, its mean value is

$$E[y_i(T_b)] = 0 \tag{10.3.20}$$

Its variance is

$$E\left[y_i^2(T_b)\right] = \frac{2\mathcal{E}_b}{T_b}\sum_{n=0}^{L_c-1}\sum_{m=0}^{L_c-1} E(c_n c_m)E(\nu_n \nu_m)$$

But $E(c_n c_m) = \delta_{mn}$. Therefore,

$$\begin{aligned} E\left[y_i^2(T_b)\right] &= \frac{2\mathcal{E}_b}{T_b}\sum_{n=0}^{L_c-1} E\left(\nu_n^2\right) \\ &= \frac{2\mathcal{E}_b}{T_b} L_c E(\nu^2) \end{aligned} \tag{10.3.21}$$

where $\nu = \nu_n$, as given by Equation (10.3.19). To determine the variance of ν, we must postulate the form of the interference.

First, let us assume that the interference is sinusoidal. Specifically, we assume that the interference is at the carrier frequency, and has the form

$$i(t) = \sqrt{2P_I}\,\cos(2\pi f_c t + \Theta_I) \tag{10.3.22}$$

where P_I is the average power and Θ_I is the phase of the interference, which we assume to be random and uniformly distributed over the interval $(0, 2\pi)$. If we substitute for

$i(t)$ in Equation (10.3.19), we obtain

$$v_n = \int_{nT_c}^{(n+1)T_c} \sqrt{2P_I}\cos(2\pi f_c t + \Theta_I)\cos(2\pi f_c t + \phi)\,dt$$
$$= \frac{1}{2}\sqrt{2P_I}\int_{nT_c}^{(n+1)T_c} \cos(\Theta_I - \phi)\,dt = \frac{T_c}{2}\sqrt{2P_I}\cos(\Theta_I - \phi) \qquad (10.3.23)$$

Since Θ_I is a random variable, v_n is also random. Its mean value is zero; i.e.,

$$E(v_n) = \frac{T_c}{2}\sqrt{2P_I}\int_0^{2\pi} \frac{1}{2\pi}\cos(\Theta_I - \phi)\,d\Theta_I = 0 \qquad (10.3.24)$$

Its mean-square value is

$$E\left(v_n^2\right) = \frac{T_c^2 P_I}{2}\,\frac{1}{2\pi}\int_0^{2\pi} \cos^2(\Theta_I - \phi)\,d\Theta_I$$
$$= \frac{T_c^2 P_I}{4} \qquad (10.3.25)$$

We may now substitute for $E(v^2)$ into Equation (10.3.21). Thus, we obtain

$$E\left[y_i^2(T_b)\right] = \frac{\mathcal{E}_b P_I T_c}{2} \qquad (10.3.26)$$

The ratio of $\{E[y(T_b)]\}^2$ to $E[y_i^2(T_b)]$ is the SNR the detector. In this case we have

$$(\text{SNR})_D = \frac{\mathcal{E}_b^2}{\mathcal{E}_b P_I T_c/2} = \frac{2\mathcal{E}_b}{P_I T_c} \qquad (10.3.27)$$

To see the effect of the spread-spectrum signal, we express the transmitted energy $\mathcal{E}_b$ as

$$\mathcal{E}_b = P_S T_b \qquad (10.3.28)$$

where P_S is the average signal power. Then, if we substitute for $\mathcal{E}_b$ in Equation (10.3.27), we obtain

$$(\text{SNR})_D = \frac{2P_S T_b}{P_I T_c} = \frac{2P_S}{P_I/L_c} \qquad (10.3.29)$$

where $L_c = T_b/T_c$ is the processing gain. Therefore, the spread-spectrum signal has reduced the power of the interference by the factor L_c.

Another interpretation of the effect of the spread-spectrum signal on the sinusoidal interference is obtained if we express $P_I T_c$ in Equation (10.3.29) as follows. Since $T_c \simeq 1/W$, we have

$$P_{IJ} T_c = P_I/W \equiv I_0 \qquad (10.3.30)$$

where I_0 is the power-spectral density of an equivalent interference in a bandwidth W. Therefore, in effect, the spread-spectrum signal has spread the sinusoidal interference over the wide bandwidth W, creating an equivalent spectrally flat noise with

power-spectral density I_0. Hence,

$$(\text{SNR})_D = \frac{2\mathcal{E}_b}{I_0} \tag{10.3.31}$$

Example 10.3.1

The SNR required at the detector to achieve reliable communication in a DS spread-spectrum communication system is 13 dB. If the interference-to-signal power at the receiver is 20 dB, determine the processing gain required to achieve reliable communication.

Solution We are given $(P_I/P_S)_{\text{dB}} = 20$ dB or, equivalently, $P_I/P_S = 100$. We are also given $(\text{SNR})_D = 13$ dB, or equivalently, $(\text{SNR})_D = 20$. The relation in Equation (10.2.29) may be used to solve for L_c. Thus,

$$L_c = \frac{1}{2}\left(\frac{P_I}{P_S}\right)(\text{SNR})_D = 1000$$

Therefore, the processing gain required is 1000 or, equivalently, 30 dB.

As a second case, let us consider the effect of an interference $i(t)$ that is a zero-mean broadband random process with a constant power-spectral density over the bandwidth W of the spread-spectrum signal, as illustrated in Figure 10.42. Note that the total interference power is

$$P_I = \int_{-\infty}^{\infty} \mathcal{S}_{ii}(f)\,df = W I_0 \tag{10.3.32}$$

The variance of the interference component at the input to the detector is given by Equation (10.3.21). To evaluate the moment $E(\nu^2)$, we substitute the bandpass representation of $i(t)$, given by Equation (10.3.16), into Equation (10.3.19). By neglecting the double frequency terms (terms involving $\cos 4\pi f_c t$) and making use of the statistical properties of the quadrature components, namely $E[i_c(t)] = E[(i_s(t)] = 0$, and

$$\begin{aligned} R_{i_c}(\tau) &= E[i_c(t)i_c(t+\tau)] = E[i_s(t)i_s(t+\tau)] \\ &= I_0 \frac{\sin \pi W\tau}{\pi\tau} \end{aligned} \tag{10.3.33}$$

we obtain the result

$$E(\nu^2) = \frac{1}{4}\int_0^{T_c}\int_0^{T_c} R_{i_c}(t_1 - t_2)\,dt_1\,dt_2 \tag{10.3.34}$$

This is an integral of the autocorrelation function over the square defined by the region $0 \le t_1 \le T_c$ and $0 \le t_2 \le T_c$, as shown in Figure 10.43. If we let $\tau = t_1 - t_2$, $E(\nu^2)$

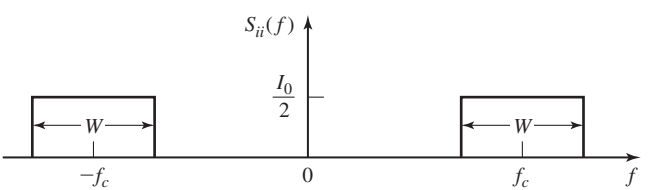

Figure 10.42 Power-spectral density of broadband interference.

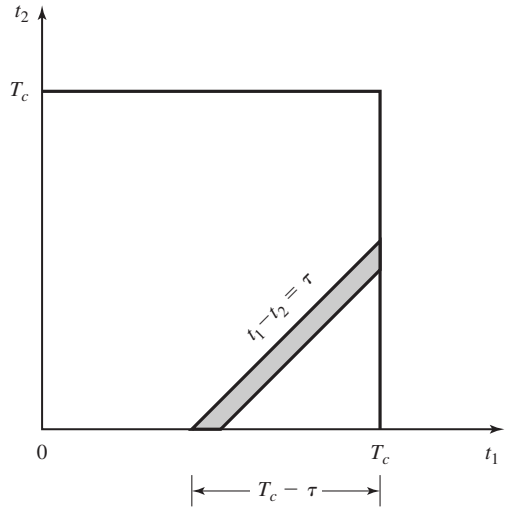

Figure 10.43 Region of integration of the autocorrelation function $R_{cc}(t_1, t_2)$.

can be reduced to the single integral (see Figure 10.43)

$$\begin{aligned} E(v^2) &= \frac{1}{4}\int_{-T_c}^{T_c}(T_c - |\tau|)R_{n_c}(\tau)\,dt \\ &= \frac{I_0 T_c}{4}\int_{-T_c}^{T_c}\left(1 - \frac{|\tau|}{T_c}\right)\frac{\sin \pi W\tau}{\pi\tau}\,d\tau \\ &= \frac{P_I T_c}{4W}\int_{-T_c}^{T_c}\left(1 - \frac{|\tau|}{T_c}\right)\frac{\sin \pi W\tau}{\pi\tau}\,d\tau \end{aligned} \tag{10.3.35}$$

Since $T_c \approx \alpha/W$, where $\alpha > 0$, the above integral may be expressed as

$$J(\alpha) = 2\int_0^{\alpha}\left(1 - \frac{x}{\alpha}\right)\frac{\sin \pi x}{\pi x}\,dx \tag{10.3.36}$$

and it can be numerically evaluated for any value of α. Figure 10.44 illustrates $J(\alpha)$. Note that $J(\alpha) \leq 1$ for any value of α and that $J(\alpha) \to 1$ as $\alpha \to \infty$.

By combining the results in Equations (10.3.21), (10.3.35) and (10.3.36), we conclude that the variance of the interference component $y_i(T_b)$ for the broadband interference is

$$E\left[y_i^2(T_b)\right] = \frac{\mathcal{E}_b P_I T_c}{2} J(\alpha) \tag{10.3.37}$$

Therefore, the SNR at the detector is

$$(\text{SNR})_D = \frac{2\mathcal{E}_b}{I_0 J(\alpha)} \tag{10.3.38}$$

If we compare Equation (10.3.31) with Equation (10.3.38) we observe that the SNR for the case of the broadband interference is larger due to the factor $J(\alpha)$. Hence, the

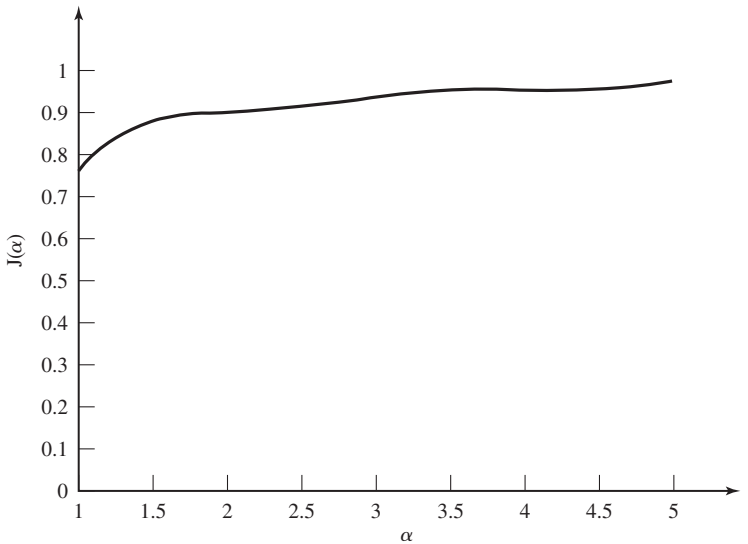

Figure 10.44 Plot of the function $I(\alpha)$ given in (10.3.30).

sinusoidal interference results in a somewhat larger degradation in the performance of the DS spread-spectrum system compared to that of a broadband interference.

The probability of error for a DS spread-spectrum system with binary PSK modulation is easily obtained from the SNR at the detector, if we make an assumption on the probability distribution of the sample $y_i(T_b)$. From Equation (10.3.18) we note that $y_i(T_b)$ consists of a sum L_c uncorrelated random variables $\{c_n \nu_n, 0 \leq n \leq L_c - 1\}$, all of which are identically distributed. Since the processing gain L_c is usually large in any practical system, we may use the Central Limit Theorem to justify a Gaussian probability distribution for $y_i(T)$. Under this assumption, the probability of error for the sinusoidal interference is

$$P_b = Q\left(\sqrt{\frac{2\mathcal{E}_b}{I_0}}\right) \tag{10.3.39}$$

where I_0 is the power-spectral density of an equivalent broadband interference. A similar expression holds for the case of a broadband interference, where the SNR at the detector is increased by the factor $1/J(\alpha)$.

The Interference Margin. We may express $\frac{\mathcal{E}_b}{I_0}$ in the Q-function in Equation (10.3.39) as

$$\frac{\mathcal{E}_b}{I_0} = \frac{P_S T_b}{P_I/W} = \frac{P_S/R}{P_I/W} = \frac{W/R}{P_I/P_S} \tag{10.3.40}$$

Also, suppose we specify a required $\mathcal{E}_b/I_0$ to achieve a desired level of performance. Then, using a logarithmic scale, we may express Equation (10.3.40) as

$$\begin{aligned} 10\log\frac{P_I}{P_S} &= 10\log\frac{W}{R} - 10\log\left(\frac{\mathcal{E}_b}{I_0}\right) \\ \left(\frac{P_I}{P_S}\right)_{\text{dB}} &= \left(\frac{W}{R}\right)_{\text{dB}} - \left(\frac{\mathcal{E}_b}{I_0}\right)_{\text{dB}} \end{aligned} \tag{10.3.41}$$

The ratio $(P_I/P_S)_{\text{dB}}$ is called the *interference margin*. This is the relative power advantage that an interference may have without disrupting the communication system.

Example 10.3.2

Suppose we require an $(\mathcal{E}_b/I_0)_{\text{dB}} = 10$ dB to achieve reliable communication. What is the processing gain that is necessary to provide an interference margin of 20 dB?

Solution Clearly, if $W/R = 1000$, then $(W/R)_{\text{dB}} = 30$ dB and the interference margin is $(P_J/P_S)_{\text{dB}} = 20$ dB. This means that the average interference power at the receiver may be 100 times the power P_S of the desired signal and we can still maintain reliable communication.

Performance of Coded Spread-Spectrum Signals. As shown in Chapter 9, when the transmitted information is coded by a binary linear (block or convolutional) code, the SNR at the output of a soft-decision decoder is increased by the coding gain, defined as

$$\text{coding gain} = R_c d_{\min}^H \tag{10.3.42}$$

where R_c is the code rate and $d_{\min}^H$ is the minimum Hamming distance of the code. Therefore, the effect of coding is to increase the interference margin by the coding gain. Thus, Equation (10.3.41) may be modified as

$$\left(\frac{P_I}{P_S}\right)_{\text{dB}} = \left(\frac{W}{R}\right)_{\text{dB}} + (CG)_{\text{dB}} - \left(\frac{\mathcal{E}_b}{I_0}\right)_{\text{dB}} \tag{10.3.43}$$

where $(CG)_{\text{dB}}$ denotes the coding gain.

10.3.3 Some Applications of DS Spread-Spectrum Signals

In this subsection, we briefly describe the use of DS spread-spectrum signals in three applications. First, we consider an application in which the signal is transmitted at very low power, so that a listener trying to detect the presence of the signal would encounter great difficulty. A second application is multiple-access radio communications. A third application involves the use of a DS spread-spectrum signal to resolve the multipath in a time-dispersive radio channel.

Low-detectability Signal Transmission. In this application, the information-bearing signal is transmitted at a very low power level relative to the background channel noise and thermal noise that is generated in the front end of a receiver. If the DS spread-spectrum signal occupies a bandwidth W and the power-spectral density of the additive noise is N_0 W/Hz, the average noise power in the bandwidth W is $P_N = WN_0$.

The average received signal power at the intended receiver is P_R. If we wish to hide the presence of the signal from receivers that are in the vicinity of the intended receiver, the signal is transmitted at a power level such that $P_R/P_N \ll 1$. The intended receiver can recover the weak information-bearing signal from the background noise with the aid of the processing gain and the coding gain. However, any other receiver which has no knowledge of the PN code sequence is unable to take advantage of the processing gain and the coding gain. Consequently, the presence of the information-bearing signal is difficult to detect. We say that the transmitted signal has a *low probability of being intercepted* (LPI) and it is called an *LPI signal*.

The probability of error given in Section 10.3.2 applies as well to the demodulation and decoding of LPI signals at the intended receiver.

Example 10.3.3

A DS spread-spectrum signal is designed so that the power ratio P_R/P_N at the intended receiver is 10^{-2}; (a) if the desired $\mathcal{E}_b/N_0 = 10$ for acceptable performance, determine the minimum value of the processing gain; and (b) suppose that the DS spread-spectrum signal is transmitted via radio to a receiver at a distance of 2000 Km. The transmitter antenna has a gain of 20 dB, while the receiver antenna is omnidirectional. The carrier frequency is 3 MHz, the available channel bandwidth $W = 10^5$ Hz and the receiver has a noise temperature of 300 K. Determine the required transmitter power and the bit rate of the DS spread-spectrum system.

Solution (a) We may write $\mathcal{E}_b/N_0$ as

$$\frac{\mathcal{E}_b}{N_0} = \frac{P_R T_b}{N_0} = \frac{P_R L_c T_c}{N_0} = \left(\frac{P_R}{W N_0}\right) L_c = \left(\frac{P_R}{P_N}\right) L_c$$

Since $\mathcal{E}_b/N_0 = 10$ and $P_R/P_N = 10^{-2}$, it follows that the necessary processing gain is $L_c = 1000$.

(b) The expression for the received signal power is

$$P_{R\text{dB}} = P_{T\text{dB}} - L_{s\text{dB}} + G_{T\text{dB}}$$

where $L_{s\text{dB}}$ is the free-space path loss and $G_{T\text{dB}}$ is the antenna gain. The path loss is

$$L_{s\text{dB}} = 20 \log\left(\frac{4\pi d}{2}\right)$$

where the wavelength $\lambda = 100$ meters. Hence,

$$L_{s\text{dB}} = 20 \log(8\pi \times 10^4) = 108\,\text{dB}$$

Therefore,

$$\begin{aligned} P_{T\text{dB}} &= P_{R\text{dB}} + 108 - 20 \\ &= P_{R\text{dB}} + 88 \end{aligned}$$

The received power level can be obtained from the condition $P_R/P_N = 10^{-2}$. First of all, $P_N = WN_0$, where $N_0 = kT = 4 \times 10^{-21}$ W/Hz and $W = 10^5$ Hz. Hence,

$$P_N = 4.1 \times 10^{-16} W$$

and

$$P_R = 4.1 \times 10^{-18} W$$

or, equivalently, $P_{R\text{dB}} = -174$ dBw. Therefore,

$$P_{T\text{dB}} = P_{R\text{dB}} + 88 = -86\,\text{dBW}$$

or, equivalently, $P_T = 2.5 \times 10^{-9}$ W. The bit rate is $R = W/L_c = 10^5/10^3 = 100$ bps.

Code Division Multiple Access. The enhancement in performance obtained from a DS spread-spectrum signal through the processing gain and the coding gain can be used to enable many DS spread-spectrum signals to occupy the same channel bandwidth provided that each signal has its own pseudorandom (signature) sequence. Thus, it is possible to have several users transmit messages simultaneously over the same channel bandwidth. This type of digital communication in which each transmitter-receiver user pair has its own distinct signature code for transmitting over a common channel bandwidth is called *code division multiple access (CDMA).*

In the demodulation of each DS spread-spectrum signal, the signals from the other simultaneous users of the channel appear as additive interference. The level of interference varies as a function of the number of users of the channel at any given time. A major advantage of CDMA is that a large number of users can be accommodated if each user transmits messages for a short period of time. In such a multiple access system, it is relatively easy either to add new users or to decrease the number of users without reconfiguring the system.

Next, we determine the number of simultaneous signals that can be accommodated in a CDMA system. For simplicity, we assume that all signals have identical average powers. In many practical systems, the received signal power level from each user is monitored at a central station and power control is exercised over all simultaneous users by use of a control channel that instructs the users on whether to increase or decrease their power level. With such power control, if there are N_u simultaneous users, the desired signal-to-noise interference power ratio at a given receiver is

$$\frac{P_S}{P_N} = \frac{P_S}{(N_u - 1)P_S} = \frac{1}{N_u - 1} \tag{10.3.44}$$

From this relation, we can determine the number of users that can be accommodated simultaneously. The following example illustrates the computation.

Example 10.3.4

Suppose that the desired level of performance for a user in a CDMA system is an error probability of 10^{-6}, which is achieved when $\mathcal{E}_b/I_0 = 20$ (13 dB). Determine the maximum number of simultaneous users that can be accommodated in a CDMA system if the bandwidth-to-bit-rate ratio is 1000 and the coding gain is $R_c d_{\min}^H = 4$ (6 dB).

Solution From the relationships given in Equations (10.3.43) and (10.3.44), we have

$$\frac{\mathcal{E}_b}{I_0} = \frac{W/R}{N_u - 1} R_c d_{\min}^H = 20$$

If we solve for N_u we obtain

$$N_u = \frac{W/R}{20} R_c d_{\min}^H + 1$$

For $W/R = 1000$ and $R_c d_{\min}^H = 4$, we obtain the result that $N_u = 201$.

In determining the maximum number of simultaneous users of the channel, we implicitly assumed that the pseudorandom code sequences used by the various users are uncorrelated and that the interference from other users adds on a power basis only. However, orthogonality of the pseudorandom sequences among the N_u users is generally difficult to achieve, especially if N_u is large. In fact, the design of a large set of pseudorandom sequences with good correlation properties is an important problem that has received considerable attention in the technical literature. We shall briefly treat this problem in Section 10.3.5.

CDMA is a viable method for providing digital cellular telephone service to mobile users. In Section 10.4 we describe the basic characteristics of the North American digital cellular system that employs CDMA.

Communication Over Channels with Multipath. In Section 10.1, we described the characteristics of fading multipath channels and the design of signals for effective communication through such channels. Examples of fading multipath channels include ionospheric propagation in the HF frequency band (3–30 MHz) where the ionospheric layers serve as signal reflectors, and in mobile radio communication systems, where the multipath propagation is due to reflection from buildings, trees, and the other obstacles located between the transmitter and the receiver.

Our discussion on signal design in Section10.1.5 focused on frequency selective channels, where the signal bandwidth W is larger than the coherence bandwidth B_{cb} of the channel. If $W > B_{cb}$, we considered two approaches to signal design. One approach is to subdivide the available bandwidth W into N subchannels such that the bandwidth per channel $\frac{W}{N} < B_{cb}$. In this way, each subchannel is frequency nonselective and the signals in each subchannel satisfy the condition that the symbol interval $T \gg T_m$, where T_m is the multipath spread of the channel. Thus, intersymbol interference is avoided. A second approach is to design the signal to utilize the entire signal bandwidth W and transmit it on a single carrier. In this case, the channel is frequency selective and the multipath components with differential delays of $\frac{1}{W}$ or greater become resolvable.

DS spread spectrum is a particularly effective way to generate a wideband signal for resolving multipath signal components. By separating the multipath components, we may also reduce the effects of fading. For example, in LOS communication systems where there is a direct path and a secondary propagation path resulting from signal reflecting from buildings and surrounding terrain, the demodulator at the receiver may synchronize to the direct-signal component and ignore the existence of the multipath component. In such a case, the multipath component becomes a form of interference (ISI) on the demodulation of subsequent transmitted signals.

ISI can be avoided if we are willing to reduce the symbol rate $\frac{1}{T}$ such that $T \gg T_m$. In this case, we employ a DS spread-spectrum signal with bandwidth W to resolve the

multipath. Thus, the channel is frequency selective and the appropriate channel model is the tapped-delay-line model with time-varying coefficients as shown in Figure 10.4. The optimum demodulator for this channel is a filter matched to the tapped-delay channel model called the RAKE demodulator, as previously described in Section 10.1.5.

10.3.4 Effect of Pulsed Interference and Fading

In Section 10.3.2, we evaluated the effectiveness of a DS spread-spectrum system in the presence of narrowband and broadband interference. We observed that the processing gain and the coding gain provide the means for suppressing the detrimental effects of these types of interference. In this section, we consider the effect of pulsed interference and the effect of fading on the performance of a DS spread-spectrum system.

Let us consider an interfering signal that consists of short bursts of spectrally flat Gaussian noise that covers the entire signal bandwidth. We call this type of an interfering signal *pulsed interference*. It may occur in a CDMA digital cellular system in which a mobile transmitter located near a base station is transmitting at a high power; i.e., operating without power control. Suppose that the interferer is average-power limited, with an average power P_I in the signal bandwidth W. Hence, $I_0 = P_I/W$. The interferer transmits pulses at a power level P_I/β for β percent of the time. Thus, the probability that the interferer is transmitting at a given instant is β. For simplicity, we assume that an interference pulse spans an integer number of bits (or symbols). When the interferer is not transmitting, the transmitted bits are assumed to be received error-free, and when the interferer is transmitting, the probability of error for an uncoded DS spread-spectrum system is

$$\begin{aligned} P(\alpha) &= \frac{\beta}{2}\, Q\left(\sqrt{\frac{2\mathcal{E}_b}{I_0/\beta}}\right) \\ &= \frac{\beta}{2}\, Q\left(\sqrt{\frac{2\beta W/R}{P_I/P_S}}\right) \end{aligned} \tag{10.3.45}$$

where W/R is the processing gain and P_I/P_S is the interference-to-signal power ratio.

Let us consider the value of the duty cycle β that maximizes the probability of error for the communication system. Upon differentiating Equation (10.3.45) with respect to β, we find the worst-case pulse interference occurs when

$$\beta^* = \begin{cases} \frac{0.71}{\mathcal{E}_b/I_0} & \frac{\mathcal{E}_b}{I_0} \geq 0.71 \\ 1, & \frac{\mathcal{E}_b}{I_0} < 0.71 \end{cases} \tag{10.3.46}$$

and the corresponding probability of error is

$$P_2 = \begin{cases} \frac{0.082}{\mathcal{E}_b/I_0} = \frac{0.082 P_I/P_s}{W/R}, & \frac{\mathcal{E}_b}{I_0} \geq 0.71 \\ Q\left(\sqrt{\frac{2\mathcal{E}_b}{I_0}}\right) = Q\left(\sqrt{\frac{2W/R}{P_I/P_S}}\right), & \frac{\mathcal{E}_b}{I_0} < 0.71 \end{cases} \tag{10.3.47}$$

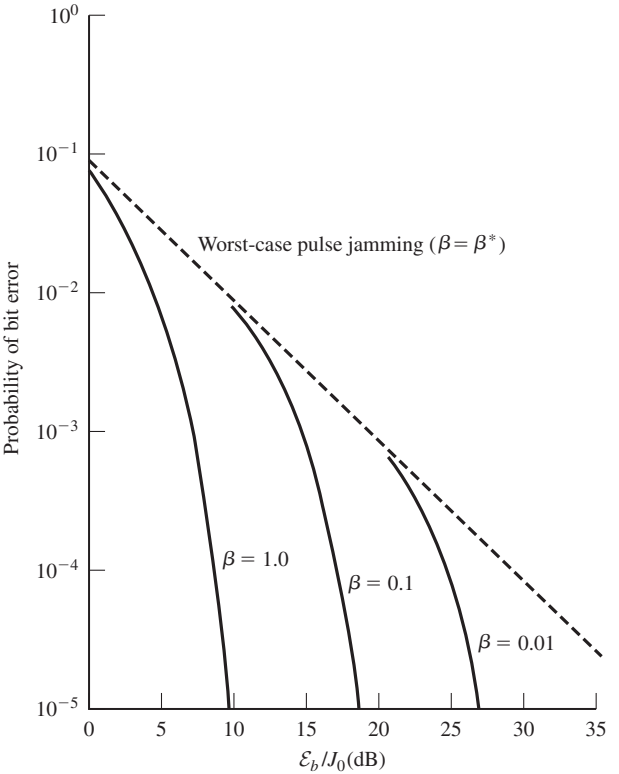

Figure 10.45 Performance of DS binary PSK with pulse interference.

The error rate performance given by (10.3.45) for $\beta = 1.0, 0.1$, and 0.01 along with the worst-case performance based on β^* is plotted in Figure 10.45. When we compare the error rate for continuous wideband Gaussian noise interference ($\beta = 1$) with worst-case pulse interference, we find a large difference in performance; e.g., approximately 40 dB at an error rate of 10^{-6}. This is, indeed, a large penalty.

We should point out that practical consideration may prohibit an interferer from achieving small values of β at a high peak power. Nevertheless, the error probability given by Equation (10.3.47) serves as an upper bound on the performance of uncoded binary PSK with worst-case pulse interference. Clearly, the performance of the DS spread-spectrum system in the presence of pulse interference is poor.

If we simply add coding to the DS spread-spectrum system, the performance in SNR is improved by an amount equal to the coding gain, which in most cases is limited to less than 10 dB. The reason that the addition of coding does not improve the performance significantly is that the interfering signal pulse duration (duty cycle) may be selected to affect many consecutive coded bits. Consequently, the code word error probability is high due to the burst characteristics of the interference.

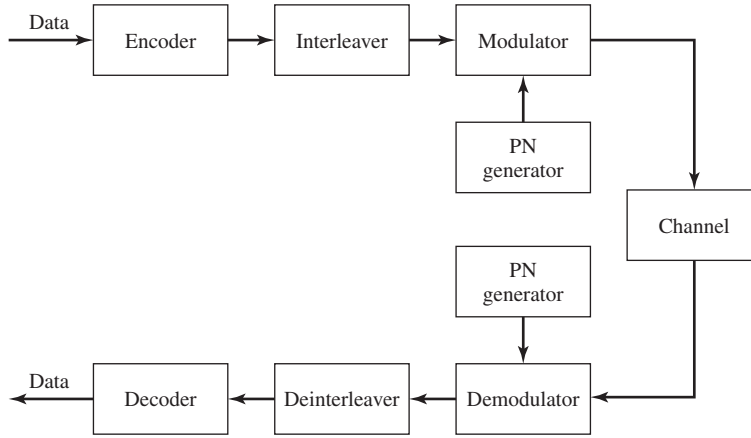

Figure 10.46 Block diagram of communication system.

In order to improve the performance of the coded DS spread-spectrum system, we should interleave the coded bits prior to transmission over the channel. The effect of interleaving is to make the coded bits that are affected by the interferer statistically independent. Figure 10.46 illustrates a block diagram of a DS spread-spectrum system that employs coding and interleaving. By selecting a sufficiently long interleaver so that the burst characteristics of the interference are eliminated, the penalty in performance due to pulse interference is significantly reduced; e.g., to the range of 3–5 dB for conventional binary block or convolutional codes.

Signal fading has a similar effect on the performance of the DS spread-spectrum system. In a frequency nonselective channel, when the signal is in a deep fade, the communication system experiences a burst of errors. By use of coding and interleaving the coded bits so that the fading on the bits in any code word is statistically independent (through interleaving, the bits in a burst of errors belong to different code words), the error-rate performance of the system decreases as the inverse of the SNR raised to the power of the diversity provided by the code. This order of diversity is equal to the Hamming distance $d_{\min}^H$ of the block code (or d_{free}^H of the convolutional code) for soft-decision decoding and $d_{\min}^H/2$ for hard-decision decoding.

10.3.5 Generation of PN Sequences

A pseudorandom or pseudonoise (PN) sequence is a code sequence of 1's and 0's whose autocorrelation has the properties similar to those of white noise. In this section, we briefly describe the construction of some PN sequences and their autocorrelation and crosscorrelation properties. For a comprehensive treatment of this subject, the interested reader may refer to the book by Golomb (1967) and the paper by Sarwate and Pursley (1980).

By far the most widely known binary PN code sequences are the maximum-length shift-register sequences. A maximum-length shift-register sequence, or m-sequence for

TABLE 10.3 SHIFT-REGISTER CONNECTIONS FOR GENERATING ML SEQUENCES

m	Stages connected to modulo-2 adder	m	Stages connected to modulo-2 adder	m	States connected to modulo-2 adder
2	1, 2	13	1, 10, 11, 13	24	1, 18, 23, 24
3	1, 3	14	1, 5, 9, 14	25	1, 23
4	1, 4	15	1, 15	26	1, 21, 25, 26
5	1, 4	16	1, 5, 14, 16	27	1, 23, 26, 27
6	1, 6	17	1, 15	28	1, 26
7	1, 7	18	1, 12	29	1, 28
8	1, 5, 6, 7	19	1, 15, 18, 19	30	1, 8, 29, 30
9	1, 6	20	1, 18	31	1, 29
10	1, 8	21	1, 20	32	1, 11, 31, 32
11	1, 10	22	1, 22	33	1, 21
12	1, 7, 9, 12	23	1, 19	34	1, 8, 33, 34

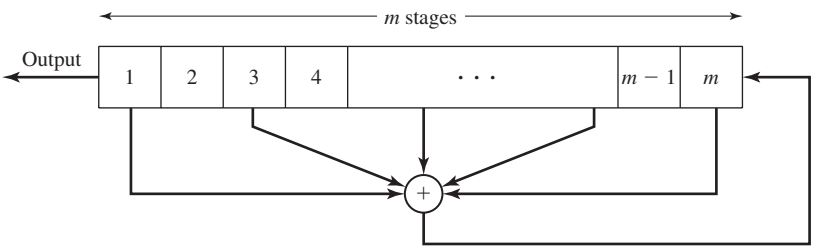

Figure 10.47 General m-stage shift register with linear feedback.

short, has a length $L = 2^m - 1$ bits and is generated by an m-stage shift register with linear feedback as illustrated in Figure 10.47. The sequence is periodic with period L. Each period has a sequence of 2^{m-1} ones and $2^{m-1} - 1$ zeros. Table 10.3 lists shift register connections for generating maximum-length sequences.

In DS spread-spectrum applications, the binary sequence with elements $\{0, 1\}$ is mapped into a corresponding binary sequence with elements $\{-1, 1\}$. We shall call the equivalent sequence $\{c_n\}$ with elements $\{-1, 1\}$ a *bipolar sequence*.

An important characteristic of a periodic PN sequence is its autocorrelation function which is usually defined in terms of the bipolar sequences $\{c_n\}$ as

$$R_c(m) = \sum_{n=1}^{L} c_n c_{n+m}, \quad 0 \le m \le L - 1 \tag{10.3.48}$$

where L is the period of the sequence. Since the sequence $\{c_n\}$ is periodic with period L, the autocorrelation sequence $\{R_c(m)\}$ is also periodic with period L.

Ideally, a PN sequence should have an autocorrelation function that has correlation properties similar to white noise. That is, the ideal autocorrelation sequence for $\{c_n\}$ is $R_c(0) = L$ and $R_c(m) = 0$ for $1 \le m \le L - 1$. In the case of m-sequences, the

autocorrelation sequence is

$$R_c(m) = \begin{cases} L, & m = 0 \\ -1, & 1 \le m \le L-1 \end{cases} \tag{10.3.49}$$

For long m-sequences, the size of the off-peak values of $R_c(m)$ relative to the peak value $R_c(0)$; i.e., the ratio $R_c(m)/R_c(0) = -1/L$, is small and, from a practical viewpoint, inconsequential. Therefore, m-sequences are very close to ideal PN sequences when viewed in terms of their autocorrelation function.

In some applications, the crosscorrelation properties of PN sequences are as important as the autocorrelation properties. For example, in CDMA each user is assigned a particular PN sequence. Ideally, the PN sequences among users should be mutually uncorrelated so that the level of interference experienced by one user from transmissions of other users adds on a power basis. However, the PN sequences used in practice by different users exhibit some correlation.

To be specific, let us consider the class of m-sequences. It is known that, the periodic cross correlation function between a pair of m-sequences of the same period, can have relatively large peaks. Table 10.4 lists the peak magnitude $R_{\max}$ for the periodic crosscorrelation between pairs of m-sequences for $3 \le m \le 12$. Also listed in Table 10.4 is the number of m-sequences of length $L = 2^m - 1$ for $3 \le m \le 12$. We observe that the number of m-sequences of length L increases rapidly with m. We also observe that, for most sequences, the peak magnitude $R_{\max}$ of the crosscorrelation function is a large percentage of the peak value of the autocorrelation function. Consequently, m-sequences are not suitable for CDMA communication systems. Although it is possible to select a small subset of m-sequences that have relatively smaller crosscorrelation peak value than $R_{\max}$, the number of sequences in the set is usually too small for CDMA applications.

Methods for generating PN sequences with better periodic crosscorrelation properties than m-sequences have been developed by Gold (1967, 1968) and by

TABLE 10.4 PEAK CROSSCORRELATIONS OF m SEQUENCES AND GOLD SEQUENCES

	m sequences				Gold sequences	
m	$L = 2^{m-1}$	Number	Peak cross-correlation $R_{\max}$	$R_{\max}/R(0)$	$R_{\max}$	$R_{\min}/R(0)$
3	7	2	5	0.71	5	0.71
4	15	2	9	0.60	9	0.60
5	31	6	11	0.35	9	0.29
6	63	6	23	0.36	17	0.27
7	127	18	41	0.32	17	0.13
8	255	16	95	0.37	33	0.13
9	511	48	113	0.22	33	0.06
10	1023	60	383	0.37	65	0.06
11	2047	176	287	0.14	65	0.03
12	4095	144	1407	0.34	129	0.03

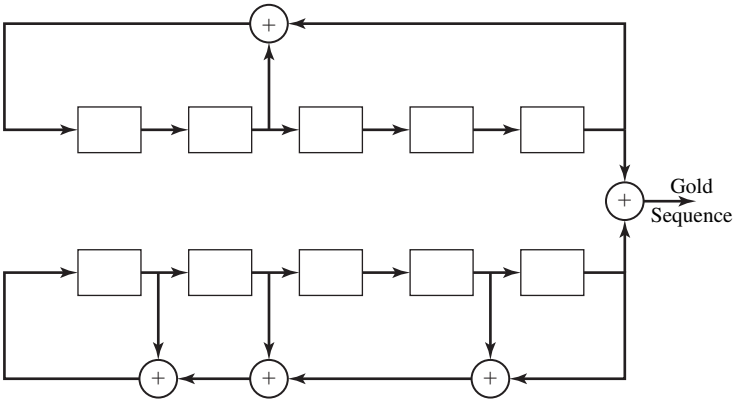

Figure 10.48 Generation of Gold sequences of length 31.

Kasami (1966). Gold sequences are constructed by taking a pair of specially selected m-sequences, called *preferred* m-*sequences,* and forming the modulo-2 sum of the two sequences, for each of L cyclicly shifted versions of one sequence relative to the other sequence. Thus, L Gold sequences are generated as illustrated in Figure 10.48. For m odd, the maximum value of the crosscorrelation function between any pair of Gold sequences is $R_{\max} = \sqrt{2L}$. For m even, $R_{\max} = \sqrt{L}$.

Kasami (1966) described a method for constructing PN sequences by decimating an m-sequence. In Kasami's method of construction, every $2^{m/2}+1$ bit of an m-sequence is selected. This method of construction yields a smaller set of PN sequences compared with Gold sequences, but their maximum crosscorrelation value is $R_{\max} = \sqrt{L}$.

It is interesting to compare the peak value of the crosscorrelation function for Gold sequences and for Kasami sequences with a known lower bound for the maximum crosscorrelation between any pair of binary sequences of length L. Given a set of N sequences of period L, a lower bound on their maximum crosscorrelation is

$$R_{\max} \geq L\sqrt{\frac{N-1}{NL-1}} \tag{10.3.50}$$

which, for large values of L and N, is well approximated as $R_{\max} \geq \sqrt{L}$. Hence, we observe that Kasami sequences satisfy the lower bound and, hence, they are optimal. On the other hand, Gold sequences with m odd have a $R_{\max} = \sqrt{2L}$. Hence, they are slightly suboptimal.

Besides the well-known Gold sequences and Kasami sequences, there are other binary sequences that are appropriate for CDMA applications. The interested reader is referred to the papers by Scholtz (1979), Olsen (1977), and Sarwate and Pursley (1980).

Finally, we should point out that although we discussed the periodic crosscorrelation function between pairs of periodic sequences, many practical CDMA systems use aperiodic sequences that have impulse-like autocorrelation function. In

such a case, it is partial-period crosscorrelation between two sequences that is important. The partial-period crosscorrelation properties of periodic PN sequences has been widely investigated and discussed in the technical literature.

10.3.6 Frequency-Hopped Spread Spectrum

In frequency-hopped (FH) spread spectrum, the available channel bandwidth W is subdivided into a large number of nonoverlapping frequency slots. In any signaling interval the transmitted signal occupies one or more of the available frequency slots. The selection of the frequency slot (s) in each signal interval is made pseudorandomly according to the output from a PN generator.

A block diagram of the transmitter and receiver for an FH spread-spectrum system is shown in Figure 10.49. The modulation is either binary or M-ary FSK (MFSK). For example, if binary FSK is employed, the modulator selects one of two frequencies, say f_0 or f_1, corresponding to the transmission of a 0 for a 1. The resulting binary FSK signal is translated in frequency by an amount that is determined by the output sequence from a PN generator, which is used to select a frequency f_c that is synthesized by the frequency synthesizer. This frequency is mixed with the output of the FSK modulator and the resultant frequency-translated signal is transmitted over the channel. For example, by taking m bits from the PN generator, we may specify $2^m - 1$ possible carrier frequencies. Figure 10.50 illustrates an FH signal pattern.

At the receiver, there is an identical PN sequences generator, synchronized with the received signal, which is used to control the output of the frequency synthesizer. Thus, the pseudorandom frequency translation introduced at the transmitter is removed at the demodulator by mixing the synthesizer output with the received signal. The resultant signal is then demodulated by means of an FSK demodulator. A signal for maintaining synchronism of the PN sequence generator with the FH received signal is usually extracted from the received signal.

Although binary PSK modulation generally yields better performance than binary FSK, it is difficult to maintain phase coherence in the synthesis of the frequencies used in the hopping pattern and, also, in the propagation of the signal over the channel

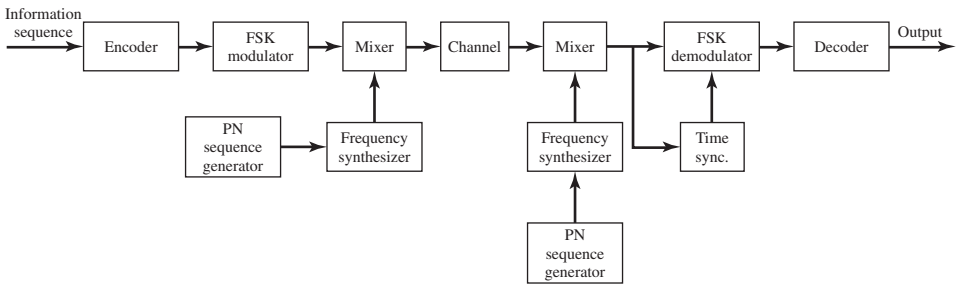

Figure 10.49 Block diagram of an FH spread-spectrum system.

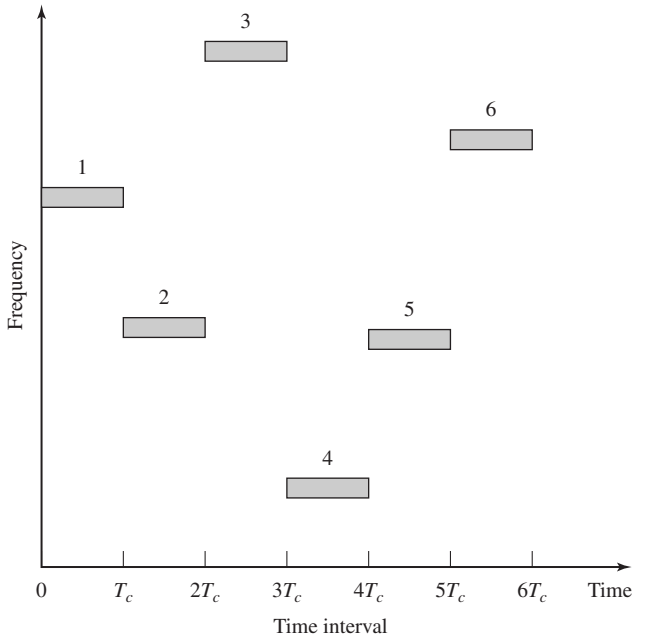

Figure 10.50 An example of an FH pattern.

as the signal is hopped from one frequency to the another over a wide bandwidth. Consequently, FSK modulation with noncoherent demodulation is usually employed in FH spread-spectrum systems.

The frequency-hopping rate, denoted as R_h, may be selected to be either equal to the symbol rate, or lower than the symbol rate, or higher than the symbol rate. If R_h is equal to or lower than the symbol rate, the FH system is called a *slow-hopping* system. If R_h is higher than the symbol rate; i.e., there are multiple hops/symbol, the FH system is called a *fast-hopping* system. However, there is a penalty incurred in subdividing an information symbol into several frequency-hopped elements, because the energy from these separate elements is combined noncoherently.

FH spread-spectrum signals may be used in CDMA where many users share a common bandwidth. In some cases, an FH signal is preferred over a DS spread-spectrum signal because of the stringent synchronization requirements inherent in DS spread-spectrum signals. Specifically, in a DS system, timing and synchronization must be established to within a fraction of a chip interval $T_c = 1/W$. On the other hand, in an FH system, the chip interval T_c is the time spent in transmitting a signal in a particular frequency slot of bandwidth $B \ll W$. But this interval is approximately $1/B$, which is much larger than $1/W$. Hence, the timing requirements in an FH system are not as stringent as in a DS system.

Next, we shall evaluate the performance of FH spread-spectrum systems under the condition that the system is either slow hopping or fast hopping.

Slow Frequency-Hopping Systems. Let us consider a slow frequency-hopping system in which the hop rate $R_h = 1$ hop/bit. We assume that the interference on the channel is broadband and is characterized as AWGN with power-spectral density I_0. Under these conditions, the probability of error for the detection of noncoherently demodulated binary FSK is

$$P_b = \frac{1}{2} e^{-\rho_b/2} \tag{10.3.51}$$

where $\rho_b = \mathcal{E}_b/I_0$ is the SNR/bit.

As in the case of a DS spread-spectrum system, we observe that $\mathcal{E}_b$, the energy/bit, can be expressed as $\mathcal{E}_b = P_S T_b = P_S/R$, where P_S is the average transmitted power and R is the bit rate. Similarly, $I_0 = P_I/W$, where P_I is the average power of the broadband interference and W is the available channel bandwidth. Therefore, the SNR ρ_b can be expressed as

$$\rho_b = \frac{\mathcal{E}_b}{I_0} = \frac{W/R}{P_I/P_S} \tag{10.3.52}$$

where W/R is the processing gain and P_I/P_S is the interference margin for the FH spread-spectrum signal.

Slow FH spread-spectrum systems are particularly vulnerable to partial-band interference that may result in FH CDMA systems. To be specific, suppose that the partial-band interference is modeled as a zero-mean Gaussian random process with a flat power-spectral density over a fraction of the total bandwidth W and zero in the remainder of the frequency band. In the region or regions where the power-spectral density is nonzero, its value is $\mathcal{S}_I(f) = I_0/\beta$, where $0 < \beta \leq 1$. In other words, the interference average power P_I is assumed to be constant.

Let us consider the worst-case partial-band interference by selecting the value of β that maximizes the error probability. In an uncoded slow-hopping system with binary FSK modulation and noncoherent detection, the transmitted frequencies are selected with uniform probability in the frequency band W. Consequently, the received signal will be corrupted by interference with probability β. When the interference is present, the probability of error is $1/2 \exp(-\beta\rho_b/2)$ and when it is not, the detection of the signal is assumed to be error free. Therefore, the average probability of error is

$$\begin{aligned} P_b(\beta) &= \frac{\beta}{2} e^{-\beta\rho_b/2} \\ &= \frac{\beta}{2} exp\left(-\frac{\beta W/R}{2P_I/P_S}\right) \end{aligned} \tag{10.3.53}$$

Figure 10.51 illustrates the error rate as a function of ρ_b for several values of β. By differentiating $P_b(\beta)$, and solving for the value of β that maximizes $P_b(\beta)$, we find that

$$\beta^* = \begin{cases} 2/\rho_b, & \rho_b \geq 2 \\ 1, & \rho_b < 2 \end{cases} \tag{10.3.54}$$

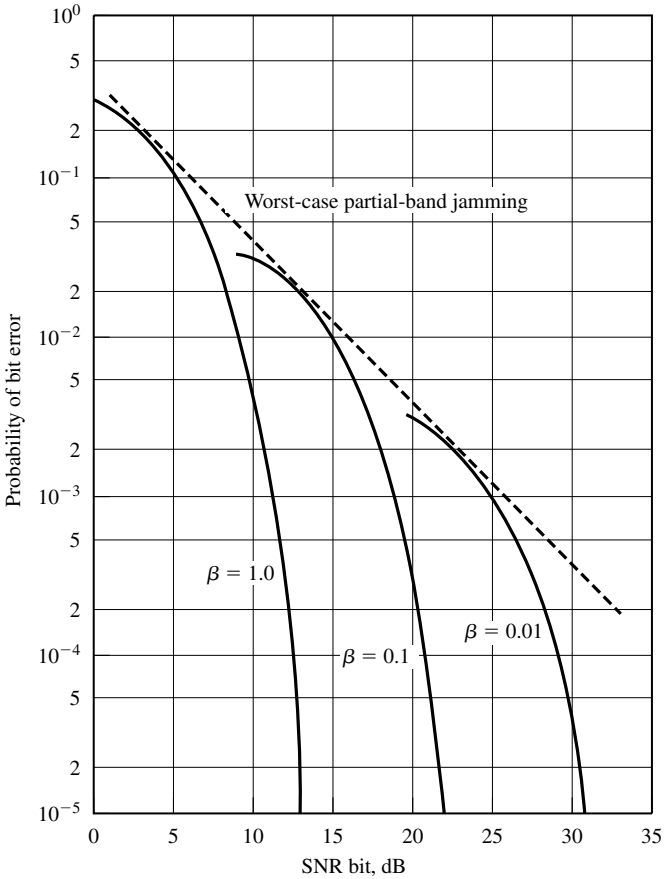

Figure 10.51 Performance of binary FSK with partial-band interference.

The corresponding error probability for the worst-case partial-band interference is

$$P_b = \begin{cases} e^{-1}/\rho_b, & \rho_b \geq 2 \\ \frac{1}{2}e^{-\rho_b/2}, & \rho_b < 2 \end{cases} \tag{10.3.55}$$

which is also shown in Figure 10.51. Whereas the error probability decreases exponentially for full-band interference as given by Equation (10.3.51), the error probability for worst-case partial-band interference decreases only inversely with $\mathcal{E}_b/I_0$. This result is similar to the error probability for DS spread-spectrum signals in the presence of pulse interference. It is also similar to the error probability for binary FSK in a Rayleigh fading channel.

In our discussion of signal design for efficient and reliable communication over a fading channel in Section 10.1, we found that diversity, which can be obtained by simple

repetition of the transmitted information bit on different frequencies (or by means of block or convolutional coding), provides a significant improvement in performance relative to uncoded signal transmission. It should not be surprising that the same type of signal coding is also effective on partial-band interference channels. In fact, it has been shown by Viterbi and Jacobs (1975) that by optimizing the code design for the partial-band interference, the communication system can achieve an average bit-error probability of

$$P_b = e^{-\rho_b/4} \tag{10.3.56}$$

Therefore, the probability of error achieved with the optimum code design decreases exponentially with an increase in SNR and is within 3 dB of the performance obtained in an AWGN channel. Thus, the penalty due to partial-band interference is reduced significantly.

Fast Frequency-Hopping Systems. In fast FH systems, the frequency-hop rate R_h is some multiple of the symbol rate. Basically, each (M-ary) symbol interval is subdivided into N subintervals, which are called *chips* and one of M frequencies is transmitted in each subinterval. Fast frequency-hopping systems are particularly attractive for military communications. In such systems, the hop rate R_h may be selected sufficiently high so that a potential intentional interferer does not have sufficient time to detect the presence of the transmitted frequency and to synthesize a jamming signal that occupies the same bandwidth.

To recover the information at the receiver, the received signal is first de-hopped by mixing it with the hopped carrier frequency. This operation removes the hopping pattern and brings the received signal in all subintervals (chips) to a common frequency band that encompasses the M possible transmitted frequencies. The signal in each subinterval is then passed through the M matched filters (or correlators) tuned to the M possible transmitted frequencies which are sampled at the end of each subinterval and passed to the detector. The detection of the FSK signals is noncoherent. Hence, decisions are based on the magnitude of the matched filter (or correlator) outputs.

Since each symbol is transmitted over N chips, the decoding may be performed either on the basis of hard decisions or soft decisions. The following example illustrates the decoding based on hard decisions.

Example 10.3.5

Suppose that binary FSK is used to transmit binary symbols, and each symbol is transmitted over N frequency hops, where N is odd. Determine the probability of error for an AWGN channel if hard-decision decoding is used.

Solution The probability of error for noncoherent detection of binary FSK for each hop is

$$p = \frac{1}{2} e^{-\rho_b/2N} \tag{10.3.57}$$

where

$$\frac{\rho_b}{N} = \frac{\mathcal{E}_b/N}{N_0} \tag{10.3.58}$$

is the SNR/chip and $\mathcal{E}_b$ is the total bit energy. The decoder decides in favor of the transmitted frequency that is larger in at least $(N+1)/2$ chips. Thus, the decision is made on the basis of a majority vote given the decisions on the N chips. Consequently, the probability of a bit error is

$$P_b = \sum_{m=(N+1)/2}^{N} \binom{N}{m} p^m (1-p)^{N-m} \tag{10.3.59}$$

where p is given by Equation (10.3.57). We should note that the error probability P_b for hard-decision decoding of the N chips will be higher than the error probability for a single hop/bit FSK system, which is given by Equation (10.3.51), when the SNR/bit ρ_b is the same in the two systems (see Problem 10.20).

The alternative to hard-decision decoding is soft-decision decoding in which the magnitudes (or magnitudes squared) of the corresponding matched-filter outputs are summed over the N chips and a single decision is made based on the frequency giving the largest output. For example, if binary orthogonal FSK is used to transmit the information, the two soft-decision metrics for the N chips based on square-law combining are

$$\begin{aligned} DM_1 &= \sum_{k=1}^{N} \left| \frac{\mathcal{E}_b}{N} + \nu_{1k} \right|^2 \\ DM_2 &= \sum_{k=1}^{N} |\nu_{2k}|^2 \end{aligned} \tag{10.3.60}$$

where $\{\nu_{1k}\}$ and $\{\nu_{2k}\}$ are the noise components from the two matched filters for the N chips. Since frequency f_1 is assumed to have been transmitted, a decision error occurs when $DM_2 > DM_1$. The probability of this event error for additive Gaussian noise may be obtained in closed form, although its derivation is cumbersome. The final result is (see Appendix A)

$$P_b = \frac{1}{2^{2N-1}} e^{-\rho_b/2} \sum_{i=0}^{N-1} K_i \left(\frac{\rho_b}{2} \right)^i \tag{10.3.61}$$

where the set $\{K_i\}$ are constants, which may be expressed as

$$K_i = \frac{1}{i!} \sum_{r=0}^{N-1-i} \binom{2N-1}{r} \tag{10.3.62}$$

The error probability for soft-decision decoding given by Equation (10.3.61) is lower than that for hard-decision decoding given by Equation (10.3.59) for the same $\mathcal{E}_b/N_0$. The difference in performance is the loss in hard-decision decoding. However, Equation (10.3.62) is higher than the error probability for single-hop FSK, which is given by Equation (10.3.51) for the AWGN channel. The difference in performance between Equation (10.3.51) and Equation (10.3.61) for the same SNR is due to the

noncoherent (square-law) combining at the decoder. This loss is usually called the *noncoherent combining loss* of the system.

If soft-decision decoding is used in the presence of partial-band interference, it is important to scale (or normalize) the matched-filter outputs in each hop, so that a strong interference that falls within the transmitted signal band in any hop does not dominate the output of the combiner. A good strategy in such a case is to normalize, or clip, the matched-filter outputs from each hop if their values exceed some threshold that is set near (slightly above) the mean of the signal-plus-noise power level. Alternatively, we may monitor the noise power level and scale the matched filter outputs for each hop by the reciprocal of the noise power level. Thus, the noise power levels from the matched filter outputs are normalized. Therefore, with proper scaling, a fast FH spread-spectrum system will not be as vulnerable to partial-band interference because the transmitted information/bit is distributed (or spread) over N frequency hops.

Applications of FH Spread Spectrum. FH spread spectrum is a viable alternative to DS spread spectrum for protection against narrowband and broadband interference that is encountered in CDMA. In CDMA systems based on frequency hopping each transmitter-receiver pair is assigned its own pseudorandom frequency-hopping pattern. Aside from this distinguishing feature, the transmitters and receivers of all users may be identical; i.e., they have identical encoders, decoders, modulators, and demodulators.

CDMA systems based on FH spread-spectrum signals are particularly attractive for mobile (land, air, sea) users because timing (synchronization) requirements are not as stringent as in a DS spread-spectrum system. In addition, frequency-synthesis techniques and associated hardware have been developed that make it possible to frequency-hop over bandwidths that are significantly larger, by one or more orders of magnitude, than those currently possible with DS spread-spectrum signals. Consequently, larger processing gains are possible by FH, which more than offset the loss in performance inherent in noncoherent detection of the FSK-type signals.

FH is also effective against intentional interference. As we have described above, an FH M-ary ($M \geq 2$) FSK system that employs coding, or simply repeats the information symbol on multiple hops (repetition coding), is very effective against a partial-band interference. As a consequence, the interferer's threat is reduced to that of an equivalent broadband noise interference whose transmitter power is spread across the channel bandwidth W.

10.3.7 Synchronization of Spread-Spectrum Systems

Time synchronization of the receiver to the received spread-spectrum signal may be separated into two distinct phases. There is an initial acquisition phase, during which time the receiver establishes time synchronization by detecting the presence of a special initial acquisition sequence. The initial acquisition phase is followed by the transmission of data, during which period the receiver must track the signal timing.

Acquisition Phase. In a DS spread-spectrum system, the PN code sequence [illegible] small fraction of the chip interval $T_c = 1/W$.

The problem of initial synchronization may be viewed as one in which we attempt to synchronize the receiver clock to the transmitter clock. Usually, extremely accurate and stable time clocks are used in spread-spectrum systems in order to reduce the time uncertainty between the receiver clock and the transmitter clock. Nevertheless, there is always an initial timing uncertainty that is due to propagation delay in the transmission of the signal through the channel. This is especially a problem when communication is taking place between two mobile users. In any case, the usual procedure for establishing initial synchronization is for the transmitter to send a known pseudorandom sequence to the receiver. The receiver is continuously in a search mode looking for this sequence in order to establish initial synchronization.

Suppose that the initial timing uncertainty is T_u seconds and the chip duration is T_c. Since initial synchronization takes place in the presence of additive noise and, perhaps other interference, it is necessary to dwell for $T_d = NT_c$ sec in order to test synchronism at each time instant, where N is some positive integer. If we search over the time uncertainty interval in (coarse) time steps of $T_c/2$, then the time required to establish initial synchronization is

$$T_{\text{init sync}} = \frac{T_u}{T_c/2} T_d = 2NT_u$$

Clearly, the synchronization sequence transmitted to the receiver must be at least as long as $2NT_c$ sec in order for the receiver to have sufficient time to perform the necessary search in a serial fashion.

In principle, matched filtering or crosscorrelation are optimum methods for establishing initial synchronization in the presence of additive Gaussian noise. A filter matched to the known data waveform generated from the known pseudorandom sequence continuously compares its output with a predetermined threshold. When the threshold is exceeded, initial synchronization is established and the demodulator enters the "data receive" mode.

Alternatively, we may implement a *sliding correlator* as shown in Figure 10.52. The correlator cycles through the time uncertainty, usually in discrete-time intervals of $T_c/2$ seconds or less. The crosscorrelation is performed over the time interval NT_c, where N is the number of chips in the synchronization sequence, and the correlator

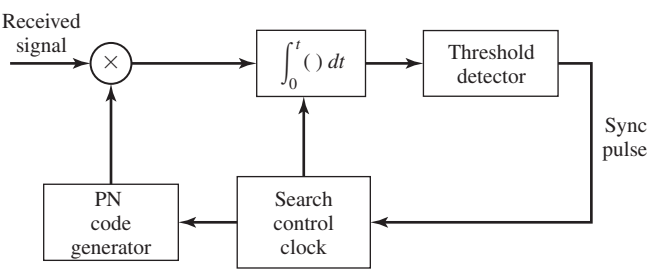

Figure 10.52 A sliding correlator for DS signal acquisition.

output is compared with a threshold to determine if the known signal sequence is present. If the threshold is not exceeded, the known reference sequence is advanced by $T_c/2$ sec and the correlation process is repeated. These operations are performed until a signal is detected or until the search has been performed over the time uncertainty interval T_u. In the case of the latter outcome, the search process is repeated.

A similar procedure may be used for FH signals. In this case, the problem is to synchronize the PN code sequence generated at the receiver that controls the hopped-frequency pattern. To accomplish this initial synchronization, a known frequency-hopped signal is transmitted to the receiver. The initial acquisition system at the receiver looks for this known FH signal pattern. For example, a band of matched filters tuned to the transmitted frequencies in the known pattern may be employed. Their outputs must be properly delayed, envelope or square-law detected, weighted, if necessary, and added to produce the signal output which is compared with a threshold. A signal present (signal acquisition) is declared when the threshold is exceeded. The search process is usually performed continuously in time until a threshold is exceeded. A block diagram illustrating their signal acquisition scheme is given in Figure 10.53. As an alternative, a single matched-filter and envelope detector may be used preceded by a frequency-hopping pattern generator and followed by a threshold detector. This configuration,

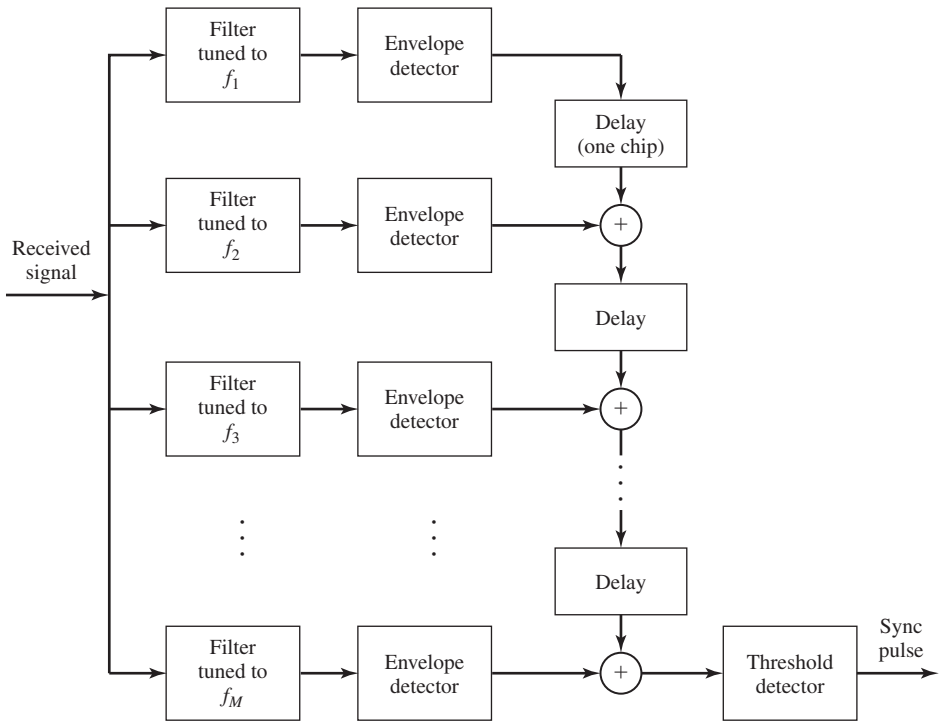

Figure 10.53 System for acquisition of an FH signal.

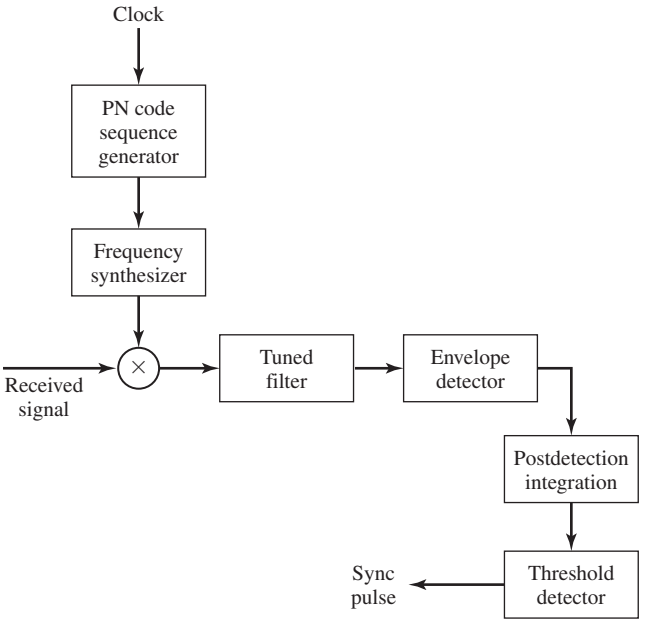

Figure 10.54 Alternative system for acquisition of an FH signal.

which is shown in Figure 10.54, is based on a serial search and is akin to the sliding correlator for DS spread-spectrum signals.

The sliding correlator for DS signals and its counterpart shown in Figure 10.54 for FH signals basically perform a serial search that is generally time consuming. As an alternative, one may employ some degree of parallelism by having two or more such correlators operating in parallel and searching over nonoverlapping time slots. In such a case, the search time is reduced at the expense of a more complex and costly implementation.

During the search mode, there may be false alarms that occur occasionally due to additive noise and other interference. To handle the occasional false alarms, it is necessary to have an additional method or circuit that checks to confirm that the received signal at the output of the correlator remains above the threshold. With such a detection strategy, a large noise pulse that causes the matched-filter output to exceed the threshold will have only a transient effect on synchronization, since the matched-filter output will fall below the threshold once the large noise pulse passes through the filter. On the other hand, when a signal is present, the correlator or matched-filter output will remain above the threshold for the duration of their transmitted signal. Thus, if confirmation fails, the search for signal synchronization is resumed.

In the above discussion, we considered only time uncertainty in establishing initial synchronization. However, another aspect of initial synchronization is frequency uncertainty. If the transmitter and, or, the receiver are mobile, the relative velocity between them results in a Doppler frequency shift in the received signal relative to the transmitted signal. Since the receiver does not know the relative velocity, a priori, the Doppler

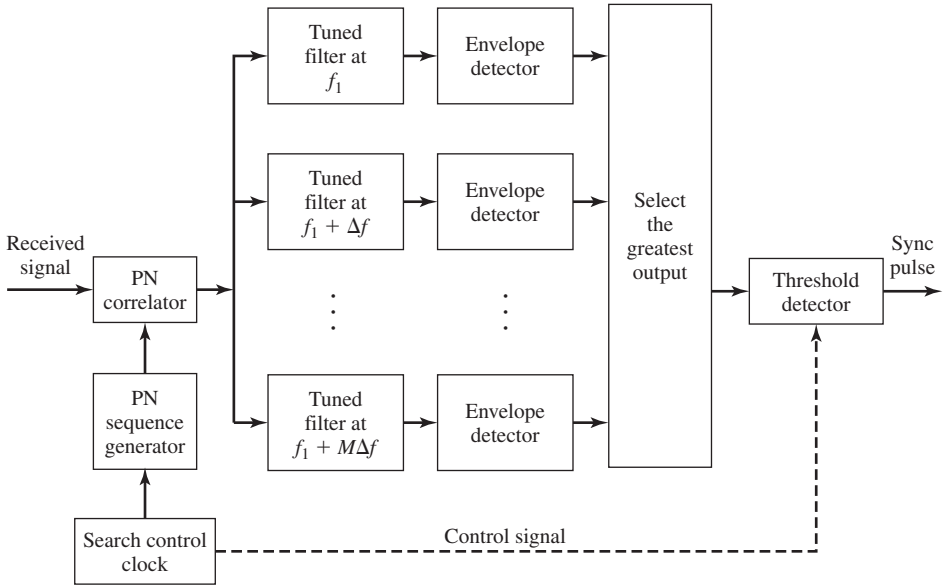

Figure 10.55 Initial search for the Doppler frequency offset in a DS system.

frequency-shift is unknown and must be determined by means of a frequency-search method. Such a search is usually accomplished in parallel over a suitably quantized frequency uncertainty interval and serially over the time uncertainty interval. A block diagram of this scheme for DS spread-spectrum signals is shown in Figure 10.55. Appropriate Doppler frequency-search methods can also be devised for FH signals.

Tracking. Once the signal is acquired, the initial synchronization process is stopped and fine synchronization and tracking begins. The tracking maintains the PN code generator at the receiver in synchronism with the received signal. Tracking includes fine-chip synchronization.

For a DS spread-spectrum signal, tracking is usually performed by means of a tracking loop, called a *delay-locked loop* (DLL), as shown in Figure 10.56. In this tracking loop, the received signal is applied to two multipliers, where it is multiplied by two outputs from the local PN code generator which are delayed relative to each other by an amount of $2\delta \leq T_c$. Thus, the product signals are the crosscorrelations between the received signal and the PN sequence at the two values of delay. These products are bandpass filtered, envelope (or square-law) detected, and then subtracted. This difference signal is applied to the loop filter that drives the voltage-controlled clock (VCC). The VCC output serves as the clock for the PN code signal generator.

If the synchronism is not exact, the filtered output from one correlator will exceed the other and the VCC will be appropriately advanced or delayed. At the equilibrium point, the two filtered-correlator outputs will be equally displaced from the peak value, and the PN code generator will be synchronized to the received signal

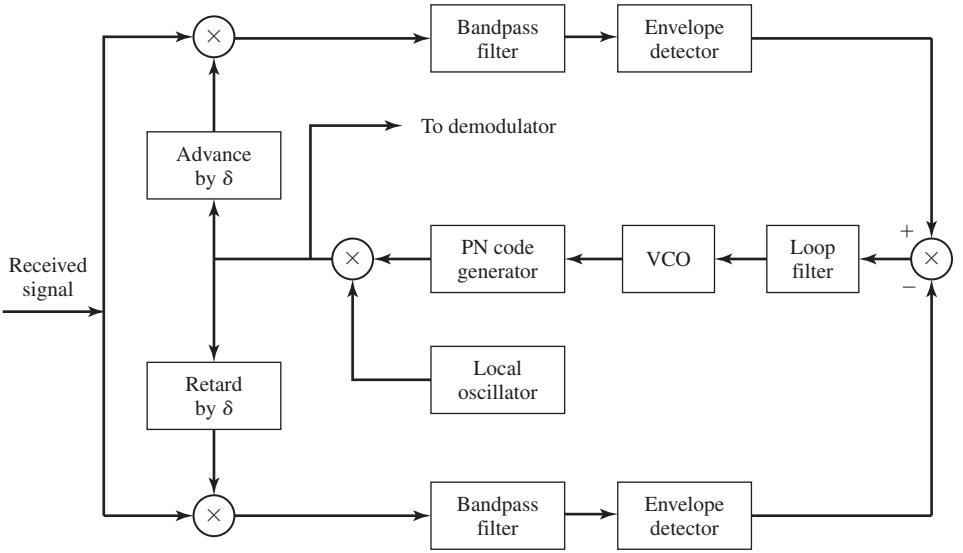

Figure 10.56 DLL for PN code tracking.

which is fed to the demodulator. We observe that this implementation of the DLL for tracking the DS signal is equivalent to the early–late gate bit-tracking synchronizer previously described in Section 7.8.1.

An alternative method for time tracking a DS signal is to use a tau-dither loop (TDL), which is illustrated by the block diagram in Figure 10.57. The TDL employs only a single "arm" instead of the two "arms" shown in Figure 10.56. By providing a suitable gating waveform, it is possible to make this single "arm" implementation appear to be equivalent to the two "arm" realization. In this case, the crosscorrelator output is regularly sampled at two values of delay, by stepping the code clock forward and backward in time by an amount δ. The envelope of the crosscorrelation that is

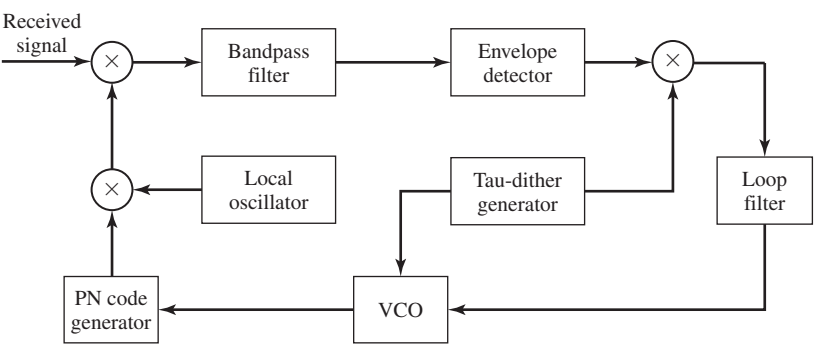

sampled at $\pm\delta$ has an amplitude modulation whose phase relative to the tau-dither modulator determines the sign of the tracking error.

One advantage of the TDL is the less costly implementation resulting from elimination of one of the two arms that are employed in the conventional DLL. A second and less apparent advantage is that the TDL does not suffer from performance degradation that is inherent in the DLL when the amplitude gain in the two arms is not properly balanced.

Both the DLL and the TDL generate an error signal by sampling the signal correlation function at $\pm\delta$ off the peak, as shown in Figure 10.58(a). This generates an error signal as shown in Figure 10.58(b). The analysis of the performance of the DLL is similar to that for the PLL, previously described in Section 5.2. If it were not for the envelope detectors in the two arms of the DLL, the loop resembles a Costas loop. In general, the variance of the time-estimation error in the DLL is inversely proportional to the loop SNR, which depends on the input SNR to the loop and on the loop bandwidth. Its performance is somewhat degraded as in the squaring PLL by the nonlinearities inherent in the envelope detectors, but this degradation is relatively small.

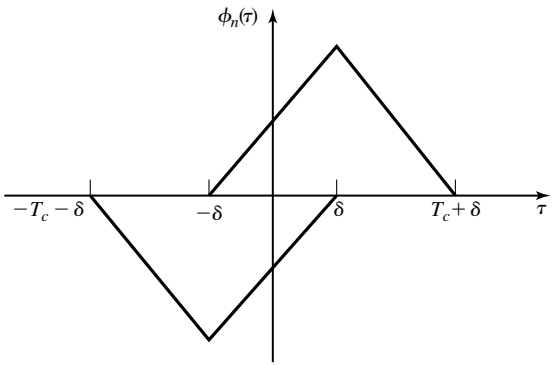

(a)

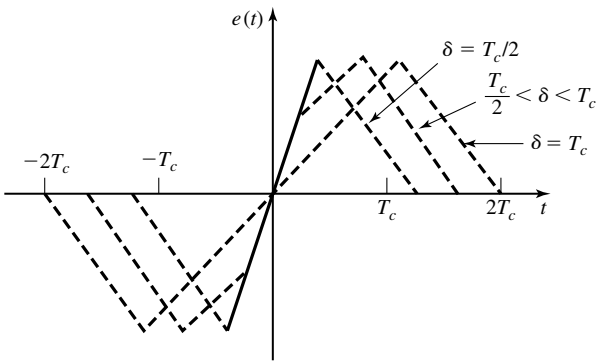

(b)

Figure 10.58 Autocorrelation function and typical error signal for (a) DLL or DLL.

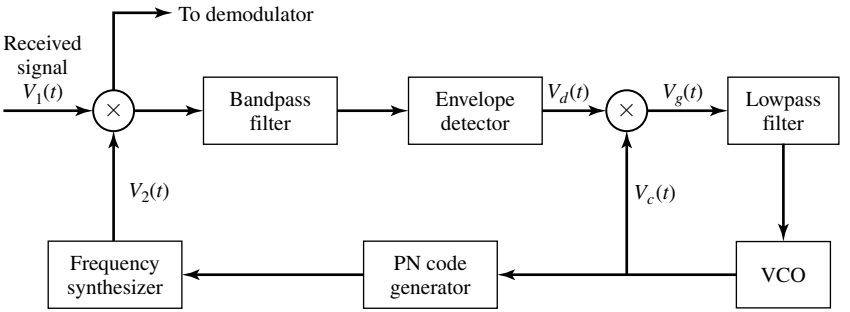

Figure 10.59 Tracking method for FH signals. (From paper by Pickholtz et al.; © 1992 IEEE. Reprinted with permission.)

A tracking method for FH spread-spectrum signals is illustrated in Figure 10.59. This method is based on the premise that, although initial acquisition has been achieved, there is a small timing error between the received signal and the received clock. The bandpass filter is tuned to a single intermediate frequency and its bandwidth is of the order of $1/T_c$, where T_c is the chip interval. Its output is envelope detected and then multiplied by the clock signal to produce a three-level signal, as shown in Figure 10.60,

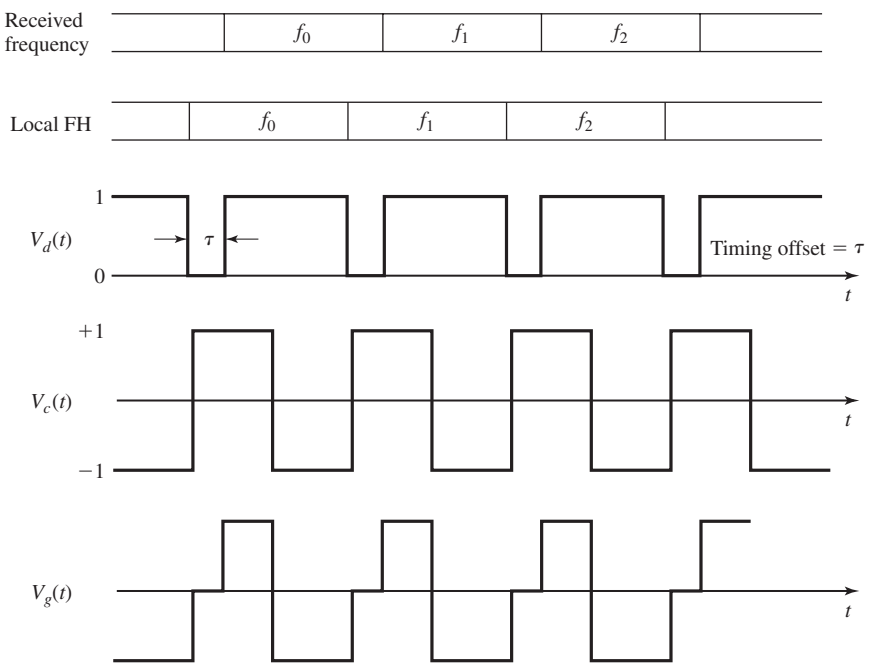

Figure 10.60 Waveforms for the tracking method of FH signals shown in

which drives the loop filter. Note that when the chip transitions from the locally generated sinusoidal waveform do not occur at the same time as the transitions in the incoming received signal, the output of the loop filter will be either negative or positive, depending on whether the VCC is lagging or advanced relative to the timing of the input signal. This error signal from the loop filter will provide the control signal for adjusting the VCC timing signal so as to drive the frequency synthesized FH signal to proper synchronism with the received signal.

10.4 DIGITAL CELLULAR COMMUNICATION SYSTEMS

In this section, we present an overview of two types of digital cellular communication systems that are currently in use. One is the GSM (Global System for Mobile Communication) system that is widely used in Europe and other parts of the world. It employs time-division multiple access (TDMA) to accommodate multiple users. The second is the CDMA system based on Interim Standard 95 (IS-95) that is widely used in North America and some countries in the Far East.

10.4.1 The GSM System

GSM was developed in Europe for the purpose of providing a common digital cellular communication system that would serve all of Europe. It is now widely used in many parts of the world. The GSM system employs the frequency band 890–915 MHz for signal transmission from mobile transmitters to base-station receivers (uplink or reverse link) and the frequency band 935–960 MHz for transmission from the base stations to the mobile receivers (downlink or forward link). The two 25 MHz-frequency bands are each subdivided into 125 channels, where each channel has a bandwidth of 200 KHz. To reduce interference from transmissions in adjacent cells, different sets of frequencies are assigned to adjacent base stations and frequencies are reused according to some

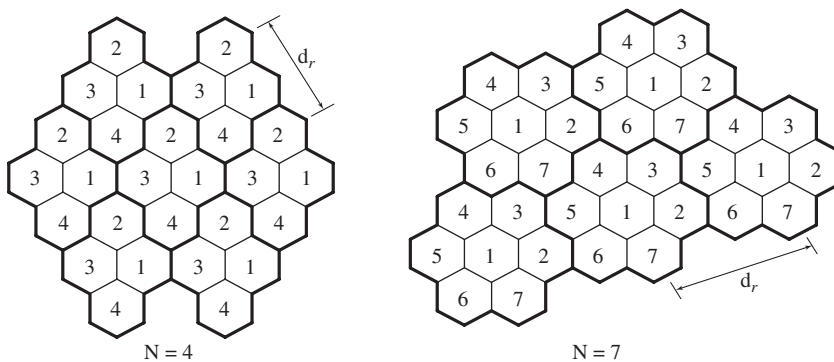

Figure 10.61 Frequency reuse in cellular system with reuse factor $N = 4$ or $N = 7$.

design plan, such as the frequency plans shown in Figure 10.61, where the frequency reuse factor is either $N = 4$ or $N = 7$. We observe that larger values of N increase the distance d_r between two base stations using the same set of frequencies, thus, reducing co-channel interference. On the other hand, a large value of N reduces the spectral efficiency of the cellular system, since fewer frequencies are assigned to each cell. The maximum radius for a cell is 35 Km.

Each 200 KHz-frequency band accommodates 8 users by creating 8 TDMA nonoverlapping time slots, as shown in Figure 10.62. The eight time slots constitute a frame of duration 4.615 msec, and each time slot has a time duration of 576.875 μsec. The information data from the users is transmitted in bursts at a rate of 270.833 Kbps. Figure 10.63 illustrates the basic GSM frame structure, in which 26 frames are grouped

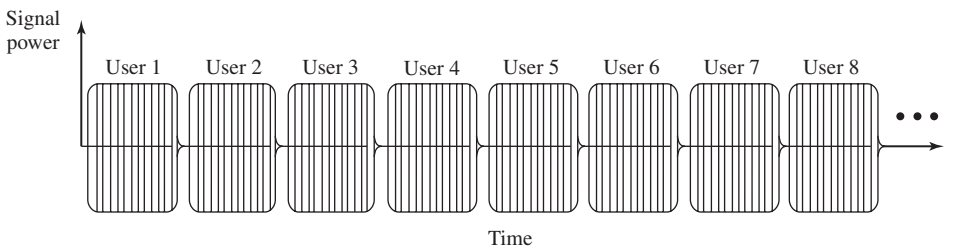

Figure 10.62 TDMA frame in GSM.

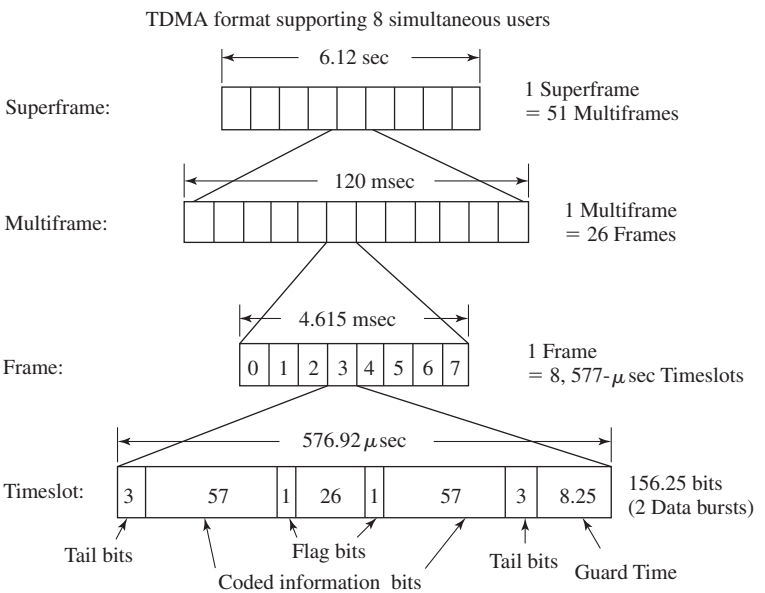

Figure 10.63 GSM frame structure.

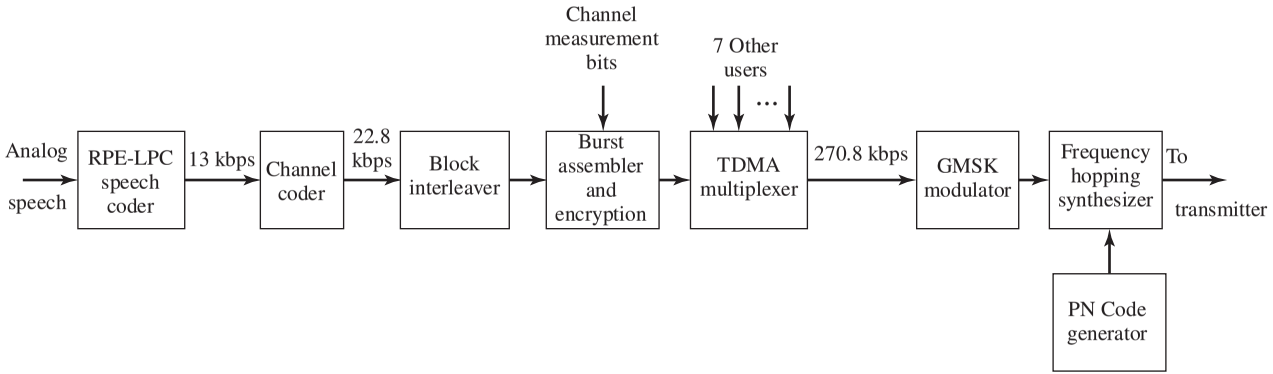

(a) Modulator

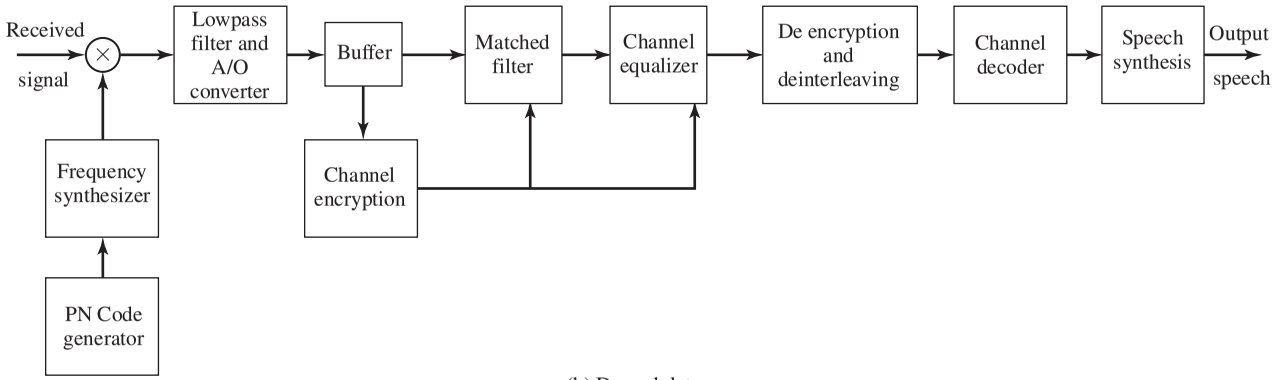

(b) Demodulator

Figure 10.64 Functional block diagram of modulator and demodulator for GSM.

to form a multiframe and 51 multiframes are grouped to form a superframe. The framing hierarchy is convenient in facilitating synchronization and network control. To reduce the effect of fading and interference and, thus, provide signal diversity, the carrier frequency is hopped at the frame rate of (nominally) 217 hops/sec.

The functional block diagram of the transmitter and receiver in the GSM system is shown in Figure 10.64. The speech coder is based on a type of linear predictive coding (LPC) called residual pulse-excited (RPE) linear-predictive coding (RPE-LPC). RPE-LPC delivers 260 bits in each 20 msec time interval, hence, a bit rate of 13 Kbps. The most significant bits are encoded by a rate $1/2$, constraint length $L = 5$ convolutional encoder, and the coded and uncoded bits are block interleaved to produce data at a rate of 22.8 Kbps. Thus, the 260 information bits are transformed into 456 coded bits in each 20 msec time interval. The coded bit stream is encrypted and, then, organized for burst transmission in time slots that carry 114 coded bits and some overhead bits, as shown in Figure 10.63, including a sequence of 26 bits which is used to measure the characteristics of the channel in each time slot. Therefore, the 456 coded bits are transmitted in four consecutive bursts, where each burst contains 114 coded bits and occupies one time slot.

The modulation used to transmit the bits in each time slot is GMSK with $BT = 0.3$, which is a signal pulse that is illustrated in Figure 10.27(e). The output of the GMSK modulator is translated in frequency to the desired carrier frequency, which is hopped to a different frequency in each frame.

At the receiver, the received signal is dehopped and translated to baseband, thus creating in-phase (I) and quadrature (Q) signal components, which are sampled and buffered. The 26 known transmitted bits are used to measure the channel characteristics and, thus, to specify the matched filter to the channel corrupted signal. The data bits are passed through the matched filter and the matched-filter output is processed by a channel equalizer, which may be realized either as a decision-feedback equalizer (DFE) or an ML sequence detector that is efficiently implemented via the Viterbi algorithm. The bits in a burst at the output of the equalizer are deassembled, deencrypted, deinterleaved, and passed to the channel decoder. The decoded bits are used to synthesize the speech signal that was encoded via RPE-LPC.

In addition to the time slots (channels) that are used for transmission of the digitized speech signals, there are additional channels that are allocated to various control and synchronization functions, such as paging, frequency correction, synchronization, and requests for access to send messages. These control channels are additional time slots that contain known sequences of bits for performing the control functions.

Table 10.5 provides a summary of the basic parameters in the GSM system.

10.4.2 CDMA System Based on IS-95

As described in Section 10.3, the enhancement in performance obtained from a DS spread-spectrum signal through the processing gain and coding gain can be used to enable many DS spread-spectrum signals to simultaneously occupy the same channel bandwidth, provided that each signal has its own distinct pseudorandom sequence.

TABLE 10.5 SUMMARY OF PARAMETERS IN GSM SYSTEM

System Parameter	Specification
Uplink frequency band	890–915 MHz
Downlink frequency band	935–960 MHz
Number of carriers/band	125
Bandwidth/carrier	200 KHz
Multiple-access method	TDMA
Number of users/carrier	8
Data rate/carrier	270.8 Kbps
Speech-coding rate	13 KHz
Speech encoder	RPE-LPC
Coded-speech rate	22.8 kbps
Modulation	GMSK with $BT = 0.30$
Demodulation	Matched filter + equalizer
Interleaver	Block
Frequency-hopping rate	217 hops/sec

Direct-sequence CDMA has been adopted as one multiple-access method for digital cellular voice communications in North America. This first generation digital cellular (DMA) communication system was developed by Qualcomm, and has been standardized and designated as IS-95 by the Telecommunications Industry Association (TIA) for use in the 800 MHz- and 1900 MHz-frequency bands. A major advantage of CDMA over other multiple-access methods is that the entire frequency band is available at each base station; i.e., the frequency reuse factor $N = 1$.

The nominal bandwidth used for transmission from a base station to the mobile receivers (forward link) is 1.25 MHz, and a separate channel, also with a bandwidth of 1.25 MHz, is used for signal transmission from mobile receivers to a base station (reverse link). The signals transmitted in both the forward and the reverse links are DS spread-spectrum signal having a chip rate of 1.2288×10^6 chips/sec (Mchips/s).

Forward Link. A block diagram of the modulator for the signals transmitted from a base station to the mobile receivers is shown in Figure 10.65. The speech coder is a code-excited linear-predictive (CELP) coder which generates data at the variable rates of 9600, 4800, 2400, and 1200 bits/s, where the data rate is a function of the speech activity of the user, in frame intervals of 20 ms. The data from the speech coder are encoded by a rate $1/2$, constraint length $L = 9$ convolutional code. For lower speech activity, where the data rates are 4800, 2400, or 1200 bits/s, the output symbols from the convolutional encoder are repeated either twice, four times, or eight times so as to maintain a constant bit rate of 9600 bits/s. At the lower speech activity rates, the transmitter power is reduced by either 3, 6, or 9 dB, so that the transmitted energy/bit remains constant for all speech rates. Thus, a lower speech activity results in a lower transmitter power and, hence, a lower level of interference to other users.

The encoded bits for each frame are passed through a block interleaver, which is needed to overcome the effects of burst errors that may occur in transmission through the channel. The data bits at the output of the block interleaver, which occur at a rate

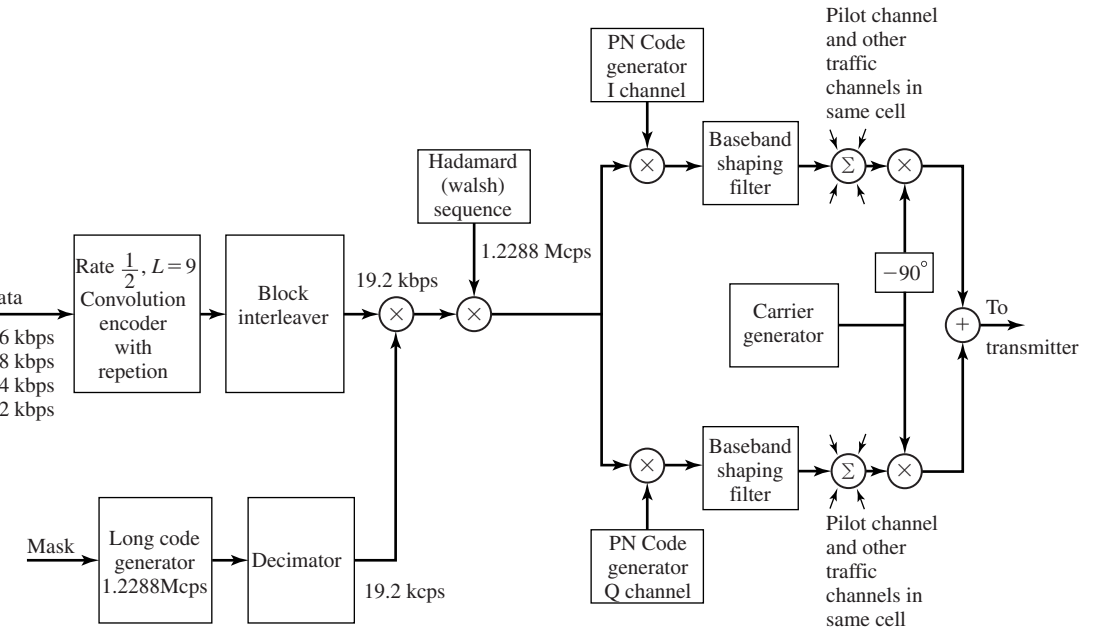

Figure 10.65 Block diagram of IS-95 forward link.

of 19.2 kbits/s, are scrambled by multiplication with the output of a long code (period $N = 2^{42} - 1$) generator running at the chip rate of 1.2288 M chips/s, but whose output is decimated by a factor of 64 to 19.2 kchips/s. The long code is used to uniquely identify a call of a mobile station on the forward and reverse links.

Each user of the channel is assigned a Hadamard (also called Walsh) sequence of length 64. There are 64 orthogonal Hadamard sequences assigned to each base station, and, thus, there are 64 channels available. One Hadamard sequence (the all-zero sequence) is used to transmit a pilot signal, which serves as a means for measuring the channel characteristics, including the signal strength and the carrier phase offset. These parameters are used at the receiver in performing phase-coherent demodulation. Another Hadamard sequence is used for providing time synchronization. One channel, and possibly more if necessary, is used for paging. That leaves up to 61 channels for allocation to different users.

Each user, using the Hadamard sequence assigned to it, multiplies the data sequence by the assigned Hadamard sequence. Thus, each encoded data bit is multiplied by the Hadamard sequence of length 64. The resulting binary sequence is now spread by multiplication with two PN sequences of length $N = 2^{15}$, so as to create in-phase (I) and quadrature (Q) signal components. Thus, the binary data signal is converted to a four-phase signal and both the I and Q components are filtered by baseband spectral-shaping filters. Different base stations are identified by different offsets of these PN sequences. The signals for all the 64 channels are transmitted synchronously so that,

in the absence of channel multipath distortion, the signals of other users received at any mobile receiver do not interfere because of the orthogonality of the Hadamard sequences.

At the receiver, a RAKE demodulator is used to resolve the major multipath signal components, which are then phase-aligned and weighted according to their signal strength using the estimates of phase and signal strength derived from the pilot signal. These components are combined and passed to the Viterbi soft-decision decoder.

Reverse Link. The modulator for the reverse link from a mobile transmitter to a base station is different from that for the forward link. A block diagram of the modulator is shown in Figure 10.66. An important consideration in the design of the modulator is that, signals transmitted from the various mobile transmitters to the base station are asynchronous and, hence, there is significantly more interference among users. Second, the mobile transmitters are usually battery operated and, consequently, these transmissions are power limited. To compensate for these major limitations, a $L = 9$, rate $1/3$ convolutional code is used in the reverse link. Although this code has essentially the same coding gain in an AWGN channel as the rate $1/2$ code used in the forward link, it has a much higher coding gain in a fading channel. As in the case of the forward link, for lower speech activity, the output bits from the convolutional encoder are repeated either two, or four, or eight times. However, the coded bit rate is 28.8 kbits/s.

For each 20-ms frame, the 576 encoded bits are block-interleaved and passed to the modulator. The data is modulated using an $M = 64$ orthogonal signal set using Hadamard sequences of length 64. Thus, a 6-bit block of data is mapped into one of the 64 Hadamard sequences. The result is a bit (or chip) rate of 307.2 kbits/s at the output of the modulator. We note that 64-ary orthogonal modulation at an error probability of 10^{-6} requires approximately 3.5 dB less SNR/bit than binary antipodal signaling.

To reduce interference to other users, the time position of the transmitted code symbol repetitions is randomized so that, at the lower speech activity, consecutive bursts do not occur evenly spaced in time. Following the randomizer, the signal is spread by the output of the long code PN generator, which is running at a rate of 1.2288 Mchips/s. Hence, there are only four PN chips for every bit of the Hadamard sequence from the modulator, so the processing gain in the reverse link is very small. The resulting 1.2288 Mchips/s binary sequences of length $N = 2^{15}$, whose rate is also 1.2288 Mchips/s, create I and Q signals (a QPSK signal) which are filtered by baseband spectral-shaping filters and then passed to quadrature mixers. The Q-channel signal is delayed in time by one-half PN chip relative to the I-channel signal prior to the baseband filter. In effect, the signal at the output of the two baseband filters is an offset QPSK signal.

Although the chips are transmitted as an offset QPSK signal, the demodulator employs noncoherent demodulation of the $M = 64$ orthogonal Hadamard waveforms to recover the encoded data bits. A computationally efficient (fast) Hadamard transform is used to reduce the computational complexity in the demodulation process. The output of the demodulator is then fed to the Viterbi detector, whose output is used to synthesize the speech signal.

Table 10.6 provides a summary of the basic parameters in the IS-95 system.

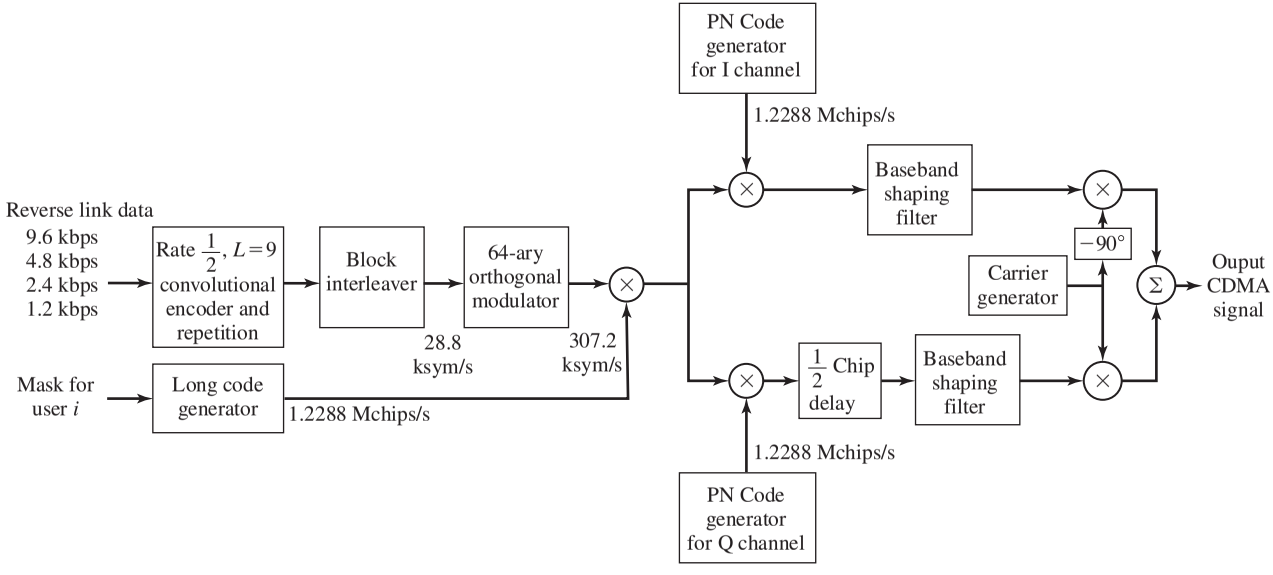

Figure 10.66 Block diagram of IS-95 reverse link.

TABLE 10.6 SUMMARY OF PARAMETERS IN IS-95 SYSTEM

System Parameter	Specification
Uplink frequency band	824–849 MHz
Downlink frequency band	869–894 MHz
Number of carriers/band	20
Bandwidth/carrier	1.25 MHz
Multiple-access method	CDMA
Number of users/carrier	60
Chip rate	1.2288 Mcps
Speech coder	Variable rate CELP
Speech rate	9600, 4800, 2400, 1200 bps
Interleaver	Block
Channel encoder	$R = 1/2,\ L = 9(D)$ $R = 1/3,\ L = 9(U)$
Modulation	BPSK with QPSK Spreading (D) 64-ary Orthogonal with QPSK Spreading (U)
Demodulation	RAKE matched filter with maximal-ratio combining
Signature sequences	Hadamard (Walsh) of length 64
PN sequence	$N = 2^{42} - 1$ (Long code) $N = 2^{15}$ (Spreading codes)

10.5 FURTHER READING

In this chapter, we focused our topics dealing with wireless communications. First, we treated digital transmission on fading multipath channels. Our treatment of this topic was indeed very brief and focused primarily on the Rayleigh fading channel model. For the most part, this is due to the wide acceptance of this model for describing the fading effects on many radio channels and to its mathematical tractability. Although other statistical models, such as the Ricean fading model, may be more appropriate for characterizing fading on some real channels, such as microwave LOS, the general approach for providing reliable communications by means of signal diversity is still applicable.

More extensive and advanced treatments on fading channels are found in books by Schwartz et al. (1966) and Proakis (2001). The pioneering work on the characterization of fading multipath channels and on signal and receiver design for reliable digital communications over such channels was done by Price (1954, 1956). This early work was followed by additional significant contributions from Price and Green (1958, 1960), Kailath (1960, 1961), and Green (1962). Diversity transmission and diversity-combining techniques under a variety of channel conditions have been treated in the papers by Pierce (1958), Brennan (1959), Turin (1961, 1962), Pierce and Stein (1960), Barrow (1963), Bello and Nelin (1962a,b, 1963), Price (1962a,b), and Lindsey (1964).

CPFSK and CPM are especially suitable for wireless digital communications because these types of digital modulations are bandwidth efficient and have the additional desirable property of having a constant envelope. Therefore, high efficiency nonlinear

power amplifiers can be used in transmission of the signals. CPFSK and CPM have been treated extensively in the technical journals and in textbooks. A thorough treatment of CPM can be found in the book by Anderson et al. (1986). The journal papers by Aulin and Sundberg (1981, 1982a,b, 1984) and by Aulin et al. (1981) provide detailed analysis of the performance characteristics of CPM. The tutorial paper by Sundberg (1986) gives a very readable overview of CPM, its demodulation and its performance characteristics. This paper also contains a comprehensive list of references.

Our third topic of this chapter was a brief, introductory treatment of spread-spectrum modulation and demodulation and the performance evaluation of this type of signaling in the presence of several different types of interference. Historically, the primary application of spread-spectrum modulation has been in the design of secure digital communications systems for military use. However, in the last two decades we have seen a trend toward commercial use of spread-spectrum modulation, especially its use in mobile cellular communications, in multiple-access communications via satellites, and in interoffice radio communications.

A historical account on the development of spread-spectrum communications covering the period 1920–1960 is given in a paper by Scholtz (1982). Tutorial treatments of spread-spectrum modulation that deal with basic concepts are found in papers by Scholtz (1977) and Pickholtz et al. (1982). These papers also contain a large number of references to the previous work. Two tutorial papers by Viterbi (1979, 1985) contain a basic analysis of the performance characteristics of DS and FH spread-spectrum signals.

Comprehensive treatments of various aspects concerning the analysis and design of spread-spectrum signals and systems, including synchronization techniques, are found in books by Simon et al. (1985), Ziemer and Peterson (1985), and Holmes (1982). Also, special issues of the *IEEE Transactions on Communications* (August 1977, May 1982) are devoted to spread-spectrum communications. These special issues contain a collection of papers devoted to a variety of topics, including multiple-access techniques, synchronization techniques, and performance analysis with various types of channel interference. A number of important papers that have been published in IEEE journals have been reprinted in book form by the IEEE press, (see Dixon, ed. (1976) and Cook et al. (1983)).

In the last section of this chapter, we presented two examples of digital cellular communication systems designed for voice transmission. One system, called GSM, is based on TDMA to accommodate multiple users, while the second system employs CDMA.

PROBLEMS

10.1 In the transmission and reception of signals to and from moving vehicles, the transmitted signal frequency is shifted in direct proportion to the speed of the vehicle. The so-called *Doppler frequency shift* imparted to a signal that is received in a vehicle traveling at a velocity v relative to a (fixed) transmitter is given by

the formula

$$f_D = \pm\frac{v}{\lambda}$$

where λ is the wavelength, and the sign depends on the direction (moving toward or moving away) that the vehicle is traveling relative to the transmitter. Suppose that a vehicle is traveling at a speed of 100 km/hr relative to a base station in a mobile cellular communication system. The signal is a narrowband signal transmitted at a carrier frequency of 1 GHz.

1. Determine the Doppler frequency shift.
2. What should be the bandwidth of a Doppler frequency tracking loop if the loop is designed to track Doppler frequency shifts for vehicles traveling at speeds up to 100 km/hr?
3. Suppose the transmitted signal bandwidth is 1 MHz centered at 1 GHz. Determine the Doppler frequency spread between the upper and lower frequencies in the signal.

10.2 A multipath fading channel has a multipath spread of $T_m = 1$ s and a Doppler spread $B_d = 0.01$ Hz. The total channel bandwidth at bandpass available for signal transmission is $W = 5$ Hz. To reduce the effect of intersymbol interference, the signal designer selects a pulse duration of $T = 10$ sec.

1. Determine the coherence bandwidth and the coherence time.
2. Is the channel frequency selective? Explain.
3. Is the channel fading slowly or rapidly? Explain.
4. Suppose that the channel is used to transmit binary data via (antipodal) coherently detected PSK in a frequency diversity mode. Explain how you would use the available channel bandwidth to obtain frequency diversity and determine how much diversity is available.
5. For the case in (4), what is the approximate SNR required/diversity to achieve an error probability of 10^{-6}?

10.3 The probability of error for binary DPSK and binary FSK with noncoherent detection in an AWGN channel is

$$P_b = \frac{1}{2}e^{-c\rho_b}$$

where $c = 1$ for DPSK and $c = \frac{1}{2}$ for FSK, and $\rho_b = \frac{\alpha^2\mathcal{E}_b}{N_0}$, where α is the attenuation factor. By averaging P_b over the Rayleigh distributed variable α, as indicated by Equation (10.1.25), verify the expression for the probability of error for DPSK and FSK in a Rayleigh fading channel.

10.4 A communication system employs dual antenna diversity and binary orthogonal FSK modulation. The received signals at the two antennae are

$$r_1(t) = \alpha_1 s(t) + n_1(t)$$
$$r_2(t) = \alpha_2 s(t) + n_2(t)$$

where α_1 and α_2 are statistically i.i.d. Rayleigh random variables, and $n_1(t)$ and $n_2(t)$ are statistically independent, zero-mean white Gaussian random processes with power-spectral density $N_0/2$ W/Hz. The two signals are demodulated, squared, and then combined (summed) prior to detection.

1. Sketch the functional block diagram of the entire receiver including the demodulator, the combiner, and the detector.
2. Plot the probability of error for the detector and compare the result with the case of no diversity.

10.5 A binary communication system transmits the same information on two diversity channels. The two received signals are

$$r_1 = \pm\sqrt{\mathcal{E}_b} + n_1$$
$$r_2 = \pm\sqrt{\mathcal{E}_b} + n_2$$

where $E(n_1) = E(n_2) = 0$, $E(n_1^2) = \sigma_1^2$ and $E(n_2^2) = \sigma_2^2$, and n_1 and n_2 are uncorrelated Gaussian variables. The detector bases its decision on the linear combination of r_1 and r_2; i.e.,

$$r = r_1 + kr_2$$

1. Determine the value of k that minimizes the probability of error.
2. Plot the probability of error for $\sigma_1^2 = 1$, $\sigma_2^2 = 3$ and either $k = 1$ or k is the optimum value found in (1). Compare the results.

10.6 Suppose the binary antipodal signals $\pm s(t)$ are transmitted over a fading channel and the received signal is

$$r(t) = \pm\alpha s(t) + n(t), \quad 0 \le t \le T$$

where $n(t)$ is zero-mean white Gaussian noise with autocorrelation function $\frac{N_0}{2}\delta(\tau)$. The energy in the transmitted signal is $\mathcal{E} = \int_0^T |s(t)|^2\, dt$. The channel gain α is specified by the PDF $p(\alpha) = 0.1\delta(\alpha) + 0.9\delta(\alpha - 2)$.

1. Determine the average probability of error P_e for the demodulator which employs a filter matched to $s(t)$.
2. What value does P_e approach as $\frac{\mathcal{E}}{N_0}$ approaches infinity?
3. Suppose the same signal is transmitted over two statistically *independently*

fading channels with gains α_1 and α_2, where

$$p(a_k) = 0.1\delta(\alpha_k) + 0.9\delta(\alpha_k - 2), \quad k = 1, 2$$

The noises on the two channels are statistically independent and identically distributed. The demodulator employs a matched filter for each channel and simply adds the two filter outputs to form the decision variable. Determine the average P_e.

4. For the case in (c) what value does P_e approach as $\frac{\mathcal{E}}{N_0}$ approaches infinity?

10.7 In a MSK signal, the initial state for the phase is either 0 or π radians. Determine the terminal phase state for the following four input pairs of input data: (a) 00, (b) 01, (c) 10, (d) 11.

10.8 A continuous-phase FSK signal with $h = 1/2$ is represented as

$$s(t) = \pm\sqrt{\frac{2\mathcal{E}_b}{T_b}}\cos\left(\frac{\pi t}{2T_b}\right)\cos 2\pi f_c t \pm \sqrt{\frac{2\mathcal{E}_b}{T_b}}\sin\left(\frac{\pi t}{2T_b}\right)\sin 2\pi f_c t \qquad 0 \le t \le 2T_b$$

where the $\pm$ signs depend on the information bits transmitted.

1. Show that this signal has a constant amplitude.
2. Sketch a block diagram of the modulator for synthesizing the signal.
3. Sketch a block diagram of the demodulator and detector for recovering the information.

10.9 Sketch the phase-tree, the state trellis, and the state diagram for partial-response CPM with $h = \frac{1}{2}$ and

$$g(t) = \begin{cases} \frac{1}{4T}, & 0 \le t \le 2T \\ 0, & \text{otherwise} \end{cases}$$

10.10 Determine the number of terminal phase states in the state trellis diagram for (a) a full response binary CPFSK with either $h = \frac{2}{3}$ or $\frac{3}{4}$ and (b) a partial response $L = 3$ binary CPFSK with either $h = \frac{2}{3}$ or $\frac{3}{4}$.

10.11 A rate $1/2$ convolutional code with $d_{\text{free}} = 10$ is used to encode a data sequence occurring at a rate of 1000 bits per second. The modulation is binary PSK. The DS spread spectrum sequence has a chip rate of 10 MHz.

1. Determine the coding gain.
2. Determine the processing gain.
3. Determine the interference margin assuming an $\mathcal{E}_b/I_0 = 10$.

10.12 Demonstrate that a DS spread-spectrum signal without coding provides no improvement in performance against additive white Gaussian noise.

10.13 A total of 30 equal-power users are to share a common communication channel [illegible] a DS spread

spectrum and binary PSK. Determine the minimum chip rate in order to obtain a bit-error probability of 10^{-5}. Additive noise at the receiver may be ignored in this computation.

10.14 A CDMA system is designed based on DS spread spectrum with a processing gain of 1000 and binary PSK modulation. Determine the number of users, if each user has equal power and the desired level of performance is an error probability of 10^{-6}. Repeat the computation if the processing gain is changed to 500.

10.15 A DS spread-spectrum system transmits at a rate of 1000 bps in the presence of a tone interference. The interference power is 20 dB greater than the desired signal and the required $\mathcal{E}_b/I_0$ to achieve satisfactory performance is 10 dB.

1. Determine the spreading bandwidth required to meet the specifications.
2. In the case of a pulse interference, determine the pulse duty cycle that results in worst-case performance and the corresponding probability of error.

10.16 A DS spread-spectrum system is used to resolve the multipath signal component in a two-path radio signal propagation scenario. If the path length of the secondary path is 300 m longer than that of the direct path, determine the minimum chip rate necessary to resolve the multipath component.

10.17 A CDMA system consists of 15 equal-power users that transmit information at a rate 10,000 bps each using a DS spread-spectrum signal operating at a chip rate of 1 MHz. The modulation is binary PSK.

1. Determine the $\mathcal{E}_b/I_0$, where I_0 is the spectral density of the combined interference.
2. What is the processing gain?
3. How much should the processing gain be increased to allow for doubling the number of users without affecting the output SNR?

10.18 An FH binary orthogonal FSK system employs a $m = 15$ stage linear feedback shift register that generates a maximal length sequence. Each state of the shift register selects one of N nonoverlapping frequency bands in the hopping pattern. The bit rate is 100 bits/sec and the hop rate is once/bit. The demodulator employs noncoherent detection.

1. Determine the hopping bandwidth for this channel.
2. What is the processing gain?
3. What is the probability of error in the presence of AWGN?

10.19 Consider the FH binary orthogonal FSK system described in Problem 10.18. Suppose that the hop rate is increased to two hops/bit. The receiver uses square-law combining to combine the signal over the two hops.

1. Determine the hopping bandwidth for the channel.
2. What is the processing gain?
3. What is the error probability in the presence of AWGN?

10.20 In a fast FH spread-spectrum system, the information is transmitted via FSK, with noncoherent detection. Suppose there are $N = 3$ hops/bit, with hard-decision decoding of the signal in each hop.

1. Determine the probability of error for this system in an AWGN channel with power-spectral density $\frac{N_0}{2}$ and an SNR = 13 dB (total SNR over the three hops).
2. Compare the result in (1) with the error probability of an FH spread-spectrum system that hops once/bit.

10.21 A slow FH binary FSK system with noncoherent detection operates at an $\mathcal{E}_b/I_0 = 10$, with a hopping bandwidth of 2 GHz, and a bit rate of 10 Kbps.

1. What is the processing gain for the system?
2. In the case of a partial-band interference, what is the bandwidth occupancy for worst-case performance?
3. What is the probability of error for the worst-case partial-band interference?

10.22 A DS binary PSK spread spectrum has a processing gain of 500. What is the interference margin against a continuous tone interference if the desired error probability is 10^{-5}?

10.23 Repeat Problem 10.22 for a pulsed noise interference with a duty cycle of 1%.

10.24 Consider the DS spread-spectrum signal

$$c(t) = \sum_{n=-\infty}^{\infty} c_n p(t - nT_c)$$

where c_n is a periodic m-sequence with a period $L = 127$ and $p(t)$ is a rectangular pulse of duration $T_c = 1\ \mu$sec. Determine the power-spectral density of the signal $c(t)$.

10.25 Suppose that $\{c_{1i}\}$ and $\{c_{2i}\}$ are two binary (0, 1) periodic sequences with periods L_1 and L_2, respectively. Determine the period of the sequence obtained by forming the modulo-2 sum of $\{c_{1i}\}$ and $\{c_{2i}\}$.

10.26 An $m = 10$ maximum-length shift register is used to generate the pseudorandom sequence in a DS spread-spectrum system. The chip duration is $T_c = 1\ \mu$sec, and the bit duration is $T_b = LT_c$, where L is the length (period) of the m-sequence.

1. Determine the processing gain of the system in dB.
2. Determine the interference margin if the required $\mathcal{E}_b/I_0 = 10$ and the interference is a tone interference with an average power I_{av}.

10.27 Figure P10-27 illustrates the average power multipath delay profile for (a) suburban and urban areas and (b) hilly terrain area, in cellular communication. In a GSM system, the bit rate is 270.8 Kbps and in IS-95 system (forward link) the bit rate is 19.2 Kbps. Determine the number of bits affected by intersymbol interference in the transmission of the signal through the channels (a) and (b)

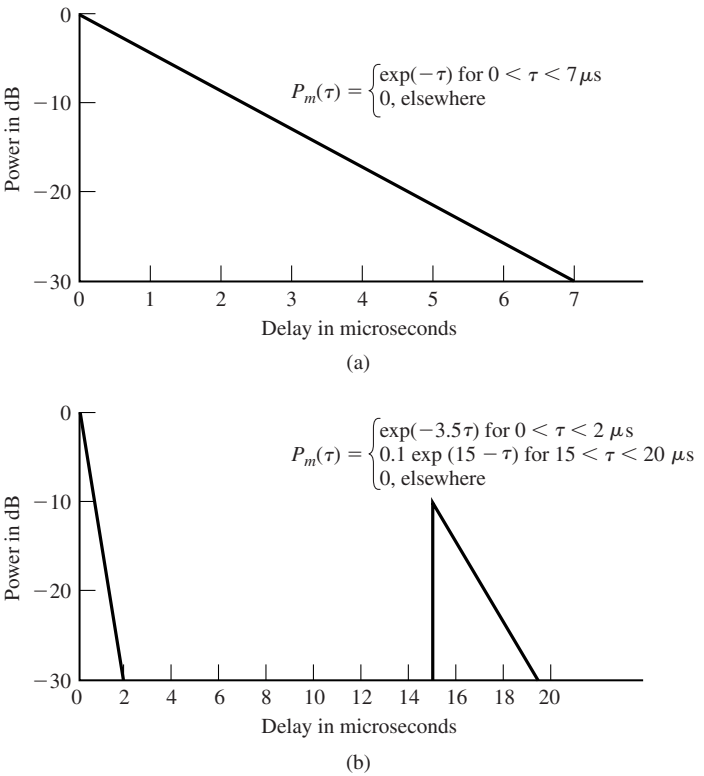

Figure P-10.27

10.28 For the multipath delay problem shown in Figure P10-27, determine the number of taps in a RAKE demodulator that would be needed to span the multipath for channels (a) and (b). Of the total number of RAKE taps, how many will contain signal components and how many will have no signal for channel (b)?

10.29 A widely used model for the Doppler power spectrum of a mobile radio channel is the so-called *Jake's model,* given as

$$\mathcal{S}(f) = \begin{cases} \frac{1}{\pi f_m} \frac{1}{\sqrt{1-(f/f_m)^2}}, & |f| \leq f_m \\ 0, & \text{otherwise} \end{cases}$$

where $f_m = vf_0/c$ is the maximum Doppler frequency, v is the vehicle speed in m/s, f_0 is the carrier frequency, and c is the speed of light (3×10^8 m/s). Determine f_m for an automobile traveling at 100 Km/hr, for a train traveling at 200 Km/hr and plot $\mathcal{S}(f)$ for the two vehicles for a cellular communication system with a carrier frequency of 900 MHz. What are the spread factors of the channel for the two vehicles if the multipath delay profile is the one shown in Figure P10-27?